Current Biology

A neuropeptidergic circuit gates selective escape behavior of Drosophila larvae

--Manuscript Draft--

Manuscript Number:	CURRENT-BIOLOGY-D-21-00284R3
Full Title:	A neuropeptidergic circuit gates selective escape behavior of Drosophila larvae
Article Type:	Research Article
Corresponding Author:	Peter Soba, Ph.D. University Medical Campus Hamburg-Eppendorf Hamburg, GERMANY
First Author:	Bibi Nusreen Imambocus
Order of Authors:	Bibi Nusreen Imambocus
	Fangmin Zhou
	Andrey Formozov
	Annika Wittich
	Federico M Tenedini
	Chun Hu
	Kathrin Sauter
	Ednilson Macarenhas Varela
	Fabiana Herédia
	Andrea P Casimiro
	André Macedo
	Philipp Schlegel
	Chung-Hui Yang
	Irene Miguel-Aliaga
	J Simon Wiegert
	Michael J Pankratz
	Alisson M Gontijo
	Albert Cardona
	Peter Soba, Ph.D.
Abstract:	Animals display selective escape behaviors when faced with environmental threats. Selection of the appropriate response by the underlying neuronal network is key to maximize chances of survival, yet the underlying network mechanisms are so far not fully understood. Using synapse-level reconstruction of the Drosophila larval network paired with physiological and behavioral readouts, we uncovered a circuit that gates selective escape behavior for noxious light through acute and input-specific neuropeptide action. Sensory neurons required for avoidance of noxious light and escape in response to harsh touch, each converge on discrete domains of neuromodulatory hub neurons. We show that acute release of hub neuron-derived Insulin-like peptide 7 (Ilp7) and cognate Relaxin-family receptor (Lgr4) signaling in downstream neurons is required for noxious light avoidance, but not harsh touch responses. Our work highlights a role for compartmentalized circuit organization and neuropeptide release from regulatory hubs, acting as central circuit elements gating escape responses.
Additional Information:	
Question	**Response**

Standardized datasets A list of datatypes considered standardized under Cell Press policy is available here. Does this manuscript report new standardized datasets?	No
Original Code Does this manuscript report original code?	Yes
Reviewers must have anonymous access to these standardized datasets that is free-of-cost. Please provide dataset locations and instructions for access here. If applicable, include accession numbers and reviewer tokens. Please consult these Author's guides for more information: "Standardized datatypes, datatype-specific repositories, and general-purpose repositories recommended by Cell Press" and "How standardized datasets and original code accompany Cell Press manuscripts from submission through publication" or email us at current-biology@cell.com. as follow-up to "**Original Code** Does this manuscript report original code? "	code and scripts for analysis of two choice assays: https://github.com/formozov/larva_tracking_Imambocus_et_al

University Medical Center Hamburg-Eppendorf
Center for Molecular Neurobiology / ZMNH
Research group:
Neuronal Patterning and Connectivity

Dr. Peter Soba
Martinistraße 52
20246 Hamburg
Germany
Phone: +49 (0) 40 7410-58281
Fax: +49 (0) 40 7410-58270
peter.soba@zmnh.uni-hamburg.de
www.sobalab.com
Delivery address:
Falkenried 94 / Martinistr. 85
20251 Hamburg, Germany

Universitätsklinikum Hamburg-Eppendorf | Martinistraße 52 | 20246 Hamburg
Zentrum für Molekulare Neurobiologie | Forschungsgruppe Dr. Peter Soba

Geoffrey North
Editor in Chief
–Current Biology–

Dear Geoff,

Thank you very much for the positive response that our manuscript entitled "**A neuropeptidergic circuit gates selective escape behavior of *Drosophila* larvae**" by Imambocus *et al*. will in principle be accepted for publication in *Current Biology*.

We have fully addressed the editorial comments and completed the Final File Checklist. Please note that we have reduced the main manuscript length significantly and put all our effort into getting close to the 5000 word count. We sincerely hope that you find the finalized version satisfactory.

Sincerely,

Peter

Peter Soba

Heisenberg Group Leader

LIMES-Institute, University of Bonn

Hosted at: ZMNH, University Medical Center Hamburg-Eppendorf

CURRENT-BIOLOGY-D-21-00284

We would like to thank the reviewers for their helpful comments and suggestions. As no further changes were requested by the reviewers, we adjusted the overall manuscript according to the Final File Checklist of Current Biology.

REVIEWER COMMENTS:

Reviewer #1: I find the revised manuscript to be further improved by addition of the pupariation and developmental assay. The rewording of "photonociception" to "noxious light avoidance" clarifies further. To repeat my comment to the first revision: I have no further comments to this excellent and significant piece of work in our field.

Response: We thank the reviewer for the very positive assessment of our work and we are grateful for the excellent comments and suggestions throughout the review process.

Reviewer #2: I praise the authors for their remarkable receptivity to the suggestions of the reviewers. In their second revision, the authors provided new material to address the concerns raised by reviewers #3 and #4. Their argumentation is both rigorous and cautious. The authors added experimental evidence that rule out the possibility that thermal effects explain the developmental photo-toxicty of prolonged exposure to blue light. The authors also provided new results establishing that Ilp7 function is necessary for larvae to exhibit preferential pupation in the dark. Finally, the authors clarified the contribution of different light-sensing pathways on the emergence of acute noxious light responses. Through the peer-review process, the work has improved from an excellent manuscript to an outstanding manuscript. It seems now timely for the work to be made accessible to the readership of Current Biology.

Response: We thank the reviewer for the very positive assessment and we are grateful for the excellent comments and suggestions made throughout the review process.

CELL PRESS DECLARATION OF INTERESTS FORM

If submitting materials via Editorial Manager, please complete this form and upload with your final submission. Otherwise, please email as an attachment to the editor handling your manuscript.

Please complete each section of the form and insert any necessary "Declaration of Interests" statement in the text box at the end of the form. A matching statement should be included in a "Declaration of Interests" section in the manuscript.

Institutional Affiliations

We require that you list the current institutional affiliations of all authors, including academic, corporate, and industrial, on the title page of the manuscript. ***Please select one of the following:***

- (●) All affiliations are listed on the title page of the manuscript.
- ( ) I or other authors have additional affiliations that we have noted in the "Declaration of Interests" section of the manuscript and on this form below.

Funding Sources

We require that you disclose all funding sources for the research described in this work. ***Please confirm the following:***

- (●) All funding sources for this study are listed in the "Acknowledgments" section of the manuscript.*

*A small number of front-matter article types do not include an "Acknowledgments" section. For these, reporting funding sources is not required.

Competing Financial Interests

We require that authors disclose any financial interests and any such interests of immediate family members, including financial holdings, professional affiliations, advisory positions, board memberships, receipt of consulting fees, etc., that:

(1) could affect or have the perception of affecting the author's objectivity, *or*
(2) could influence or have the perception of influencing the content of the article.

Please select one of the following:

- (●) We, the authors and our immediate family members, have no financial interests to declare.
- ( ) We, the authors, have noted any financial interests in the "Declaration of Interests" section of the manuscript and on this form below, and we have noted interests of our immediate family members.

Advisory/Management and Consulting Positions

We require that authors disclose any position, be it a member of a board or advisory committee or a paid consultant, that they have been involved with that is related to this study. We also require that members of our journal advisory boards disclose their position when publishing in that journal. ***Please select one of the following:***

- (●) We, the authors and our immediate family members, have no positions to declare and are not members of the journal's advisory board.
- ( ) The authors and/or their immediate family members have management/advisory or consulting relationships noted in the "Declaration of Interests" section of the manuscript and on this form below.

Patents

We require that you disclose any patents related to this work by any of the authors or their institutions. ***Please select one of the following:***

- (●) The authors and our immediate family members, have no related patents to declare.
- ( ) We, the authors, have a patent related to this work, which is noted in the "Declaration of Interests" section of the manuscript and on this form below, and we have noted the patents of immediate family members.

Please insert any "Declaration of Interests" statement in this space. This exact text should also be included in the "Declaration of Interests" section of the manuscript. If no authors have a competing interest, please insert the text, "The authors declare no competing interests."

The authors declare that no competing interests exist.

On behalf of all authors, I declare that I have disclosed all competing interests related to this work. If any exist, they have been included in the "Declaration of Interests" section of the manuscript.

Name: Peter Soba

Manuscript number (if available): CURRENT-BIOLOGY-D-21-00284

Graphical Abstract

Click here to access/download;Graphical Abstract;graphical abstractv4.tif

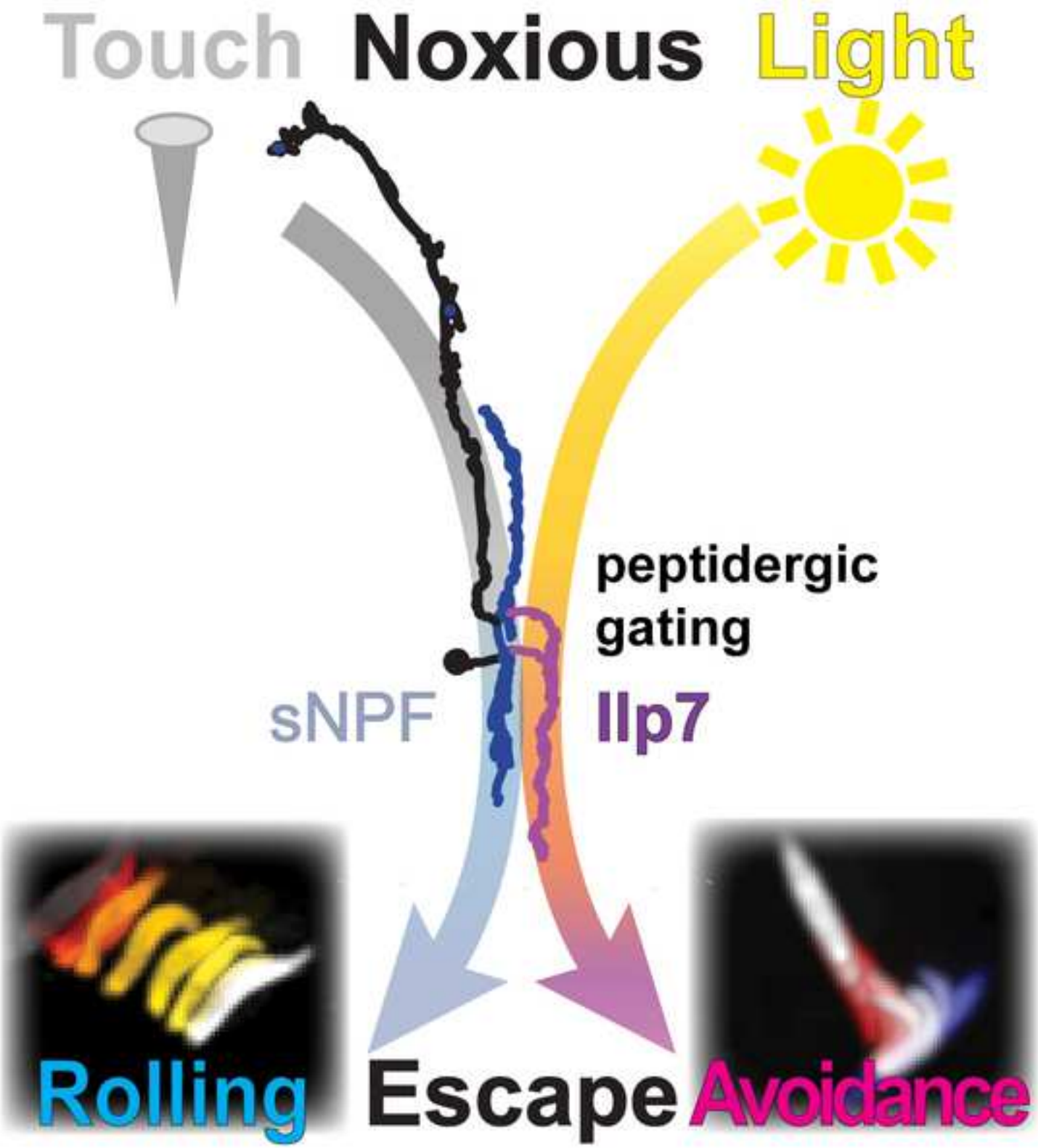

A neuropeptidergic circuit gates selective escape behavior of *Drosophila* larvae

Bibi Nusreen Imambocus[1,2], Fangmin Zhou[1,2], Andrey Formozov[2], Annika Wittich[2], Federico Tenedini[2], Chun Hu[2,#], Kathrin Sauter[2], Ednilson Macarenhas Varela[3], Fabiana Herédia[3], Andreia P. Casimiro[3], André Macedo[3], Philipp Schlegel[1,†], Chung-Hui Yang[4], Irene Miguel-Aliaga[5,6], J. Simon Wiegert[2], Michael J. Pankratz[1], Alisson M. Gontijo[3,7], Albert Cardona[8,9,10], Peter Soba[1,2,11,*]

[1]LIMES Institute, Department of Molecular Brain Physiology and Behavior, University of Bonn, Carl-Troll-Str. 31, 53115 Bonn, Germany
[2]Center for Molecular Neurobiology (ZMNH), University Medical Center Hamburg-Eppendorf, Falkenried 94, 20251 Hamburg, Germany.
[3]Integrative Biomedicine Laboratory, CEDOC, Chronic Diseases Research Center, NOVA Medical School, Faculdade de Ciências Médicas, Universidade Nova de Lisboa, Rua do Instituto Bacteriológico 5, 1150-082 Lisbon, Portugal.
[4]Department of Neurobiology, Duke University Medical School, 427E Bryan Research, Durham, NC 27710, USA
[5]MRC London Institute of Medical Sciences, Du Cane Road, London W12 0NN, UK
[6]Institute of Clinical Sciences, Faculty of Medicine, Imperial College London, Du Cane Road, London W12 0NN, UK.
[7]The Discoveries Centre for Regenerative and Precision Medicine, Lisbon Campus, Av. Rovisco Pais, 1049-001 Lisbon, Portugal
[8]HHMI Janelia Research Campus, 19700 Helix Dr, Ashburn, VA 20147, USA
[9]MRC Laboratory of Molecular Biology, Francis Crick Avenue, Cambridge CB2 0QH, UK
[10]Department of Physiology, Development & Neuroscience, University of Cambridge, Downing Street, Cambridge CB2 3EJ, UK

#present address: Key Laboratory of Brain, Cognition and Education Sciences, Ministry of Education, China; Institute for Brain Research and Rehabilitation, South China Normal University, 510631 Guangzhou, China
[†]present address: Department of Zoology, University of Cambridge, Downing Street, Cambridge CB2 3EJ, UK
[11]Lead contact
[*]Correspondence: psoba@uni-bonn.de

Summary

Animals display selective escape behaviors when faced with environmental threats. Selection of the appropriate response by the underlying neuronal network is key to maximize chances of survival, yet the underlying network mechanisms are so far not fully understood. Using synapse-level reconstruction of the *Drosophila* larval network paired with physiological and behavioral readouts, we uncovered a circuit that gates selective escape behavior for noxious light through acute and input-specific neuropeptide action. Sensory neurons required for avoidance of noxious light and escape in response to harsh touch, each converge on discrete domains of neuromodulatory hub neurons. We show that acute release of hub neuron-derived Insulin-like peptide 7 (Ilp7) and cognate Relaxin-family receptor (Lgr4) signaling in downstream neurons is

required for noxious light avoidance, but not harsh touch responses. Our work highlights a role for compartmentalized circuit organization and neuropeptide release from regulatory hubs, acting as central circuit elements gating escape responses.

Keywords

escape behavior, nociception, light avoidance, neuromodulation, neuropeptide, GPCR, connectomics, sensory gating

Introduction

Animals employ stimulus-specific, optimized strategies to deal with acute threats and noxious stimuli, including escape or avoidance behaviors [1–3]. In the somatosensory system of vertebrates as well as invertebrates, noxious stimuli are sensed by nociceptive neurons and their activation results in acute escape or avoidance [4–7]. A specific noxious stimulus thereby elicits a stereotyped response with high fidelity, e.g. jumping in mice or corkscrew-like rolling in *Drosophila* larvae in response to noxious heat [6,8]. Selection of the appropriate behavioral response minimizes risk and increases the likelihood of survival.

The neuronal networks underlying escape responses range from simple reflex to extensive circuits[8–13]. Recent reconstruction of such networks at the synaptic level and neuronal circuit mapping have revealed extensive integration and interaction of circuits mediating distinct responses [8–10,14]. Integration and processing of sensory information starts at the sensory level, where different types of sensory neurons are converging on common 2nd order neurons, which are in turn part of interconnected circuits providing feedback and feedforward information. How such circuits can specifically gate stimulus-specific information to support selected actions is not fully understood and difficult to deduce from pure anatomical network connectivity. Selection of behavior can occur probabilistically in a "winner takes it all" fashion, e.g. by reciprocal inhibition of circuits regulating mutually exclusive behaviors[10,15]. Differences in the activation pattern of sensory neuron subsets can result in different sensations and behavioral responses, as shown for combinatorial coding in mechanosensation and olfaction, suggesting extensive integration and processing in such networks [16–19]. Adding to the complexity of circuit computation are neuropeptides, which are expressed by many neurons across species [20–23]. They can be released in parallel to small synaptic neurotransmitters to exert modulatory functions [24–27]. In most cases, their precise role, site of release and action remains unclear, although they strongly contribute to network function and behavior.

To get detailed insight into the encoding of discrete escape responses at the circuit and neuromodulatory level, we took advantage of the escape behavior of *Drosophila* larva, given its experimental accessibility and the ability to map the neuronal wiring diagram with nanometer resolution. Recent reconstruction of *Drosophila* larval brain circuits [14,28,29] has revealed a complex somatosensory network capable of processing different mechanical and noxious stimuli [14,30–32] comparable to its vertebrate counterpart [33–35]. At the sensory level, class IV dendritic arborization (C4da) neurons are polymodal neurons able to detect noxious touch, heat and UV/blue light, which generate two different escape behaviors [6,36,37]: heat and harsh mechanical touch (mechanonociception) cause corkscrew-like rolling, while exposure to UV or blue light results in reorientation, avoidance and dark preference. *Drosophila* larvae can sense UV, blue and green light via different light-sensitive cells: Bolwig's organ (BO) consists of a group of cells in the larval head region and is sensitive to all of these wavelengths[38]; C4da neurons detect only noxious short wavelength light in the UV and blue spectral range, presumably via the light sensitive

Gr28b receptor[37]. Avoidance responses to noxious light in acute and two-choice light avoidance assays have been shown to rely on both, BO and C4da neuron function[36,37]. While the circuit mechanism for light avoidance has not been studied in detail so far, mechanonociception requires integration of three mechanosensory subtypes (namely C2da, C3da and C4da) by dorsal pair insulin-like peptide 7 (Dp7) neurons[39], which provide neuropeptidergic feedback via short Neuropeptide F (sNPF). sNPF action in turn promotes C4da and downstream partner (A08n) neuron responses, thus facilitating rolling escape behavior[30]. As Dp7 neurons integrate input from the mechano- and light-sensitive C4da neurons and have neuromodulatory functions, we reasoned they are potential candidates for computing distinct behavioral outputs depending on the type of sensory input.

Results

Neuromodulatory Dp7 neurons integrate sensory input required for noxious light avoidance

To explore the larval somatosensory escape circuit for noxious light avoidance (Fig. 1A,B), we first sought to confirm the noxious effect of short wavelength light on development by rearing freshly hatched larvae either under blue or green light (470 nm or 525 nm at 2.5 $\mu W/mm^2$). Only blue light exposure resulted in lethality during development at larval or white pupal stages (Fig. 1C). Thus, *Drosophila* larvae might have evolved avoidance behaviors to avoid short wavelength light (e.g., bright sunlight) during their development. We therefore explored the circuits underlying escape behavior in response to noxious light using a two-choice preference assay[36,40], in which larvae in an arena were allowed to choose between darkness or white light of physiological relevance (365-600 nm with 6.9-3.3 $\mu W/mm^2$, respectively). After placing larvae close to the dark/light boundary, controls (w^{1118}) preferentially redistributed to the dark side within less than 5 min and maintained this preference for at least 15 min (Fig. S1A,B, Video S1). This allowed us to reliably assess light avoidance by analyzing larval distribution after 15 min as previously described[36] (see STAR methods for details).

To test for a potential function of Dp7 neurons in noxious light avoidance, we genetically hyperpolarized them by expressing the inward rectifying potassium channel Kir2.1 (*Dp7-LexA*[30]). In contrast to controls, silencing of Dp7 neurons strongly impaired larval light avoidance (Fig. 1D, S1C,D). We next tested whether Dp7 neurons are functionally activated in response to noxious light by expressing the calcium sensor GCaMP7s[41]. To prevent crosstalk of the stimulus with excitation/emission of the sensor, we used a narrow 365 nm light pulse (10 s, 60 $\mu W/mm^2$). We found that UV-light exposure gave rise to robust calcium responses in the soma of Dp7 neurons in live larvae (Fig. 1E, Video S2), strongly suggesting that Dp7 neurons are part of an innate noxious light sensing circuit.

We next asked whether Dp7 neuron-derived neuropeptides are involved in noxious light avoidance. Dp7 neurons express multiple neuropeptides including sNPF and Insulin-like peptide 7 (Ilp7), of which sNPF, but not Ilp7, is required for mechanonociception[30,42]. Interestingly, we found that light avoidance was impaired in $Ilp7^{ko}$, but not *sNPF* mutant animals (Fig. 1F). Temporal analysis showed that larvae eventually distributed almost evenly across the arena suggesting they are not able to maintain dark preference (Fig. S1A,B). We analyzed light-dependent changes in larval locomotion in the dark or during exposure to noxious blue light. Control larvae displayed mildly elevated locomotion speed in blue light conditions with a concomitant reduction in turning rates, presumably to escape the uniform noxious stimulus (Fig. S1E,F). In contrast, $Ilp7^{ko}$ animals displayed comparable speed, but lower turning rates in

darkness, while slowing down and increasing turning under noxious light conditions. This suggests that in the absence of Ilp7, noxious light is still inducing locomotion changes, but responses are virtually inverted compared to controls. *Drosophila* larvae maintain light avoidance throughout development and preferentially pupariate in the dark[36]. *Ilp7^{ko}* animals formed pupae slightly earlier than controls (median *Ilp7^{ko}*: 119 h AEL, *w^{1118}*: 112 h AEL), but displayed reduced preference for pupariation in the dark (Fig. S1G,H), suggesting that Ilp7 is required for light avoidance throughout development. Lastly, we rescued Ilp7 expression in *Ilp7^{ko}* animals using a Dp7-neuron-specific line, which completely restored light avoidance (*Dp7-Gal4>UAS-Ilp7*, Fig. 1G, Fig. S1I). Taken together, these data show that Dp7 neuron function and Ilp7 are required and that Dp7 neuron-derived Ilp7 is sufficient for noxious light avoidance.

Dp7 neurons integrate noxious light input from multiple somatosensory subcircuits

To gain more insight into the larval noxious light circuit, we first identified the partially reconstructed Dp7 neurons from the electron microscopy (EM) brain volume of the first instar larva[14,24]. To confirm dendritic and axonal compartments of Dp7 neurons, we expressed a dendritic marker (DenMark[43]) that labeled its medial and lateral arbors within the ventral nerve cord (VNC), but not the ascending arbor projecting to the brain lobes (Fig. S2A). We then reconstructed Dp7 neurons and traced all of their synaptic partners (Fig. 1H, S2B-F). Dp7 neurons receive most synaptic input in the VNC and provide output mostly in the subesophageal zone (SEZ) and brain lobe region along its dorsally projecting axon (Fig. 1H, S2C-F). Dp7 neurons receive input from several subtypes of sensory neurons in the VNC (Fig. 1H, Fig.S2E) suggesting they are a somatosensory hub. We confirmed connectivity of Dp7 neurons with somatosensory neurons (C2da, C3da, C4da) as well as with C4da neuron-connected A08n neurons[30] at the EM level (Fig. S2E). Moreover, we identified a subset of tracheal dendrite (named v`td2[44]) neurons as the sensory class with the highest Dp7 neuron connectivity (Fig. S2D,E). In contrast, the anatomically similar subset of v'td1 neurons was only weakly connected to Dp7 neurons at the connectome level (Fig. S2D,E, see also Fig. 2A). Overall, four sensory circuits were found to converge on Dp7 neurons (Fig. 2A,B): direct monosynaptic connections from C4da and v`td2 to Dp7 neurons and two 2-hop polysynaptic pathways. We identified a strong link via A08n neurons previously shown to receive numerous synaptic inputs from C4da neurons[28,30,45]. Furthermore, the v`td2 to Dp7 neuron link was strongly interconnected via so far uncharacterized midline projection (MIP) neurons (Fig. 2A, S3A-D).

As C4da neurons respond to UV and blue light and are involved in light avoidance[36,37], we tested if A08n neurons as a major downstream output connected to Dp7 neurons play a role as well. Unlike silencing of C4da neurons or ablation of BO, A08n neuron silencing did not result in significantly decreased light avoidance (Fig. S3E,F). However, we detected robust calcium transients in A08n neurons in response to UV light (Fig. S3G). Therefore, A08n neurons might only play a minor role in larval light avoidance suggesting C4da neurons might contribute to noxious light avoidance via other pathways.

V`td2 neurons are the major presynaptic partner of Dp7 neurons and co-labeled with C4da neurons by a reporter line of the putative light sensor Gr28b[37,44] suggesting a role in noxious light sensing. We confirmed synaptic and functional connectivity between v'td2 and Dp7 neurons using a v'td2-specific Gal4 line (*73B01-Gal4*[44], named *v'td2-Gal4* hereafter). Synapse-specific GFP reconstitution across synaptic partners (SybGRASP[46]) showed that v'td2 form synaptic contacts with Dp7 neuron lateral dendritic arbors and along the proximal axonal segment (Fig.

S3H). Consistently, we also detected robust Dp7 neuron calcium responses upon optogenetic activation of v'td2 neurons with CsChrimson (Fig. S3I). We then tested if v'td2 neurons are required for larval light avoidance. Similarly to Dp7 neurons, Kir2.1-mediated silencing of v`td2 neurons significantly impaired light avoidance (Fig. 2C). We further carried out calcium imaging of v`td2 neurons in intact larvae, which showed that, similarly to C4da neurons, acute responses to UV light stimulation (Fig. 2D, Video S3). V`td1 sensory neurons, on the other hand, did not show calcium responses to UV stimulation (Fig. 2E, Video S3), in line with the low connectivity to the Dp7 network (Fig. 2A). We then tested if v'td2 neurons could mediate acute avoidance behavior in response to optogenetic activation. We expressed and activated CsChrimson using different lines labeling v'td2 neurons, which resulted mostly in stop and turn or backward locomotion responses (Fig. 2F, Video S4). At high, but not low activation intensities, one of the three utilized v'td2 lines also induced significant rolling responses, likely due to strong expression of CsChrimson. While we cannot rule out that v'td2 neuron activation can result in nociceptive rolling, Kir2.1-mediated silencing with the same driver line did not affect mechanonociceptive behavior including rolling escape responses (Fig. 2G). Thus, in contrast to C4da or A08n neurons, which are required for nociceptive rolling responses towards noxious touch[30], v'td2 neuron activation induces acute avoidance behavior and is required for noxious light avoidance but not mechanonociception. Together with our connectome analysis these findings show that at least two sensory subcircuits, C4da-A08n and v'td2 neurons, converge on Dp7 neurons and are involved in somatosensory UV light sensing, with v'td2 but not A08n neurons strongly contributing to noxious light avoidance behavior.

Compartmental organization of Dp7 hub neurons

To identify members of the noxious light avoidance circuit downstream of Dp7 neurons, we analyzed the reconstructed synaptic wiring diagram. We identified abdominal Leucokinin (ABLK) neurons, which receive direct input from Dp7, plus strong 2-hop synaptic connections from v`td2 via MIP neurons (Fig. 3A). We inspected the topographical relationship of the mapped neurons and found that v`td2, MIP, and ABLK neurons anatomically converge on the ventrolateral dendritic arbor of Dp7 neurons (Fig. 3B), which extends along the ventrolateral neuropil (Fig. S4A). MIP and v`td2 neurons further extend mediodorsally along the axonal arbor of Dp7 neurons in the thoracic segments of the larval VNC and SEZ (Fig. S3C,D). However, 75-100% of synapses of v'td2 to MIP or Dp7 and MIP to ABLK neurons reside on the Dp7 ventrolateral dendrite (Fig. 3B,C). This suggests convergence of noxious light inputs and outputs within this Dp7 domain. In contrast, the mechanonociceptive circuit comprising C2da, C3da, C4da, and A08n neurons[30], of which C4da and A08n also process noxious light information, primarily provides synaptic inputs on the medioventral dendritic arbor of Dp7 neurons (Fig. 3D, S4A). Within the lateral region, Dp7 neurons receive extensive synaptic input from v`td2 neurons, which form concurrent (polyadic) synapses with MIP neurons. MIP neurons, in turn, innervate adjoining ABLK neuron processes also extending along the ventrolateral neuropil (Fig. 3E, S4B,C). This suggests that v'td2-MIP-ABLK neurons form a functional unit with the Dp7 ventrolateral arbor and that processing of mechanonociceptive and noxious light information might preferentially occur in distinct Dp7 arbor domains.

Interestingly, the synaptic contact region of v'td2-MIP-ABLK neurons on the lateral arbor of Dp7 neurons also coincides with Ilp7 neuropeptide localization (Fig. 3B, 4A), suggesting this could be a site of local peptide release. Analysis of Dp7 neurons in the EM volume revealed in total five putative fusion events of large dense-core vesicles (LDCVs), one of them occurring

from Dp7 neurons to neighboring ABLK neurons (Fig. 3F, arrow, from region marked with asterisk in Fig. 3B). This indicated the possibility that Ilp7 is released from Dp7 neurons in direct vicinity of ABLK neurons.

Dp7 and Ilp7-dependent output to ABLK neurons in response to noxious light

Based on their converging input from the noxious light sensing circuit, we next asked whether ABLK neurons are relevant downstream outputs. We silenced Leucokinin (Lk)-expressing neurons (*Lk-Gal4*[47]) by expressing Kir2.1 and performed light avoidance assays, which resulted in a strongly decreased dark preference (Fig. 4B). As Lk is expressed in additional neurons in the SEZ (SELK) and brain lobes (ALK and LHLK), we genetically suppressed expression of Kir2.1 only in ABLK neurons (*tsh-Gal80*, see Fig. S4H). Silencing of the remaining Lk-positive neurons did not result in light avoidance defects suggesting a specific dependence on ABLK neuron function. We also tested Hugin-VNC neuron function in light avoidance, which are downstream partners of Dp7 neurons, but receive major sensory input from non-UV responsive v`td1 neurons (Fig. 3A). Consistent with our connectome and functional analysis, we did not detect any significant defects when silencing Hugin-VNC neurons with a specific Gal4 line[48] (Fig. 4B). Our results show that ABLK, but not Hugin-VNC neurons, are specifically involved in noxious light avoidance.

We analyzed potential light-dependent locomotion changes when silencing v'td2, Ilp7 or ABLK neurons. Average locomotion speed in the dark or during noxious blue light illumination was comparable to control (Fig. S4D), but overall turning rates of the animals, particularly during noxious light exposure, where reduced (Fig. S4E). This indicated impaired reorientation/turning behavior under noxious light conditions. However, loss of *Ilp7* or silencing of v'td2, Ilp7 or ABLK neurons did not impair chemotaxis towards ethyl butyrate (Fig. S4F,G) suggesting complex navigational behavior is not generally affected. We next attempted to dissect ABLK neuron-dependent acute behavior by optogenetic activation of different Lk-positive subsets (Fig. S4H,I). While we could selectively block expression in ABLK or brain lobe (ALK and LHLK) neurons using different genetic approaches, we could not suppress expression in SELK neurons. Optogenetic activation resulted in consistently strong rolling responses suggesting SELK neurons are likely involved in nociceptive rolling (Video S5).

We then assayed ABLK neuron responses to UV light using GCaMP6s and found prominent calcium transients upon stimulation (Fig. 4C, S5A, Video S2). In contrast, SELK neurons did not respond to UV light, strongly suggesting they are not involved in noxious light avoidance (Fig. S5B, Video S2). We further assessed the activation of ABLK neurons by different light intensities and wavelengths using the red-shifted calcium sensor jRCaMP1b[49]. We could detect strong and acute calcium transients in ABLK neurons at UV light intensities ranging from 20-60 $\mu W/mm^2$ (Fig. S5C). We then illuminated with different wavelengths in the range from 365 to 525 nm with the same intensity (60 $\mu W/mm^2$) revealing strong responses up to 470 nm, but not at 525 nm (Fig. S5D). These data show that ABLK neurons are responding only to light within the noxious UV and blue wavelength range and that they are a part of a noxious light sensing circuit.

We next examined if ABLK neuron responses to noxious light depend on Dp7 neuron function. To this end, we silenced Dp7 neurons using Kir2.1 expression and monitored ABLK neuron responses to UV light, which were absent under these conditions (Fig. 4C,D). To assay if

Dp7-derived Ilp7 was required for ABLK activation, we performed calcium imaging in *Ilp7*^{ko} animals and detected a 70% decrease in ABLK neuron responses after UV light stimulation (Fig 4E, F). In contrast, expression of Tetanus toxin light chain (TNT) in Dp7 neurons did not affect ABLK neuron responses to UV light (Fig. S5E) suggesting synaptic transmission from Dp7 to ABLK neurons does not play a major role in this context. However, we cannot exclude the involvement of other neuropeptides contributing to ABLK responses. To test for a contribution to ABLK neuron activation by other light sensing pathways including C4da neurons or BO, we blocked their function by TNT expression or genetic ablation (*GMR-hid*), respectively. In both cases, ABLK neuron responses to UV light were not significantly impaired (Fig. S5E). Similarly, optogenetic activation of Dp7, BO or C4da neurons using CsChrimson did not result in significant activation of ABLK neurons suggesting that neither Dp7 nor BO or C4da neurons are sufficient to activate ABLK neurons (Fig. S5F-H). Consistently, we did not find a connectomic link between the BO network with Dp7 or ABLK neurons, as well as no link between C4da and ABLK other than Dp7 neurons. Taken together, these data strongly suggest that Dp7 neurons exert Ilp7-dependent control of ABLK neuron activation by noxious light, which likely involves the v'td2-MIP-Dp7 circuit rather than C4da neurons or BO.

Acute Ilp7 release from Dp7 neurons in response to noxious light

We next investigated the peptidergic link between Dp7 and ABLK neurons in more detail by asking whether Ilp7 release from Dp7 neurons can be acutely induced by UV light stimulation. We generated an Ilp7 release reporter by fusing Ilp7 to GCaMP6s (NPRR^{Ilp7}), analogously to previously characterized neuropeptide reporters[50]. NPRR^{Ilp7} expressed in Dp7 neurons localized in a punctate pattern similar to the endogenous pattern of Ilp7, and colocalized completely with the LDCV-specific Synaptotagmin Sytα[51] (Fig. S6A,B). We next imaged NPRR^{Ilp7} responses to UV light in Dp7 neurons in live larvae. NPRR^{Ilp7} puncta in the proximal axon and ventrolateral dendrite region of Dp7 neurons displayed low baseline fluorescence consistent with low LDCV calcium levels, which increased rapidly upon UV-light illumination indicating peptide release (Fig. 5A,B, Video S6). Repeated UV-light stimulation resulted in consistent NPPR^{Ilp7} responses in LDCV puncta (Fig. 5C,D). This data is compatible with acute and rapid peptide release by partial LDCV fusion with the plasma membrane in the millisecond to second range, similarly to kiss and run-type peptide release upon electrical stimulation[50,52]. Imaging of NPPR^{Ilp7} in the Dp7 soma showed similar responses, also suggesting somatic release (Fig. S6C). In contrast, posterior Ilp7-positive neurons, which innervate the gut, did not show UV-light induced somatic NPPR^{Ilp7} responses (Fig. S6C). To further confirm that NPPR^{Ilp7} is indeed reporting LDCV fusion with the plasma membrane, we used RNAi to knock down calcium-dependent secretion activator (Cadps), a conserved protein required for LDCV release, but not biogenesis [53,54]. UV-light-induced NPPR^{Ilp7} responses in the Dp7 soma were strongly diminished upon Cadps-RNAi showing that the observed responses are LDCV release-dependent (Fig. 5E). Our data thus show that LDCVs containing Ilp7 are acutely released from Dp7 in response to UV light, thereby acting directly on neighboring ABLK neurons, reminiscent of small molecule neurotransmitter action.

Neuropeptidergic decoding of circuit responses and behavior for noxious light

As the noxious light and mechanonociceptive circuits overlap extensively at the sensory C4da and Dp7 neuron level, we asked whether Ilp7-dependent output of Dp7 to ABLK neurons is

specific for UV light. Kir2.1-mediated silencing of LK neurons, with or without the inclusion of ABLKs, did not significantly impair mechanonociceptive escape responses resulting in nocifensive rolling behavior (Fig. 6A). Instead, silencing all LK neurons mildly facilitated mechanonociceptive behavior, in line with a similar effect described for *Ilp7* deletion [30]. Moreover, in sharp contrast to UV light stimulation, we did not detect calcium responses in ABLK neurons after mechanonociceptive stimulation (Fig. 6B). Divergence of the mechanonociceptive and noxious light circuits thus occurs downstream of Dp7 neurons through Ilp7-mediated action on ABLK neurons.

While no cognate Ilp7 receptor has been identified so far, the Relaxin-family receptor Lgr4 has coevolved with Ilp7 across arthropod species, suggesting a receptor-ligand relationship [55,56]. A Gal4 reporter incorporated in the endogenous Lgr4 mRNA (*Lgr4^{T2AGal4}*) displayed expression in ABLK neurons suggesting the presence of Lgr4 (Fig. 6C). We further analyzed the localization of an ABLK-expressed HA-tagged-Lgr4, which localized along ABLK neuron projections close to endogenous Ilp7 puncta present on the ventrolateral branch of Dp7 neurons (Fig. 6D). In addition, we biochemically confirmed Ilp7 and Lgr4 interaction in S2 cells in co-immunoprecipitation assays showing that Ilp7 and Lgr4 are capable of binding *in vitro* (Fig. S6D). Binding was dependent on the presence of the extracellular Leucine-rich repeat (LRR) domain of Lgr4, but not a conserved residue (I263) required for interaction of the mammalian orthologues RXFP1 and Relaxin (Fig. S6E)..

To find out whether Lgr4 is physiologically relevant for noxious light avoidance, we tested *Lgr4^{T2AGal4}* larvae, which carry a T2A-Gal4 exon resulting in loss of *Lgr4* as confirmed by qPCR analysis (Fig. S6F). *Lgr4^{T2AGal4}* animals showed significantly reduced light avoidance, which could be fully rescued by overexpression of Lgr4 in its endogenous pattern (Fig. 6E). We then imaged calcium responses of ABLK neurons using a confirmed *Lgr4* knockout allele (*Lgr4^{ko}* [57]) showing reduced light avoidance as well (Fig. 6F,G, Fig. S6G,H). Similarly to *Ilp7^{ko}* animals, we detected a three-fold decrease in calcium transients, which was rescued upon expression of Lgr4 only in LK-positive neurons including ABLKs (Fig. 6F,G). Collectively, these results suggest that Lgr4 acts downstream of Ilp7 in ABLK neurons to promote their UV-light responses and light avoidance behavior.

Discussion

Noxious light processing in Drosophila larvae for sustained avoidance responses

All animals have to detect noxious stimuli and engage in appropriate escape actions to avoid injury or death. Consistent with previous reports[58,59], extended exposure to blue, but not green light, is noxious and lethal for developing *Drosophila* larvae. This suggests a strong need to efficiently detect and avoid short wavelength light. Extraocular UV/blue light sensors expressed in body wall neurons have been identified in several invertebrates including *C. elegans*[60] and *Drosophila*[37,61,62], and the underlying circuits seem to aid in the detection and avoidance of noxious light qualities and intensities. Previous work in *Drosophila* larva showed that besides BO, C4da neurons are involved in acute UV or blue light avoidance responses[37,63,64], likely via independent circuits. Here, we provide evidence that v'td2 neurons represent an additional set of larval body wall neurons sensing noxious light and inducing avoidance responses via peptidergic Dp7 neuron action and ABLK neuron activation. Of note, ABLK neurons have been proposed to gate binary escape decisions in response to optogenetic activation of C4da neurons using a blue light-activated channelrhodopsin[65]. Our connectomic, functional and behavioral data show that ABLK neurons are actually part of a UV- and blue-light-sensing circuit promoting acute and

sustained noxious light avoidance behavior. While ABLK neurons have known additional functions in stress response pathways[66,67] and blue light-induced rearing behavior[68], the lack of major connectivity and functional activation of ABLK by C4da neurons as shown in our work will require further investigation of their role in computing binary escape decisions.

Why do *Drosophila* larvae need three seemingly independent sensory circuits (BO, C4da and v'td2) to sense and avoid noxious light? BO is located in the larval head region, while v'td2 and C4da neurons reside in abdominal segments (A1-A7) or tile the entire body wall[38,44,69], respectively. For acute noxious light responses after exposure on the larval head region, BO and C4da neurons seem to be jointly required[37,63]. However, as shown for our v'td2-Dp7-ABLK circuit here and previously for BO[40] and C4da neurons[36], each of these sensory units is necessary for efficient light avoidance in choice assays. Under such chronic conditions, the combined action of these sensory systems covering different larval body regions might enable a sustained behavioral mode for continuous avoidance of extended periods of noxious light exposure of any body part. Although we could not identify a connectomic or functional link between BO and the circuit described here, C4da neurons might still contribute to Dp7 neuron-dependent Ilp7 release based on their ability to promote Dp7 neuron activation in mechanonociception[30]. We cannot rule out additional outputs of v'td2 neurons besides ABLK neurons, which might reside within the MIP connectome. However, it is also possible that these light sensing circuits are connected via long-range peptidergic/hormonal regulation, as BO-dependent release of PTTH (prothoracicotropic hormone) has been suggested to control C4da neuron function in light avoidance behavior[36]. This indicates that global hormonal signals might additionally coordinate the action of these circuits.

Neuromodulatory hub-mediated sensory processing

The challenge of a nervous system is to generate the correct behavioral output, like specific escape responses, based on the received sensory input. Emerging connectomic data from *Drosophila* illustrates that sensory networks fan out extensively, adding numerous partners at each subsequent level [14,28,70]. As a result, the relevant output path of any given sensory input is often difficult to identify, indicating that physical connection is not a sufficient predictor for function [22,71]. This suggests specific circuit mechanisms for selective gating of action-specific network components. Along these lines, a hub- and spoke-like circuit has been identified in *C. elegans*, where the RMG neuron forms a hub that receives spoke-like input from several sensory neurons regulating aggregation behavior via neuromodulatory signaling [72,73]. Similarly, Somatostatin-positive neurons in the spinal cord receive converging input from different mechanosensory pathways [74] and play a pivotal role in mechanical pain processing. Such convergence of multiple sensory inputs allows integration and regulation of behavioral output, suggesting that neuropeptide-expressing neurons are local network hubs. In our work, Dp7 neurons act as a regulatory hub that gates the activation of specific network responses. This might be particularly important in sensory processing, where peptidergic action can increase the computational power by organizing circuit function to generate alternative behaviors [22,27,75]. In mice, alternative escape behaviors are regulated by competitive and mutually inhibitory circuits of corticotropin-releasing factor and somatostatin-positive neurons in the central amygdala, which mediate conditioned flight or passive freezing, respectively [10]. While direct involvement of these neuromodulators has not yet been shown, oxytocin release from presynaptic terminals of hypothalamic neurons in the central amygdala attenuates fear responses in mice [76,77], suggesting extensive neuromodulatory regulation of escape and related behaviors across species. Our work revealed that discrete escape pathways are controlled by Dp7 hub neurons through input-specific neuropeptide function. Rolling in response to noxious mechanical touch [6,78] requires feedback signaling from Dp7 neurons via sNPF, but not Ilp7 peptide [30]. In contrast, noxious light avoidance

behavior requires Dp7 neuron-derived Ilp7, but not sNPF, and acts via a feedforward mechanism. Circuit-specific neuropeptide action thus generates discrete escape behaviors in this system by creating divergent networks, despite the extensive overlap between mechanonociceptive and noxious light avoidance circuits (Fig. 6H). This may raise the question of why these circuits are converging on hub neurons in the first place. First, sensory integration can facilitate escape responses as vibration[14] or blue light[79] enhance nociceptive rolling in *Drosophila* larvae. Second, escape responses might have to be tuned depending on the overall environmental context as well as the state of the animal, for which peptidergic regulation is known to be a key factor[22].

Compartmentalized modality-specific circuits and neuromodulatory action

Specific compartmentalization of sensory inputs and outputs can increase the efficiency of network computation at hub neurons through combined local synaptic and neuropeptide domains. In *C. elegans*, peptide release from PVD neuron dendrites provides local proprioceptive feedback to motor neurons[80]. Discrete functional domains have also been described for *Drosophila* mushroom body Kenyon cells displaying compartmentalized activity, which encodes context-specific functions by local dopaminergic modulation [81–83]. Here, we show convergence of UV light-responsive inputs and outputs with Ilp7 release sites on the Dp7 lateral dendritic arbor, which likely form a computational unit of the noxious light avoidance circuit. Analogous compartmental organization is likely found in the somatosensory system of adult flies[84] and also in vertebrates displaying modality-specific laminar organization of sensory inputs and corresponding outputs [16,17,85]. This suggests that integrating neuropeptide-expressing neurons receiving sensory input linked to distinct modalities, like Dp7 neurons in *Drosophila* or Somatostatin-expressing neurons in the vertebrate spinal cord [74], play a pivotal role in processing sensory stimuli. Dendrites can act as independent computational units [86] as shown in the vertebrate retina [87]. Although we could identify physical compartmentalization of input and output domains, most of the physiological responses including peptide release seem to occur globally across the entire neuron. We currently lack the tools and resolution to investigate region specific differences in calcium levels or peptide release efficiency. Nonetheless, neuromodulatory signals can still aid local processing due to circuit-specific expression of cognate receptors, as shown here by noxious light-specific responses of Lgr4-expressing ABLK neurons. In line with this notion, neuropeptide overexpression studies in zebrafish have shown that sensory responsiveness can be regulated in a peptide and modality-specific manner[88] suggesting their signaling still acts on selective circuits to enhance respective innate behaviors. Thus compartmentalized circuits with broad yet functional unit-specific neuromodulatory action might be a widespread mechanism to generate context-specific behaviors.

Neuropeptide-mediated co-transmission selects network action and behavior

Co-transmission of small molecule neurotransmitters and neuropeptides has been described in vertebrates and invertebrates [20,22,27,89], yet acute signaling function of neuropeptides in sensory behavior are not well understood. In general, neuropeptide release has been described to occur upon neuronal activity [25,50,90–92], although their action is considered slow and broad[20,22] with the ability to regulate targets distant from release sites, e.g., opioid receptor signaling in stress-induced analgesia [93], and long lasting behavioral states including sleep, foraging and social behavior [72,94,95].

Here, we show that Ilp7 is acutely released from Dp7 neurons in response to noxious light and required for full ABLK neuron activation. Residual ABLK neuron calcium transients in the absence of Ilp7, likely due to small neurotransmitter activity in this network, are not sufficient for

noxious light avoidance behavior. This suggests that Ilp7 can act as a co-transmitter required for selective network activation and behavior. Ilp7 presumably acts via Lgr4 to enable noxious light avoidance responses and behavior. Lgr4 belongs to the conserved family of Relaxin receptors[55,96–100]. Recent work indicates a role for Relaxin-3 in escape behavior through inhibition of oxytocin-producing neurons in the hypothalamus, a brain region implicated in the modulation of escape responses of vertebrates [76,101]. This suggests a conserved role of Relaxin signaling in escape responses.

Overall, our data suggest that neuropeptidergic signals can act acutely on the physical neuronal network to promote selective network activity and specific innate behaviors. Based on the widespread expression of neuropeptides and cognate GPCRs, including in escape circuits [20–23,102], further studies will have to determine if local neuromodulatory hubs with compartmentalized circuits as described here might be a general motif for computation of modality-specific sensory responses.

Acknowledgments

We would like to thank M. Petersen and A.R.M. Dias for excellent technical assistance. C. Wegener, T. Oertner, F. Morellini, J. Parrish and Q. Yuan for comments on the manuscript, B. Ye, B. Hofbauer and C. Wegener for communicating results prior to publication, P. Herrero, C. Wegener, M. Wernet and D. Anderson for fly stocks, T. Kazimier for advice and trouble-shooting with Catmaid, L. Herren for supervising Dp7 connectome reconstruction. P.S., B.N.I., and A.C. thank the Visiting Scientist program at HHMI Janelia, and HHMI Janelia for funding. Stocks obtained from the Bloomington Drosophila Stock Center (NIH P40OD018537) and Vienna Drosophila Resource Center (VDRC, www.vdrc.at) were used in this study. cDNA and cells obtained from the Drosophila Genomics Resource Center (NIH grant 2P40OD010949) were used in this study. This work was supported by the Deutsche Forschungsgemeinschaft (DFG, SO1337/4-1, SO1337/2-1/2-2, SO1337/ 7-1, to P.So., WI4485/2-2, WI4485/3-2, to J.S.W.), the DFG Heisenberg program (SO1337/6-1, to P.So.), an Alexander von Humboldt Research Fellowship (to A.F.) and EMBO Short-Term Fellowship (to E.M.V.), the European Commission FP7 (PCIG13-GA-2013-618847 to A.M.G.), the European Research Council Horizon2020 (ERC2016-StG-714762 to J.S.W.), the FCT (IF/00022/2012; Congento LISBOA-01-0145-FEDER-022170, co-financed by FCT/Lisboa2020; UID/Multi/04462/2019; PTDC/BEXBCM/1370/2014; PTDC/BIA-BID/31071/2017 to A.M.G.; PTDC/MED-NEU/30753/2017 to F.H. and A.M.G., SFRH/BPD/94112/2013 to A.M.), PD/BD/52421/2013 to F.H., and SFRH/BD/135263/2017 via PGCD – Programa Pós-Graduação Ciência Para o Desenvolvimento to E.M.V.).

Author contributions

B.N.I. performed and analyzed most experiments including connectome reconstruction and analysis, phototoxicity assays, light avoidance behavior and calcium imaging, morphological analysis and wrote the manuscript , A.W and F.Z. performed a subset of the light avoidance assays, F.Z. and A.F. performed locomotion and chemotaxis assays and analysis, A.F. wrote custom analysis scripts and code, C.H. performed and analyzed experiments in semi-intact larval preparations, F.M.T. performed and analyzed mechanonociceptive and optogenetic behavior assays, K.S. made reagents and performed co-immunoprecipitation experiments, E.M.V. performed and analyzed pupariation assays, E.M.V., A.P.C., A.M., F,H., and A.M.G. developed Lgr4 transgenes, and performed qPCR assays, P.Sch. and M.P performed connectome reconstruction and analyses, C.H.Y. and I.M.A. developed critical reagents, J.S.W. contributed to and supervised behavioral analyses and custom code, A.C. performed and supervised connectome

reconstruction, P.So. made reagents, contributed to circuit and behavioral analysis, supervised the work and wrote the manuscript.

Declaration of interests

The authors declare that no competing interests exist.

Figure Legends

Fig. 1. Ilp7-releasing Dp7 neurons are required for light avoidance.

A. Schematic representation of escape behaviors in *Drosophila* larvae. Noxious touch requires C2da, C3da and C4da neurons for rolling escape, while noxious light sensed by C4da neurons elicits avoidance behavior. **B.** For mechanonociception, Dp7 neuron-derived sNPF, but not Ilp7, enables mechanonociceptive rolling through feedback action on C4da neurons to facilitate output to A08n[30]. **C.** Developmental lethality due to exposure to blue light (470nm) but not green light (525nm) of the same intensity (2.5 μW/mm2). Percentage of freshly hatched larvae placed on food plates at 25°C dying at stages as indicated in the legend (n=5 trials, 50 larvae each, ± s.d. $^{***}P< 0.0001$, X^2-test). **D.** Inactivation of Dp7 neurons using *LexAop-Kir2.1* under the control of *Dp7-LexA*, impairs larval light avoidance (n=10 trials, $^{**}P<0.01$, $^{***}P<0.001$, one-way-ANOVA with Tukey's *post-hoc* test). **E.** UV-A light induces calcium transients in Dp7 neurons (*Ilp7-Gal4>UAS-GCaMP7s*, 365 nm, 60 μW/mm^2, mean ± s.e.m. indicated by shaded area, n=4). **F.** *Ilp7^{ko}*, but not *sNPF*, mutant animals showed decreased light-avoidance responses (n=10 trials, $^{***}P<0.001$, n.s., non-significant, one-way-ANOVA with Tukey's *post-hoc* test). **G.** Dp7-neuron-specific UAS-Ilp7 expression (with *Dp7-Gal4*) in the *Ilp7^{ko}* background restores light avoidance (n=10 trials, $^{*}P<0.05$, $^{****}P< 0.0001$, n.s., non-significant, one-way-ANOVA with Tukey's *post-hoc* test, *ilp7^{ko}* dataset same as in Fig. 1e). **G.** EM-reconstructed Dp7 neurons and their highest connected synaptic partners. Upstream partners are shown in magenta, downstream partners in green.

Fig. 2. Dp7 integrates noxious light input from multiple somatosensory circuits.

A. Dp7 neuron presynaptic connectivity analysis showing the highest input from sensory v`td2 neurons. C4da to Dp7 neuron direct connectivity is weak, but additional indirect connections were found via A08n neurons. V'td2 neurons are additionally strongly connected to Dp7 neurons via MIP neurons, while v`td1 neurons display weak connectivity with Dp7 neurons and other circuit elements. Numbers in brackets indicate number of neurons of the respective subtype, numbers on arrows indicate synapses from each neuronal subset forming direct connections. **B.** Inputs onto Dp7 neurons originating from either C4da or v`td2 neurons create 2 direct and 2 indirect subcircuits. Percentages of overall synaptic input of the target cells are shown. **C.** Silencing of v`td2 neurons using *Kir2.1* impairs light avoidance (*v'td2-Gal4>UAS-Kir2.1*, n=10 trials, **P<0.01, ****P<0.0001, one-way-ANOVA with Tukey's *post-hoc* test). **D.** UV light-induced calcium transients in v`td2 neurons (*v'td2-Gal4>GCaMP6s*, mean ± s.e.m., n=8). **E.** Quantitative comparison of calcium responses (GCaMP6s) of v`td2 and v`td1 neurons to UV light using *R35B01-Gal4*, which labels both subtypes ($\Delta F_{max}/F_0$ boxplot, n=5, $^{**}P<0.01$, unpaired two-tailed *t*-test). **F.** Optogenetic activation of CsChrimson (635 nm, high: 8.13 μW/mm^2, low:1.33 μW/mm^2) using different previously characterized Gal4 driver lines expressing in v'td2 neurons[44]. Behavioral responses included avoidance (stop, backward, turn, hunch) and nocifensive behaviors (bending and rolling), as well as different combinations (n as indicated for

each genotype). Note that all lines showed high prevalence for stop and turn or backwards behavior depending on the activation level. **G.** Mechanonociceptive behavior (rolling and bending) is not affected by silencing of v'td2 neurons (*v'td2-Gal4>UAS-Kir2.1*, n= number of animals as indicated in graph, n.s.=non-significant, X^2-test).

Fig. 3. Domain-specific organization of the noxious light avoidance network.

A. Connectivity graph of Dp7 neurons shows overlapping, but distinct subcircuits. The major outputs of v`td2 neurons are Dp7 and MIP neurons, while v`td1 neurons strongly connect to ABLK and Hugin-VNC neurons. Numbers on arrows indicate synapses from each neuronal subset forming direct connections. **B.** Overview of reconstructed Dp7, v'td2, MIP, and ABLK neuron innervation. Enlarged axon and dendrite regions of Dp7 neurons show local v'td2-Dp7, v'td2-MIP, and MIP-ABLK synapses on the lateral dendrite and anterior axon of Dp7 neurons. **C**. Relative synapse numbers in Dp7 dendritic and axonal arbor regions are shown for each partner. **D**. Synaptic connectivity of mechanosensory (C2da, C3da, C4da) and A08n neurons with Dp7. Most synapses are located on Dp7 medial dendrites providing mechanonociceptive input (indicated by shaded blue area). Except for C4da and A08n synapses, noxious light inputs (as shown in Fig. 3b) are mainly found on Dp7 lateral dendrites (indicated by shaded magenta area). **E**. v'td2 forms polyadic synapses with MIP and Dp7 neurons. Scale bar =200nm. **F.** Putative peptide release by docked LDCV (indicated by arrow) from Dp7 (blue) to adjacent ABLK neurons (green) in consecutive EM sections (region indicated by asterisk in Fig. 3b), additional LDCVs indicated by arrowheads. Scale bar =200nm.

Fig. 4. **Dp7 neuron activity and Ilp7 peptide is required for noxious light information flow to ABLK neurons.**

A. Confocal image stack (maximum projection) showing anatomical overlap of ABLK (*LK-Gal4>UAS-CD4-tdGFP*) and Ilp7 neuropeptide puncta (cyan) along the lateral dendritic region of Dp7 neurons (*Ilp7-LexA>LexAop-CD4-td-Tomato)*. Scale bar=50. **B.** Silencing of LK neurons (*Lk-Gal4>UAS-Kir2.1*), but not when precluding ABLK expression (*tsh-Gal80, Lk-Gal4>UAS-Kir2.1)*, abolishes light avoidance. Silencing Hugin-VNC neurons (Hug^{VNC}*-Gal4>UAS-Kir2.1)* does not affect light avoidance (n=10 trials/genotype, ****P<0.0001, **P<0.01, n.s., non-significant, one-way ANOVA with Tukey's *post-hoc* test). **C.** ABLK neuron calcium transients evoked by UV light with or without Dp7 neuron silencing (*Dp7-LexA, LexAop-Kir2.1*, mean ± s.e.m., n=7). **D.** Boxplot quantification (% $\Delta F_{max}/F_0$) showing ABLK neuron response to UV light *(Lk-Gal4>UAS-GCaMP6s*) with or without Ilp7 neuron silencing (*Ilp7-LexA>LexAopKir2.1*, n=7 larvae/genotype, $^{****}P<0.0001$ unpaired t test). **E**. ABLK neuron calcium transients evoked by UV light in control and $Ilp7^{ko}$ animals (mean ± s.e.m., n=7). **F.** % $\Delta F_{max}/F_0$ boxplots for Fig. 4E (n=7 larvae/genotype, unpaired *t*-test, $^{**}P<0.01$).

Fig. 5. Acute Ilp7 peptide release from Dp7 neurons in response to UV-light.

A. $NPRR^{Ilp7}$-labeled LDCVs (numbers 1-4, b: background) located along the Dp7 proximal axon. Time series (xt) along the dotted line showing acute evoked $NPRR^{Ilp7}$ fluorescence increase in response to a 10-s UV-light exposure (365 nm, 60 μW/mm^2). Scale bars=10 μm. **B.** Stacked individual traces of $NPRR^{Ilp7}$-labeled LDCVs (numbered 1-4, individual responses are stacked by 20% each for clarity) and background (b) shown in A. **C.** Repeated UV-light induced responses of individual $NPRR^{Ilp7}$ puncta located along the proximal axon or lateral dendrite of Dp7 neurons

(from 3 representative experiments). **D.** $\Delta F_{max}/F_0$ boxplot of Dp7 *NPRR*^{Ilp7} responses to UV light (n=18 LDCVs from 6 animals). **E.** Boxplot quantification (% $\Delta F_{max}/F_0$) of maximum NPRR^{Ilp7} fluorescence change in Dp7 somata upon UV light stimulation without or with Cadps-RNAi. Cadps knock-down significantly reduces NPRR^{Ilp7} responses (n=6 larvae/genotype, $^{***}P<0.001$, unpaired *t*-test).

Fig. 6. **Neuromodulatory decoding of nociceptive escape behaviors.**

A. Mechanonociceptive responses upon silencing of Lk neurons **(***Lk-Gal4 UAS-Kir2.1*), with or without ABLK silencing (*Lk-Gal4;tsh-Gal80,UAS-Kir2.1*, n=total number of larvae indicated in graphs, n.s.=not significant, *P<0.05, X^2 test,). **B.** Maximum ABLK neuron responses (% $\Delta F_{max}/F_0$) to noxious mechanical or UV light stimulations in semi-intact live larval preparations (n=8, unpaired t-test, $^{**}P<0.01$). **C.** Endogenous Lgr4 reporter expression (*Lgr4*^{T2AGal4}*,UAS-CD4-tdGFP*) in ABLK neurons detected by colocalized anti-Lk immunostaining. Overview and magnified lateral VNC region (boxed region) with ABLK neuron somata (GFP: green, Lk: magenta). Scale bars=50 μm, 10 μm for enlarged view. **D.** Lgr4-HA localization in ABLK neurons (*Lk-Gal4, UAS-Lgr4-HA*) with anti-Ilp7 immunostaining. Overview and magnified lateral VNC region (boxed region) showing ABLK neuron somata and dendrites with proximity of Lgr4 (green) and Ilp7 (magenta) puncta on the Dp7 neuron lateral arbor. Scale bars=50 μm, 10 μm. **E.** *Lgr4*^{T2AGal4} animals display reduced light avoidance, which was rescued by *UAS-Lgr4* expression (n=10,10,8 trials/genotype, $^{*}P<0.05$, $^{**}P<0.01$, one-way ANOVA with Tukey's *post-hoc* test). **F.** GCaMP6s-expressing ABLK neuron responses to UV light in control and *Lgr4*^{ko} animals, with and without UAS-Lgr4 expression (*Lk-Gal4>GCaMP6s*, n=5 animals/genotype, mean ± s.e.m.). **G.** Quantitative $\Delta F_{max}/F_0$ box plots of Fig. 6f (n=5, $^{**}P<0.01$, one-way ANOVA,with Tukey's *post-hoc* test). **H.** Model depicting neural and molecular elements shaping the larval somatosensory escape circuit with specific action of sNPF or Ilp7 on mechanonociception vs. noxious light resulting in rolling or avoidance, respectively.

STAR Methods

RESOURCE AVAILABILITY

Lead contact

Further information and requests for resources and reagents should be directed to and will be fulfilled by the Lead Contact, Peter Soba (psoba@uni-bonn.de).

Materials Availability

Lines generated and described in this study are available on request from the Lead Contact.

Data and Code Availability

All neurons reconstructed from volume EM were archived in the Virtual Fly Brain server, and are accessible via CATMAID software at this address:
https://l1em.catmaid.virtualflybrain.org/?pid=1
Microscopy and behavioural data reported in this paper is available from the lead contact upon request.
Code and scripts used to analyse larval distribution in two choice assays are available at this address:

https://github.com/formozov/larva_tracking_Imambocus_et_al
Any additional information required to reanalyse the data reported in this paper is available from the lead contact upon request.

Experimental Model and Subject Details

Drosophila melanogaster

Drosophila melanogaster were reared at 25°C and 70% humidity with a 12 light/dark cycle on standard fly food. Transgenic lines were maintained in either *white* mutant (w^-) or yellow-white (y^-, w^-) backgrounds. For analysis, 3rd instar foraging stage larvae of both sexes were used in this study (94h±2h AEL unless stated otherwise). No sex-specific effects were part of this study. For driver lines details see Key Resources Table. Driver lines were obtained from Bloomington Drosophila Stock Center or from Vienna Drosophila Stock Center unless stated otherwise. UAS-Chrimson effector was used to stimulate specific neurons. UAS-Kir2.1 or UAS-TNT was used to block specific neurons.

S2-DRSC cell line

S2-DRSC cells were cultured in Schneider's *Drosophila* medium supplemented with 10% fetal calf serum, glutamine and Penicilin/Streptomycin (ThermoFisher). Cells were passaged every 3-5 days and maintained in as semi-adherent cultures.

METHOD DETAILS

Generation of plasmids and transgenes

Dp7-Gal4 is a 2nd chromosome insertion and was generated analogously to *Dp7-LexA* [30] using a 1,099 bp fragment of the Ilp7 enhancer region at the 5′ end of the Ilp7 gene (starting from –1,131 to –33, where the ATG for Ilp7 starts at position 0). The genomic region was amplified by PCR and cloned into pCasper-AUG-GAL4. Transgenes were generated using P-element-mediated transformation. The UAS-Ilp7 transgene was generated by cloning Ilp7 cDNA via EcoRI into the pUAST vector and P-element mediated transformation. A UAS-Ilp7 insertion on the 3rd chromosome was used in this study. The Ilp7 neuropeptide release reporter ($NPRR^{Ilp7}$) was designed analogously to Ding et al.[50], by fusing GCaMP6s to the C-terminus of the Ilp7 neuropeptide. Ilp7 cDNA was obtained from the Drosophila Genetics Resource Center (DGRC) and amplified from clone FI18537 by PCR with specific primers carrying NotI and NdeI restriction sites, and fused in frame with GCaMP6s (Addgene) via NdeI/XbaI into the pUAST-AttB vector. Transgenes were made by phiC31-mediated genomic integration[103] into the AttP2 landing site (BestGene Inc., Chino Hills, CA, USA). HA-tagged Ilp7 was generated by inserting the HA sequence after the signal peptide sequence at position 34 of the Ilp7 cDNA using overlap-PCR. Primers containing the HA-tag sequence were used for amplification and cloning into the pUAST-AttB vector via NotI/XhoI.

Lgr4 cDNA was amplified from DGRC clone UFO07708 (BDGP Tagged ORF collection) by PCR using specific primers and inserted into a pUAST-AttB vector containing a C-terminal 3xflag-6xHis-tag via NotI/XhoI. The $Lgr4^{I263A}$ mutation was introduced using overlap-PCR with specific primers for the codon change and cloned via internal EcoRI/StuI sites into the original Lgr4 cDNA. To remove the Leucine-rich repeats (LRRs), Lgr4 cDNA was synthesized lacking amino acids 81-426 ($Lgr4^{\Delta 81\text{-}426}$, GeneArt, ThermoFisher) and subcloned into pUAST-AttB vector containing a C-terminal 3xflag-6xHis-tag via NotI/XhoI. All constructs were verified by sequencing.

Transgenic flies carrying UAS-Lgr4-HA (pUAST-Lgr4-CFLAGHA-BD-PHI, consisting of full length Lgr4 cDNA dually-tagged with a Flag-HA C-terminal fusion (UFO07708, BDGP Tagged ORF collection) where made using phiC31-mediated genomic integration by injection

into *y[1] M{vas-int.Dm}ZH-2A w*; M{3xP3-RFP.attP'}ZH-51C* (BestGene Inc., Chino Hills, CA, USA).

Neuronal reconstruction and circuit mapping

Neuronal reconstruction was performed on ssTEM images of the first instar larvae using the web-based software CATMAID[104]. Dp7 neurons and its partners were manually reconstructed similarly as described[14,29] and the location of pre- and post-synapses were identified. Synapses were annotated using the following 4 criteria: (1) the presence of a highly visible T-bar, (2) the presence of numerous synaptic vesicles close to the T-bars, (3) contact of pre- and post-synaptic membranes in at least 2 consecutive sections (4) the presence of a synaptic cleft. We then reconstructed the pre and postsynaptic partners of Dp7 from the synaptic sites and identified the v`td2 sensory neurons. Neuronal reconstruction validation was done as previously described[14,29] by using the iterative method**.** Pre- and post-synaptic illustrations between 2 neurons were extracted from CATMAID's 3D-visualization tools.

Immunohistochemistry and confocal imaging

Larval brains were dissected in PBS, fixed in 4% formaldehyde with PBS for 15 mins at room temperature, washed in PBST (PBS with 0.3% Triton X-100 (Roth Karlsruhe, Germany), incubated with primary antibodies at room temperature overnight, washed in PBST, incubated in secondary antibody for 1 hour) and mounted either on poly-L-lysine (Sigma) coated coverslips or on Superfrost slides in Slow Fade Gold (Thermo Fisher, Carlsbad, CA,USA). For anatomical inspection of Dp7 neurons, native fluorescence was sufficiently bright to be visualized by confocal microscopy (Zeiss LSM700). Confocal Z-Stacks were processed in Fiji (ImageJ, NIH, Bethesda).

Labeling of synapses using Syb-GRASP[46] was performed as described[105]. Larval brains were dissected in 5 mM dissection buffer (108 mM NaCl, 5 mM KCl, 4 mM NaHCO3, 1 mM NaH_2PO_4, 5 mM Trehalose, 10mM Sucrose, 5 mM HEPES, 8.2 mM MgCl2, 2 mM $CaCl_2$, pH 7.4), washed 3 times/5 seconds alternating between dissection buffer containing 5 mM KCl and 70 mM KCl, respectively, followed by 10 minutes incubation in 5 mM dissection buffer. The brains were then fixed in 4% formaldehyde/PBS for 15 minutes, followed by immunohistochemistry and mounting as described above. Confocal Z-Stacks were obtained using confocal microscopy and processed in Fiji (ImageJ, NIH, Bethesda).

Developmental toxicity assay

Wild type flies (*w[1118]*) were staged for 4 to 6 hours. After 1 day, 50 freshly hatched L1 larvae were transferred to a grape agar petri dish supplemented with yeast paste. Yeast paste was replaced daily to prevent decay. The larvae were then incubated either under green light ($2.5\mu W/mm^2$) or blue light ($2.5\mu W/mm^2$) for at least 9 days at 25°C in a custom humidified incubator (described in [106]). The temperature of the substrate or larvae was measured after 1h, 6h and 16h of blue or green light incubation and remained within the nominal temperature of the incubator (25.15±1.75 °C). After 9 days, the number of eclosed flies and the numbers of dead animals (pharate adults, white pupae, 2nd and 3rd instar larvae, 1st instar or lost upon transfer) were counted. The assay was repeated 5 times for each condition.

Light avoidance assays

After pre-staging, embryos were staged on grape agar plates supplemented with fresh yeast paste within a fixed time frame (Zeitgeber (ZT) 4-6) for 1-3 h depending on the number of fertilized eggs to minimize the risk of overcrowding.

Third instar foraging larvae (94 h ± 1.5h AEL) were subjected to a 15 min light avoidance assay as described[36,40] with modifications. Briefly, the experimental setup consisted of a dark

chamber with a white light source (365-580 nm, intensity 6.9-3.3 μW/mm^2 on light side, respectively, <0.01 μW/mm^2 on dark side) illuminating one half of a 10cm agar plate (12 ml of 2% agar dissolved in ddH_2O (Roth, Karlsruhe, Germany)). An infrared LED source surrounding the plates allowed live recording of larval distribution in darkness with a digital camera (Basler ace-2040gm, Basler, Switzerland).

For each trial, 20 larvae were preincubated in darkness for 15 min. The animals were placed in the middle of each petri dish at the light /dark junction. Each trial was run for at least 15 min, recorded by a camera at the top of the chamber using Ethovision, Pylon (Basler), or StreamPix 6 (Norpix). For each genotype, typically 10 trials consisting of 20 larvae each were performed unless noted otherwise.

Mechanonociception assays

Mechanonociceptive experiments were performed on staged 96h old 3rd instar larvae as described[30,107] using a calibrated 50 mN filament. Larvae were stimulated on mid-abdominal segments (A3–A5) twice within 2 s and the behavioral response to the 2nd stimulus was scored (no response, stop, or stop and turn as non-nocicpetive, bending and rolling as nociceptive). Each genotype was tested multiple times on different days.

Locomotion and chemotaxis assays

Larvae were staged on grape juice agar plates and fed with yeast paste. Third instar larvae (94 h ± 2 h after egg laying) were used for all experiments. For locomotion analysis under dark or blue light conditions, animals were carefully transferred to a 2% agar film on a FTIR (frustrated total internal reflection) based tracking system (FIM, University of Münster)[108] using a Basler ac2040-25gm camera (Basler, Ahrensburg, Germany). Five freely moving larvae per trial were recorded for 1 min in the dark, or for 1 min with 4.5 μW/mm^2 470 nm light illumination from a LED light source (RGB-BL-S-Q-1 R, Phlox, Aix-en-Provence, France). Locomotion was tracked with 10 frames per second.

For chemotaxis assays, 10 µl of 125mM Ethyl butyrate (Merck, Darmstadt, Germany) diluted in paraffin oil were placed in an odor container on one side of a 10 cm agar plate. Experiments were performed under minimum light conditions as for locomotion assays. Five freely moving larvae were video-captured for 5min.

Optogenetic behavioral assays

Staged third instar larvae (96 h ± 3 h AEL) were kept in darkness on grape agar plates with yeast paste containing 5 mM all-*trans*-retinal. Larvae were carefully transferred under low red light conditions to 2% agar plates with a 1 ml water film. CsChrimson was activated with 625 nm light (high: 8.13 μW/mm² or low: 1.13 μW/mm²) for 5 s. Videos were taken during the experiment and analyzed using the Fiji cell counter plugin (ImageJ, NIH, Bethesda). Rolling was defined as at least one complete 360° roll along the body axis. Bending was defined as a c-shape like twitching, typically seen before rolling behavior, and not to be confused with other described bending behavior[15]. Turning behavior describes head turning and thereby a direction changes of locomotion. Backwards behavior describes at least one wave of backwards crawling. Stop behavior describes a stop of locomotion. Hunch behavior describes a full body contraction. No behavior describes the absence of change in larval behavior. All staging, behavioral assays and analyses were performed in a blinded and randomized fashion.

Calcium imaging in intact larvae

Calcium responses were recorded from the soma of specific neurons labelled with *UAS-GCaMP(6s* or *7s)* under the control of specific neuronal Gal4-drivers. Live third instar larvae (94 ±2 h) were mounted in 90% glycerol and immobilized with a coverslip. The neuronal somata

were live imaged by confocal microscopy with a 40x/NA1.3 oil objective (Zeiss LSM700 or LSM900AS2). 400 frame times series were acquired at a frame rate of 0.24 s or 0.34 s (240 x 240 pixels) and the larva was subjected to UV light for 10 seconds (365nm, 60 μW/mm^2 CoolLED). Each larva was subjected to at least 2 pulses of UV light during the 400 frame time series with an interval of at least 15 s between pulses. For each genotype, 5-10 larvae were assayed between ZT 3 to 6. Calcium imaging was performed with identical confocal microscope settings imaging a single plane (approx. 2 μm). Only datasets without significant Z-drift (stable baseline, return to original baseline levels after stimulation) were retained for analysis.
Optogenetic activation of C4da, BO and Dp7 neurons and calcium imaging in ABLK neurons were also performed in intact 3rd instar larvae. Animals were reared in grape agar plates supplemented with all-trans retinal in the dark and imaging, with imaging in minimal light conditions. Larvae were mounted and imaged as described above. A red light pulse (635nm, intensity: 700 μW/mm^2) was given using an optical fiber coupled to CoolLED Pe4000 light source. For each genotype, 5 larvae were assayed with identical confocal settings.

To visualize NPPR^{Ilp7} release, we imaged either DP7 soma or the Dp7 lateral dendrite that features NPPR^{Ilp7} puncta as well as synaptic input and output of v`td2 and ABLK neurons, respectively. Time series with 500 frames were acquired at 0.24 s/frame (Zeiss LSM700).

Calcium imaging in semi-intact larvae

For comparison of noxious light versus mechanonociception, ABLK neuron calcium responses were assayed in semi-intact larval preparations essentially as described[30]. Staged 94 ±2 h old larvae were partially dissected on a Sylgard (Dow Corning) plate in physiological saline and ABLK neuron somata expressing GCaMP6m were imaged by confocal microscopy with a 40×/NA 1.0 water objective (Olympus FV1000MP). A micromanipulator-mounted *von Frey* filament (45 mN) was used to provide a mechanonociceptive stimulus to midabdominal segments (A3–A5). For noxious light stimulation, the larval preparation was subjected to UV light for 10 seconds (365 nm, 60 μW/mm^2 CoolLED).

Cell culture and co-immunoprecipitation assay

Biochemical interaction of Lgr4 and Ilp7 in S2 cells was assayed by transient co-transfection using a previously established protocol[109]. For S2 cell expression the following constructs were used: pUAST-AttB-Lgr4-3xflag-6xHis (wildtpype, I264A and ΔLRR variants), pUAST-AttB-Ilp7-HA, pActin-Gal4. Cells were seeded in 6 well plates and transfected at 50% density in an adherent state using Effectene (Qiagen, Venlo, Netherlands). Cells were harvested 48 h post-transfection and lysed in 500 μl lysis buffer (50 mM Tris pH7.4, 150 mM NaCl, 1% Triton X-100, protease inhibitor mix (Roche)) for 20 min on ice. After centrifugation (10 min/4˚C/10.000×g), the supernatant was incubated with mouse IgG-agarose (Sigma–Aldrich, St. Louis, MO) for 30 min at 4˚C, and subsequently with anti-flag M2 agarose beads (Sigma–Aldrich, St. Louis, MO) or anti-HA sepharose beads (Roche) for 4 hr at 4˚C. Samples were washed with lysis buffer three times, denatured and analyzed on Bis-Tris gels (ThermoFischer) and by Western blotting against Ilp7-HA (rat anti-HA, 1:5000, Roche) and Lgr4-3xflag (anti-flag M2, 1:10.000, Sigma).

qRT-PCR

The material used for each qRT–PCR sample (n=3 per genotype) was obtained from 5 synchronized L3 males 94-96 h after egg-laying for 2 h in apple plates. 48 h after the egg laying, 30 larvae were transferred from the apple plates into a vial with fly food to avoid competition. The genotypes used were *y[1] w[*] Mi{Trojan-GAL4.1}Lgr4[MI06794-TG4.1]* or *P{w[+mW.hs]=GawB}109C1, y[1] w[*]*, which served as a *yw* background control for the *Lgr4* TROJAN insertion. Male larvae were selected under the stereoscope and immediately put into dry

ice and either stored in -80 °C or processed for RNA extraction immediately. Each sample was macerated using pellet pestles, homogenized in 800 µl TriPure Isolation Reagent (Roche), and centrifuged at 12000 g for 1 min, to remove tissue debris. We added 0.5 volume of absolute ethanol (400 µl) to the supernatant and then followed manufacturer's instructions from the kit High Pure RNA Tissue Kit (Roche). An extra DNAse treatment (Turbo DNA-free kit, Ambion, Life Technologies) was performed to reduce gDNA contamination. 1 µg of RNA was used for the cDNA synthesis using the Maxima First Strand cDNA Synthesis Kit for RT–quantitative PCR (Thermo Scientific), following manufacturer's instructions but for a final volume of 10 µl.

qRT-PCR primers were designed and their specificity tested using Primer BLAST or Primer3. Primer efficiencies were determined to be between 90-100% using qPCR standard curves using serial dilutions (1x, 0,1X, and 0.01x) of gDNA extracted from the genome reference stock #2057 (BDSC) extracted using the High Pure PCR template preparation kit (Roche). The resulting melting curves did not present primer dimers in any concentration or in water.

Briefly, the experiments were performed in a Lightcycler 96 (Roche) using the FastStart Essential DNA Green Master dye and polymerase (Roche). The final volume for each reaction was 10 µl, consisting of 5 µl of dye and polymerase (master mix), 2 µl of 10 × diluted cDNA sample and 3 µl of the specific primer pairs (1 µM each).

Light avoidance pupariation assay

w^{1118} and $Ilp7^{ko}$ flies (3–6-days-old) were crossed and after 1–2 days transferred to laying pots with grape juice agar plates for 48 h. The next morning, the animals were allowed to lay eggs in fresh plates with yeast within a fixed time-frame (Zeitgeber (ZT) 4-6) for 1-2 h depending on the number of fertilized eggs to minimize the risk of overcrowding (the first plate was discarded). 3rd instar foraging larvae (94 h ± 1.5 h AEL) were then collected and placed in a tube containing standard medium. This tube was mounted in a T-shape glass device designed as described previously[36], where half of the horizontal glass tube is covered by black electrical tape. This allows larvae to wander and pupariate either in the dark or in the light side. Larvae were kept for 3 days under constant white light (2.9-4.5 $\mu W/mm^2$) at 25°C. The numbers of pupae in both dark and light sides were then counted. The Preference Index (PI) was calculated as: (number of puparia in dark- number of puparia in light)/total number of puparia.

Developmental time assay

w^{1118} and $Ilp7^{ko}$ flies (2-9 days old) were crossed and maintained at 25 °C in laying pots with grape juice agar plates for 48 h. Flies were then transferred to a fresh plate to lay eggs for 1–2 h. To control for overcrowding, 20-30 2nd instar larvae (48 h AEL) were transferred to vials containing normal Drosophila food at 25 °C. The number and timing of pupariation was assessed 3 times/day every 6-8 h until all larvae pupariated or died. Pupariation was defined as cessation of movement with evaginated spiracles and a darker color of the puparium.

QUANTIFICATION AND STATISTICAL ANALYSIS

Statistics

Sample sizes were chosen similar to previous publications and commonly used in the field[14,15,30,48,105]. For comparison of two groups, unpaired Student's *t*-test with Welch`s correction or nonparametric Mann-Whitney U test were used as appropriate. For analysis of mechanonociceptive behavior, the $\chi 2$ test was used. For multiple comparisons, one-way ANOVA with Tukey's *post-hoc* analysis was performed. All tests were two-tailed and differences were considered significant for $p < 0.05$ (*P < 0.05, **P < 0.01, ***P < 0.001, ****P < 0.0001). Statistical testing was performed using Prism (GraphPad).

Network graphs and analysis of synaptic counts

Network graphs were built by using the customised graph tools on CATMAID, where the interactions between a pair of nodes (neurons) was generated based on the absolute number of synaptic counts, using a synapse cutoff above 2^{14}. The network was build starting with the first processing layer (sensory neurons) consisting of 3 nodes, each representing a subset of sensory neurons (C4da, v`td1 and v`td2) connected to Dp7 neurons (second processing layer). Intermediate nodes from the sensory neurons to Dp7 were also extracted. The third processing layer consisted of output nodes of Dp7 neurons with a) VNC projections and b) being interconnected with sensory neurons (Hugin-VNC and ABLK). The thickness of the arrow between 2 nodes was determined automatically in CATMAID as a function of synaptic counts. Analysis of synaptic counts between different neurons connected on the lateral Dp7 domain was done using Graph Pad Prism (GraphPad, San Diego, CA, USA).

Developmental toxicity assay

Bar charts displaying percentages of animals were plotted with Excel. Statistical significance was calculated using the $\chi 2$ test (GraphPad, San Diego, CA, USA).

Light avoidance analysis

Preference index (PI) was calculated at 15 mins as: (number of larvae in dark-number of larvae in light)/total number of larvae. PI data are shown as violin plots, where the middle line shows the median. If more than 3 larvae escaped during the trial, it was discarded. Statistical analysis was performed using one-way ANOVA and Tukey`s *post-hoc* test (GraphPad, San Diego, CA, USA).

Analysis of temporal larval distribution was performed by keeping only every 200th frame, cropping and converting mp4 files to avi using a custom script (https://github.com/formozov/larva_tracking_Imambocus_et_al) and ffmpeg (https://www.ffmpeg.org). Reduced avi files were processed and analyzed in Fiji (ImageJ, NIH) using a custom macro script to create background-corrected masked images retaining intensity-based signals from larvae only. Total intensities on the dark and light side were measured over time and plotted as a preference index (PI = intensity in dark- intensity in light)/total intensity) analogously to larval distribution.

Mechanonociception analyses

Statistical significance was calculated using the $\chi 2$ test (GraphPad, San Diego, CA, USA).

Locomotion and chemotaxis analysis

For locomotion analysis, velocity and bending angles were analyzed using the FIMtrack software (https://github.com/kostasl/FIMTrack). For analysis, only animals displaying continuous locomotion and uninterrupted tracking were kept. Average locomotion speed and cumulative bending angles were analyzed and plotted for the first 30 s under dark or blue light conditions. Graphs of mean ± s.d. were plotted and analyzed using one-way ANOVA and Tukey`s post-hoc test (GraphPad, San Diego, CA, USA).

For chemotaxis, the locomotion tracks were generated using the FIMTrack software. All reconstructed tracks were considered in the analysis. The plate was virtually divided into four equidistant regions along X-axis. The first and the last regions were further restricted along the Y-axis (to take only a central band with a width equal to the radius of the plate) to set a "no-odor" and "odor" zone, respectively. The area surrounding the odor was defined as the "odor" zone, while the same area on the opposite side of the plate was defined as the "no-odor" zone. To quantify chemotaxis we used a performance index (PI), defined as $(t_{odor}-t_{noodor})/(t_{odor}+t_{noodor})$, where t_{odor} and t_{noodor} are total time that larvae spent in the odor and no-odor zones, respectively,

in the time window between 3 and 5 min of a given video recording. Graphs of mean ± s.d. were plotted and analyzed using one-way ANOVA and Tukey`s *post-hoc* test (GraphPad, San Diego, CA, USA).

Analysis of calcium imaging in intact larvae

Time series analysis was performed using image registration with the StackReg plugin (using translation function, Fiji, ImageJ) to correct for internal movement. GCaMP6 signal intensity was then quantified using a region of interest defining the neuronal soma and the Time Series Analyser V3 plugin (ImageJ). The calcium response ($\Delta F/F_0$ (%)) was calculated by subtracting the amplitude of pre-stimulation baseline (average of 19 frames) from the stimulation evoked amplitude. $\Delta F/F_0$ (%) = $(F-F_0)/F_0$ x100. Maximum fluorescence was calculated as F_{max}-F_0/F_0 x 100 ($F_{max,}$ maximum fluorescence observed during the stimulation; F_0 (average of 19 frames)). Graphs of mean ± s.e.m were plotted using Prism (GraphPad, San Diego, CA, USA). Comparison of maximum responses ($\Delta F_{max}/F_0$ (%)) were plotted and analyzed using one-way ANOVA and Tukey`s *post-hoc* test (GraphPad, San Diego, CA, USA).

Analysis for calcium imaging data upon optogenetic activation of C4da, BO and Dp7 neurons were performed as described above.

To analyse $NPPR^{Ilp7}$ release, the baseline signal was calculated from 19 frames before 40 frames of UV illumination, with 100 frames between stimulations. $NPPR^{Ilp7}$ release events were calculated for each puncta using the formula $\Delta F/F_0$ (%) = $(F-F_0)/F_0$ x100. The n number refers to individual LDCV puncta from 5 different larvae.

Analysis of calcium imaging in semi-intact larvae

Baseline (F_0) and the relative maximum intensity change (ΔF_{max}) of GCaMP6s fluorescence was analyzed. $\Delta F_{max}/F_0$ values of mechanonociceptive vs. noxious light ABLK neuron responses were plotted and compared, with the centerline representing median values, upper and lower whiskers representing S.E.M. Statistical significance was analyzed using a Mann- Whitney U-test. Somatic Dp7 calcium responses upon optogenetic activation of v`td2 neurons were also performed in semi-intact larval preparations as described above. Comparison of maximum responses ($\Delta F_{max}/F_0$ (%)) were plotted as box plots and analyzed with the Mann-Whitney test.

Video files

Video S1. Larval light avoidance assay

Processed light avoidance video for w^{1118} larvae. Circular arena with dark area (top) and light area (bottom). Video shows larval positions over 16 min (0.36 min/frame) with preferential distribution in the dark area.

Video S2. Dp7 and ABLK neuron UV light responses compared to no response in SELK neurons

Dp7 neuron calcium responses to a 10 s UV light stimulus (365 nm, 60 μW/mm^2) visualized by expression of GCaMP7s using *Ilp7-Gal4* **(left panel)**. ABLK neuron calcium responses to two separate 10 s and one short 2 s UV light stimulus (365 nm, 60 μW/mm^2) visualized by expression of GCaMP6s using *Lk-Gal4* (middle panel). No calcium response in SELK neuron to a 10 s UV light stimulus (365 nm, 60 μW/mm^2) visualized by expression of GCaMP6s using *Lk-Gal4* (right panel).

Video S3. UV light response in v'td2 and C4da, but not v'td1 neurons

V'td2 and C4da neuron calcium responses to a 10 s UV light stimulus (365 nm, 60 μW/mm^2) visualized by expression of GCaMP6s using *Gr28b.c-Gal4*, in comparison to v'td1 neurons (*35B01-Gal4>GCaMP6s*) under the same conditions.

Video S4. V'td2 neuron activation induces avoidance behavior

Optogenetic activation of v'td2 neurons using CsChrimson-Venus (5s, 635 nm, 8.13 μW/mm^2) expressed with different Gal4 driver lines: *Gr89a-Gal4*, *22C07-Gal4*, *73B01-Gal4* (high: 8.13 μW/mm^2, low: 1.13 μW/mm^2).

Video S5. Optogenetic activation of Lk neuron subsets

Optogenetic activation of different subsets of Lk neurons using CsChrimson-Venus (5s, 635 nm, 8.13 μW/mm^2): *Lk-Gal4* (left panel), *tsh-Gal80;Lk-Gal4* (middle panel), *otd-Flp, tub>Stop>Gal80; Lk-Gal4* (right panel).

Video S6. UV light-induced acute Ilp7 release from Dp7 neurons

Video of time series shown in Fig. 5A,B. $NPRR^{Ilp7}$-labeled LDCVs located along the Dp7 proximal axon showing acute evoked $NPRR^{Ilp7}$ fluorescence increase in response to a 10-s UV-light exposure (365 nm, 60 μW/mm^2, onset at 4s).

References

1. Branco, T., and Redgrave, P. (2020). The Neural Basis of Escape Behavior in Vertebrates. Annu. Rev. Neurosci. *43*, 417–439.
2. Im, S.H., and Galko, M.J. (2012). Pokes, sunburn, and hot sauce: Drosophila as an emerging model for the biology of nociception. Dev. Dyn. *241*, 16–26.
3. Hesselson, D., Walker, D.S., Massingham, J.N., Schafer, W.R., Neely, G.G., and Chew, Y.L. (2020). Invertebrate Models of Nociception. In The Oxford Handbook of the Neurobiology of Pain, J. N. Wood, ed. (Oxford University Press), pp. 60–100.
4. Basbaum, A.I., Bautista, D.M., Scherrer, G., and Julius, D. (2010). Cellular and molecular mechanisms of pain. Cell *139*, 267–284.
5. Chatzigeorgiou, M., Yoo, S., Watson, J.D., Lee, W.H., Spencer, W.C., Kindt, K.S., Hwang, S.W., Miller, D.M., Treinin, M., Driscoll, M., et al. (2010). Specific roles for DEG/ENaC and TRP channels in touch and thermosensation in C. elegans nociceptors. Nat. Neurosci. *13*, 861–868.
6. Tracey, W.D., Wilson, R.I., Laurent, G., and Benzer, S. (2003). painless, a Drosophila Gene Essential for Nociception. Cell *113*, 261–273.
7. Julius, D. (2013). TRP Channels and Pain. Annu. Rev. Cell Dev. Biol. *29*, 355–384.
8. Barik, A., Thompson, J.H., Seltzer, M., Ghitani, N., and Chesler, A.T. (2018). A Brainstem-Spinal Circuit Controlling Nocifensive Behavior. Neuron *100*, 1491-1503.e3.
9. Tovote, P., Esposito, M.S., Botta, P., Chaudun, F., Fadok, J.P., Markovic, M., Wolff, S.B.E., Ramakrishnan, C., Fenno, L., Deisseroth, K., et al. (2016). Midbrain circuits for defensive behaviour. Nature *534*, 206–212.
10. Fadok, J.P., Krabbe, S., Markovic, M., Courtin, J., Xu, C., Massi, L., Botta, P., Bylund, K., Müller, C., Kovacevic, A., et al. (2017). A competitive inhibitory circuit for selection of active and passive fear responses. Nature *542*, 96–99.
11. Dunn, T.W., Gebhardt, C., Naumann, E.A., Riegler, C., Ahrens, M.B., Engert, F., and Del Bene, F. (2016). Neural Circuits Underlying Visually Evoked Escapes in Larval Zebrafish. Neuron *89*, 613–628.
12. Kupfermann, I., Castellucci, V., Pinsker, H., and Kandel, E. (1970). Neuronal correlates of habituation and dishabituation of the gill-withdrawal reflex in Aplysia. Science (80-.). *167*, 1743–1745.
13. Bezares-Calderón, L.A., Berger, J., Jasek, S., Verasztó, C., Mendes, S., Gühmann, M., Almeda, R., Shahidi, R., and Jékely, G. (2018). Neural circuitry of a polycystin-mediated hydrodynamic startle response for predator avoidance. Elife *7*, 1–28.
14. Ohyama, T., Schneider-Mizell, C.M., Fetter, R.D., Aleman, J.V., Franconville, R., Rivera-Alba, M., Mensh, B.D., Branson, K.M., Simpson, J.H., Truman, J.W., et al. (2015). A multilevel multimodal circuit enhances action selection in Drosophila. Nature *520*, 633–639.
15. Jovanic, T., Schneider-Mizell, C.M., Shao, M., Masson, J.-B., Denisov, G., Fetter, R.D., Mensh, B.D., Truman, J.W., Cardona, A., and Zlatic, M. (2016). Competitive Disinhibition Mediates Behavioral Choice and Sequences in Drosophila. Cell *167*, 858-870.e19.
16. Abraira, V., and Ginty, D. (2013). The sensory neurons of touch. Neuron *79*, 618–639.
17. Koch, S.C., Acton, D., and Goulding, M. (2018). Spinal Circuits for Touch, Pain, and Itch. Annu. Rev. Physiol. *80*, 189–217.
18. Kaupp, U.B. (2010). Olfactory signalling in vertebrates and insects: Differences and commonalities. Nat. Rev. Neurosci. *11*, 188–200.
19. Haverkamp, A., Hansson, B.S., and Knaden, M. (2018). Combinatorial Codes and Labeled Lines: How Insects Use Olfactory Cues to Find and Judge Food, Mates, and Oviposition Sites in Complex Environments. Front. Physiol. *9*, 49.
20. van den Pol, A.N. (2012). Neuropeptide Transmission in Brain Circuits. Neuron *76*, 98–

115.
21. Taghert, P.H., and Nitabach, M.N. (2012). Peptide neuromodulation in invertebrate model systems. Neuron *76*, 82–97.
22. Bargmann, C.I., and Marder, E. (2013). From the connectome to brain function. Nat. Methods *10*, 483–490.
23. Jékely, G., Melzer, S., Beets, I., Kadow, I.C.G., Koene, J., Haddad, S., and Holden-Dye, L. (2018). The long and the short of it -A perspective on peptidergic regulation of circuits and behaviour. J. Exp. Biol. *221*.
24. Schlegel, P., Texada, M.J., Miroschnikow, A., Schoofs, A., Hï¿½ckesfeld, S., Peters, M., Schneider-Mizell, C.M., Lacin, H., Li, F., Fetter, R.D., et al. (2016). Synaptic transmission parallels neuromodulation in a central food-intake circuit. Elife *5*, 462–465.
25. Shakiryanova, D., Tully, A., Hewes, R.S., Deitcher, D.L., and Levitan, E.S. (2005). Activity-dependent liberation of synaptic neuropeptide vesicles. Nat. Neurosci. *8*, 173–178.
26. Nässel, D.R. (2009). Neuropeptide signaling near and far: How localized and timed is the action of neuropeptides in brain circuits? Invertebr. Neurosci. *9*, 57–75.
27. Nusbaum, M.P., Blitz, D.M., and Marder, E. (2017). Functional consequences of neuropeptide and small-molecule co-transmission. Nat. Rev. Neurosci. *18*, 389–403.
28. Gerhard, S., Andrade, I., Fetter, R.D., Cardona, A., and Schneider-Mizell, C.M. (2017). Conserved neural circuit structure across Drosophila larval development revealed by comparative connectomics. Elife *6*, 1–17.
29. Schneider-Mizell, C.M., Gerhard, S., Longair, M., Kazimiers, T., Li, F., Zwart, M.F., Champion, A., Midgley, F.M., Fetter, R.D., Saalfeld, S., et al. (2016). Quantitative neuroanatomy for connectomics in Drosophila. Elife *5*, 1133–1145.
30. Hu, C., Petersen, M., Hoyer, N., Spitzweck, B., Tenedini, F., Wang, D., Gruschka, A., Burchardt, L.S., Szpotowicz, E., Schweizer, M., et al. (2017). Sensory integration and neuromodulatory feedback facilitate Drosophila mechanonociceptive behavior. Nat. Neurosci. *20*, 1085–1095.
31. Burgos, A., Honjo, K., Ohyama, T., Qian, C.S., Shin, G.J., Gohl, D.M., Silies, M., Tracey, W.D., Zlatic, M., Cardona, A., et al. (2018). Nociceptive interneurons control modular motor pathways to promote escape behavior in Drosophila. Elife *7*, e26016.
32. Takagi, S., Cocanougher, B.T., Niki, S., Miyamoto, D., Kohsaka, H., Kazama, H., Fetter, R.D., Truman, J.W., Zlatic, M., Cardona, A., et al. (2017). Divergent Connectivity of Homologous Command-like Neurons Mediates Segment-Specific Touch Responses in Drosophila. Neuron *96*, 1373-1387.e6.
33. Niu, J., Ding, L., Li, J.J., Kim, H., Liu, J., Li, H., Moberly, A., Badea, T.C., Duncan, I.D., Son, Y.-J., et al. (2013). Modality-Based Organization of Ascending Somatosensory Axons in the Direct Dorsal Column Pathway. J. Neurosci. *33*, 17691–17709.
34. Osseward, P.J., and Pfaff, S.L. (2019). Cell type and circuit modules in the spinal cord. Curr. Opin. Neurobiol. *56*, 175–184.
35. Dubin, A.E., and Patapoutian, A. (2010). Nociceptors: The sensors of the pain pathway. J. Clin. Invest. *120*, 3760–3772.
36. Yamanaka, N., Romero, N.M., Martin, F.A., Rewitz, K.F., Sun, M.M., O'Connor, M.B., Léopold, P., Connor, M.B.O., Léopold, P., O'Connor, M.B., et al. (2013). Neuroendocrine Control of Drosophila Larval Light Preference. Science (80-.). *341*, 1113–1116.
37. Xiang, Y., Yuan, Q., Vogt, N., Looger, L.L., Jan, L.Y., and Jan, Y.N. (2010). Light-avoidance-mediating photoreceptors tile the Drosophila larval body wall. Nature *468*, 921–6.
38. Sprecher, S.G., Cardona, A., and Hartenstein, V. (2011). The Drosophila larval visual system: High-resolution analysis of a simple visual neuropil. Dev. Biol. *358*, 33–43.
39. Miguel-Aliaga, I., Thor, S., and Gould, A.P. (2008). Postmitotic specification of

Drosophila insulinergic neurons from pioneer neurons. PLoS Biol. *6*, e58.
40. Mazzoni, E.O., Desplan, C., and Blau, J. (2005). Circadian Pacemaker Neurons Transmit and Modulate Visual Information to Control a Rapid Behavioral Response. Neuron *45*, 293–300.
41. Dana, H., Sun, Y., Mohar, B., Hulse, B.K., Kerlin, A.M., Hasseman, J.P., Tsegaye, G., Tsang, A., Wong, A., Patel, R., et al. (2019). High-performance calcium sensors for imaging activity in neuronal populations and microcompartments. Nat. Methods *16*, 649–657.
42. Linneweber, G.A., Jacobson, J., Busch, K.E., Hudry, B., Christov, C.P., Dormann, D., Yuan, M., Otani, T., Knust, E., de Bono, M., et al. (2014). Neuronal Control of Metabolism through Nutrient-Dependent Modulation of Tracheal Branching. Cell *156*, 69–83.
43. Nicolai, L.J., Ramaekers, A., Raemaekers, T., Drozdzecki, A., Mauss, A.S., Yan, J., Landgraf, M., Annaert, W., Hassan, B.A., and Nicolaï, L.J.J. (2010). Genetically encoded dendritic marker sheds light on neuronal connectivity in Drosophila. Proc Natl Acad Sci U S A *107*, 20553–20558.
44. Qian, C.S., Kaplow, M., Lee, J.K., and Grueber, W.B. (2018). Diversity of internal sensory neuron axon projection patterns is controlled by the POU-domain protein Pdm3 in Drosophila larvae. J. Neurosci. *38*, 2125–17.
45. Kaneko, T., Macara, A.M., Li, R., Hu, Y., Iwasaki, K., Dunnings, Z., Firestone, E., Horvatic, S., Guntur, A., Shafer, O.T., et al. (2017). Serotonergic Modulation Enables Pathway-Specific Plasticity in a Developing Sensory Circuit in Drosophila. Neuron *95*, 623-638.e4.
46. Macpherson, L.J., Zaharieva, E.E., Kearney, P.J., Alpert, M.H., Lin, T.-Y., Turan, Z., Lee, C.-H., and Gallio, M. (2015). Dynamic labelling of neural connections in multiple colours by trans-synaptic fluorescence complementation. Nat. Commun. *6*, 10024.
47. de Haro, M., Al-Ramahi, I., Benito-Sipos, J., López-Arias, B., Dorado, B., Veenstra, J.A., and Herrero, P. (2010). Detailed analysis of leucokinin-expressing neurons and their candidate functions in the Drosophila nervous system. Cell Tissue Res. *339*, 321–336.
48. Schoofs, A., Hückesfeld, S., Schlegel, P., Miroschnikow, A., Peters, M., Zeymer, M., Spieß, R., Chiang, A.-S., and Pankratz, M.J. (2014). Selection of Motor Programs for Suppressing Food Intake and Inducing Locomotion in the Drosophila Brain. PLoS Biol. *12*, e1001893.
49. Dana, H., Mohar, B., Sun, Y., Narayan, S., Gordus, A., Jeremy, P., Tsegaye, G., Holt, G.T., Hu, A., Walpita, D., et al. (2016). Sensitive red protein calcium indicators for imaging neural activity. *2*, 1–24.
50. Ding, K., Han, Y., Seid, T.W., Buser, C., Karigo, T., Zhang, S., Dickman, D.K., and Anderson, D.J. (2019). Imaging neuropeptide release at synapses with a genetically engineered reporter. Elife *8*, 1–15.
51. Park, D., Li, P., Dani, A., and Taghert, P.H. (2014). Peptidergic Cell-Specific Synaptotagmins in Drosophila: Localization to Dense-Core Granules and Regulation by the bHLH Protein DIMMED. J. Neurosci. *34*, 13195–13207.
52. Wong, M.Y., Cavolo, S.L., and Levitan, E.S. (2015). Synaptic neuropeptide release by dynamin-dependent partial release from circulating vesicles. Mol. Biol. Cell *26*, 2466–74.
53. Farina, M., van de Bospoort, R., He, E., Persoon, C.M., van Weering, J.R.T., Broeke, J.H., Verhage, M., and Toonen, R.F. (2015). CAPS-1 promotes fusion competence of stationary dense-core vesicles in presynaptic terminals of mammalian neurons. Elife *4*, e05438.
54. Renden, R., Berwin, B., Davis, W., Ann, K., Chin, C.-T., Kreber, R., Ganetzky, B., Martin, T.F.J., and Broadie, K. (2001). Drosophila CAPS Is an Essential Gene that Regulates Dense-Core Vesicle Release and Synaptic Vesicle Fusion. Neuron *31*, 421–437.
55. Gontijo, A.M., and Garelli, A. (2018). The biology and evolution of the Dilp8-Lgr3

pathway: A relaxin-like pathway coupling tissue growth and developmental timing control. Mech. Dev. *154*, 44–50.
56. Veenstra, J.A., Rombauts, S., and Grbić, M. (2012). In silico cloning of genes encoding neuropeptides, neurohormones and their putative G-protein coupled receptors in a spider mite. Insect Biochem. Mol. Biol. *42*, 277–295.
57. Deng, B., Li, Q., Liu, X., Cao, Y., Li, B., Qian, Y., Xu, R., Mao, R., Zhou, E., Zhang, W., et al. (2019). Chemoconnectomics: Mapping Chemical Transmission in Drosophila. Neuron *101*, 876-893.e4.
58. Hori, M., Shibuya, K., Sato, M., and Saito, Y. (2014). Lethal effects of short-wavelength visible light on insects. Sci. Reports 2014 41 *4*, 1–6.
59. Shibuya, K., Onodera, S., and Hori, M. (2018). Toxic wavelength of blue light changes as insects grow. PLoS One *13*, e0199266.
60. Gong, J., Yuan, Y., Ward, A., Kang, L., Zhang, B., Wu, Z., Peng, J., Feng, Z., Liu, J., and Xu, X.Z.S. (2016). The C. elegans Taste Receptor Homolog LITE-1 Is a Photoreceptor. Cell *167*, 1252-1263.e10.
61. Guntur, A.R., Gu, P., Takle, K., Chen, J., Xiang, Y., and Yang, C.-H. (2015). *Drosophila* TRPA1 isoforms detect UV light via photochemical production of H_2O_2. Proc. Natl. Acad. Sci., 201514862.
62. Lazopulo, S., Lazopulo, A., Baker, J.D., and Syed, S. (2019). Daytime colour preference in Drosophila depends on the circadian clock and TRP channels. Nature *574*, 108–111.
63. Omamiuda-Ishikawa, N., Sakai, M., and Emoto, K. (2020). A pair of ascending neurons in the subesophageal zone mediates aversive sensory inputs-evoked backward locomotion in Drosophila larvae. PLoS Genet. *16*, 1–27.
64. Keene, A.C., Mazzoni, E.O., Zhen, J., Younger, M. a, Yamaguchi, S., Blau, J., Desplan, C., and Sprecher, S.G. (2011). Distinct Visual Pathways Mediate Drosophila Larval Light Avoidance and Circadian Clock Entrainment. J. Neurosci. *31*, 6527–6534.
65. Hu, Y., Wang, C., Yang, L., Pan, G., Liu, H., Yu, G., and Ye, B. (2020). A Neural Basis for Categorizing Sensory Stimuli to Enhance Decision Accuracy. Curr. Biol. *30*, 4896-4909.e6.
66. Zandawala, M., Marley, R., Davies, S.A., and Nässel, D.R. (2018). Characterization of a set of abdominal neuroendocrine cells that regulate stress physiology using colocalized diuretic peptides in Drosophila. Cell. Mol. Life Sci. *75*, 1099–1115.
67. Zandawala, M., Yurgel, M.E., Texada, M.J., Liao, S., Rewitz, K.F., Keene, A.C., and Nässel, D.R. (2018). Modulation of Drosophila post-feeding physiology and behavior by the neuropeptide leucokinin. PLOS Genet. *14*, e1007767.
68. Okusawa, S., Kohsaka, H., and Nose, A. (2014). Serotonin and downstream leucokinin neurons modulate larval turning behavior in Drosophila. J. Neurosci. *34*, 2544–58.
69. Grueber, W.B., Jan, L.Y., and Jan, Y.N. (2002). Tiling of the Drosophila epidermis by multidendritic sensory neurons. Development *129*, 2867–78.
70. Miroschnikow, A., Schlegel, P., Schoofs, A., Hueckesfeld, S., Li, F., Schneider-Mizell, C.M., Fetter, R.D., Truman, J.W., Cardona, A., and Pankratz, M.J. (2018). Convergence of monosynaptic and polysynaptic sensory paths onto common motor outputs in a Drosophila feeding connectome. Elife *7*, 1–23.
71. Swanson, L.W., and Lichtman, J.W. (2016). From Cajal to Connectome and Beyond. Annu. Rev. Neurosci. *39*, 197–216.
72. Chen, C., Itakura, E., Nelson, G.M., Sheng, M., Laurent, P., Fenk, L.A., Butcher, R.A., Hegde, R.S., and de Bono, M. (2017). IL-17 is a neuromodulator of Caenorhabditis elegans sensory responses. Nature *542*, 43–48.
73. Macosko, E.Z., Pokala, N., Feinberg, E.H., Chalasani, S.H., Butcher, R.A., Clardy, J., and Bargmann, C.I. (2009). A hub-and-spoke circuit drives pheromone attraction and social

behaviour in C. elegans. Nature *458*, 1171–1175.
74. Duan, B., Cheng, L., Bourane, S., Britz, O., Padilla, C., Garcia-Campmany, L., Krashes, M., Knowlton, W., Velasquez, T., Ren, X., et al. (2014). Identification of Spinal Circuits Transmitting and Gating Mechanical Pain. Cell *159*, 1417–1432.
75. Bentley, B., Branicky, R., Barnes, C.L., Chew, Y.L., Yemini, E., Bullmore, E.T., Vértes, P.E., and Schafer, W.R. (2016). The Multilayer Connectome of Caenorhabditis elegans. PLOS Comput. Biol. *12*, e1005283.
76. Knobloch, H.S., Charlet, A., Hoffmann, L.C., Eliava, M., Khrulev, S., Cetin, A.H., Osten, P., Schwarz, M.K., Seeburg, P.H., Stoop, R., et al. (2012). Evoked axonal oxytocin release in the central amygdala attenuates fear response. Neuron *73*, 553–566.
77. Viviani, D., Charlet, A., Van Den Burg, E., Robinet, C., Hurni, N., Abatis, M., Magara, F., and Stoop, R. (2011). Oxytocin selectively gates fear responses through distinct outputs from the central amygdala. Science (80-.). *333*, 104–107.
78. Hwang, R.Y., Zhong, L., Xu, Y., Johnson, T., Zhang, F., Deisseroth, K., and Tracey, W.D. (2007). Nociceptive neurons protect Drosophila larvae from parasitoid wasps. Curr Biol *17*, 2105–2116.
79. Wietek, J., Rodriguez-Rozada, S., Tutas, J., Tenedini, F., Grimm, C., Oertner, T.G., Soba, P., Hegemann, P., and Wiegert, J.S. (2017). Anion-conducting channelrhodopsins with tuned spectra and modified kinetics engineered for optogenetic manipulation of behavior. Sci. Rep. *7*, 14957.
80. Tao, L., Porto, D., Li, Z., Fechner, S., Lee, S.A., Goodman, M.B., Xu, X.Z.S., Lu, H., and Shen, K. (2019). Parallel Processing of Two Mechanosensory Modalities by a Single Neuron in C. elegans. Dev. Cell *51*, 617-631.e3.
81. Cohn, R., Morantte, I., and Ruta, V. (2015). Coordinated and Compartmentalized Neuromodulation Shapes Sensory Processing in Drosophila. Cell *163*, 1742–1755.
82. Boto, T., Louis, T., Jindachomthong, K., Jalink, K., and Tomchik, S.M. (2014). Dopaminergic Modulation of cAMP Drives Nonlinear Plasticity across the Drosophila Mushroom Body Lobes. Curr. Biol. *24*, 822–831.
83. Bilz, F., Geurten, B.R.H., Hancock, C.E., Widmann, A., and Fiala, A. (2020). Visualization of a Distributed Synaptic Memory Code in the Drosophila Brain. Neuron *106*, 963-976.e4.
84. Tsubouchi, A., Yano, T., Yokoyama, T.K., Murtin, C., Otsuna, H., and Ito, K. (2017). Topological and modality-specific representation of somatosensory information in the fly brain. Science (80-.). *358*, 615–623.
85. Choi, S., Hachisuka, J., Brett, M.A., Magee, A.R., Omori, Y., Iqbal, N., Zhang, D., DeLisle, M.M., Wolfson, R.L., Bai, L., et al. (2020). Parallel ascending spinal pathways for affective touch and pain. Nature *587*, 258–263.
86. Branco, T., and Häusser, M. (2010). The single dendritic branch as a fundamental functional unit in the nervous system. Curr. Opin. Neurobiol. *20*, 494–502.
87. Euler, T., Detwiler, P.B., and Denk, W. (2002). Directionally selective calcium signals in dendrites of starburst amacrine cells. Nature *418*, 845–852.
88. Woods, I.G., Schoppik, D., Shi, V.J., Zimmerman, S., Coleman, H.A., Greenwood, J., Soucy, E.R., and Schier, A.F. (2014). Neuropeptidergic signaling partitions arousal behaviors in zebrafish. J. Neurosci. *34*, 3142–3160.
89. Hökfelt, T., Barde, S., Xu, Z.-Q.D., Kuteeva, E., Rüegg, J., Le Maitre, E., Risling, M., Kehr, J., Ihnatko, R., Theodorsson, E., et al. (2018). Neuropeptide and Small Transmitter Coexistence: Fundamental Studies and Relevance to Mental Illness. Front. Neural Circuits *12*.
90. Persoon, C.M., Hoogstraaten, R.I., Nassal, J.P., van Weering, J.R.T., Kaeser, P.S., Toonen, R.F., and Verhage, M. (2019). The RAB3-RIM Pathway Is Essential for the Release of Neuromodulators. Neuron *104*, 1065-1080.e12.

91. Duggan, A.W., Morton, C.R., Zhao, Z.Q., and Hendry, I.A. (1987). Noxious heating of the skin releases immunoreactive substance P in the substantia gelatinosa of the cat: A study with antibody microprobes. Brain Res. *403*, 345–349.
92. Jan, L.Y., and Jan, Y.N. (1982). Peptidergic transmission in sympathetic ganglia of the frog. J. Physiol. *327*, 219–246.
93. Fields, H. (2004). State-dependent opioid control of pain. Nat. Rev. Neurosci. *5*, 565–575.
94. Nichols, A.L.A., Eichler, T., Latham, R., and Zimmer, M. (2017). A global brain state underlies C. elegans sleep behavior. Science (80-.). *356*, eaam6851.
95. Flavell, S.W., Pokala, N., Macosko, E.Z., Albrecht, D.R., Larsch, J., and Bargmann, C.I. (2013). Serotonin and the Neuropeptide PDF Initiate and Extend Opposing Behavioral States in C. elegans. Cell *154*, 1023–1035.
96. Garelli, A., Heredia, F., Casimiro, A.P., Macedo, A., Nunes, C., Garcez, M., Dias, A.R.M., Volonte, Y.A., Uhlmann, T., Caparros, E., et al. (2015). Dilp8 requires the neuronal relaxin receptor Lgr3 to couple growth to developmental timing. Nat. Commun. *6*, 8732.
97. Vallejo, D.M., Juarez-Carreño, S., Bolivar, J., Morante, J., and Dominguez, M. (2015). A brain circuit that synchronizes growth and maturation revealed through Dilp8 binding to Lgr3. Science (80-.). *350*, aac6767.
98. Bathgate, R.A.D., Halls, M.L., van der Westhuizen, E.T., Callander, G.E., Kocan, M., and Summers, R.J. (2013). Relaxin Family Peptides and Their Receptors. Physiol. Rev. *93*, 405–480.
99. Jaszczak, J.S., Wolpe, J.B., Bhandari, R., Jaszczak, R.G., and Halme, A. (2016). Growth coordination during Drosophila melanogaster imaginal disc regeneration is mediated by signaling through the relaxin receptor Lgr3 in the prothoracic gland. Genetics *204*, 703–709.
100. Colombani, J., Andersen, D.S., Boulan, L., Boone, E., Romero, N., Virolle, V., Texada, M., and Léopold, P. (2015). Drosophila Lgr3 Couples Organ Growth with Maturation and Ensures Developmental Stability. Curr. Biol. *25*, 2723–9.
101. Kania, A., Gugula, A., Grabowiecka, A., de Ávila, C., Blasiak, T., Rajfur, Z., Lewandowski, M.H., Hess, G., Timofeeva, E., Gundlach, A.L., et al. (2017). Inhibition of oxytocin and vasopressin neuron activity in rat hypothalamic paraventricular nucleus by relaxin-3-RXFP3 signalling. J. Physiol. *595*, 3425–3447.
102. Smith, S.J., Sümbül, U., Graybuck, L.T., Collman, F., Seshamani, S., Gala, R., Gliko, O., Elabbady, L., Miller, J.A., Bakken, T.E., et al. (2019). Single-cell transcriptomic evidence for dense intracortical neuropeptide networks. Elife *8*, 1–35.
103. Groth, A.C., Fish, M., Nusse, R., and Calos, M.P. (2004). Construction of transgenic Drosophila by using the site-specific integrase from phage phiC31. Genetics *166*, 1775–82.
104. Saalfeld, S., Cardona, A., Hartenstein, V., and Tomancak, P. (2009). CATMAID: collaborative annotation toolkit for massive amounts of image data. Bioinformatics *25*, 1984–1986.
105. Tenedini, F.M., Sáez González, M., Hu, C., Pedersen, L.H., Petruzzi, M.M., Spitzweck, B., Wang, D., Richter, M., Petersen, M., Szpotowicz, E., et al. (2019). Maintenance of cell type-specific connectivity and circuit function requires Tao kinase. Nat. Commun. *10*, 3506.
106. Ingles-Prieto, A., Furthmann, N., Crossman, S.H., Tichy, A.-M., Hoyer, N., Petersen, M., Zheden, V., Biebl, J., Reichhart, E., Gyoergy, A., et al. (2021). Optogenetic delivery of trophic signals in a genetic model of Parkinson's disease. PLOS Genet. *17*, e1009479.
107. Hoyer, N., Petersen, M., Tenedini, F., and Soba, P. (2018). Assaying Mechanonociceptive Behavior in Drosophila Larvae. BIO-PROTOCOL *8*, e2736.
108. Risse, B., Thomas, S., Otto, N., Löpmeier, T., Valkov, D., Jiang, X., and Klämbt, C. (2013). FIM, a novel FTIR-based imaging method for high throughput locomotion

analysis. PLoS One *8*, e53963.
109. Soba, P., Han, C., Zheng, Y., Perea, D., Miguel-Aliaga, I., Jan, L.Y., and Jan, Y.N. (2015). The Ret receptor regulates sensory neuron dendrite growth and integrin mediated adhesion. Elife *4*, e05491.
110. Yang, C.-H., Belawat, P., Hafen, E., Jan, L.Y., and Jan, Y.-N. (2008). Drosophila egg-laying site selection as a system to study simple decision-making processes. Science *319*, 1679–83.
111. Grönke, S., Clarke, D.-F., Broughton, S., Andrews, T.D., and Partridge, L. (2010). Molecular evolution and functional characterization of Drosophila insulin-like peptides. PLoS Genet. *6*, e1000857.
112. Karuppudurai, T., Lin, T.-Y., Ting, C.-Y., Pursley, R., Melnattur, K.V., Diao, F., White, B.H., Macpherson, L.J., Gallio, M., Pohida, T., et al. (2014). A Hard-Wired Glutamatergic Circuit Pools and Relays UV Signals to Mediate Spectral Preference in Drosophila. Neuron *81*, 603–615.
113. Baines, R.A., Uhler, J.P., Thompson, A., Sweeney, S.T., and Bate, M. (2001). Altered electrical properties in Drosophila neurons developing without synaptic transmission. J. Neurosci. Off. J. Soc. Neurosci. *21*, 1523–1531.
114. Watanabe, K., Chiu, H., Pfeiffer, B.D., Wong, A.M., Hoopfer, E.D., Rubin, G.M., and Anderson, D.J. (2017). A Circuit Node that Integrates Convergent Input from Neuromodulatory and Social Behavior-Promoting Neurons to Control Aggression in Drosophila. Neuron *95*, 1112-1128.e7.
115. Thevenaz, P., Ruttimann, U.E., and Unser, M. (1998). A pyramid approach to subpixel registration based on intensity. IEEE Trans. Image Process. *7*, 27–41.

KEY RESOURCES TABLE

REAGENT or RESOURCE	SOURCE	IDENTIFIER
Antibodies		
Rabbit anti-Ilp7	I. Miguel-Aliaga, MRC clinical Sciences Center, London, UK[39]	N/A
Rabbit anti-Leucokinin	Dr. Dick Nässel, Stockholm University, Sweden	N/A
Chicken polyclonal anti-GFP	Abcam	Abcam Cat# ab13970, RRID:AB_300798
Rat monoclonal anti-HA	Roche	Roche Cat# ROAHAHA, RRID:AB_2687407
Mouse monoclonal anti-Flag M2	Sigma-Aldrich	Sigma-Aldrich Cat# P2983, RRID:AB_439685
Alexa Fluor 488 Donkey anti-mouse	Jackson Immunoresearch	Jackson ImmunoResearch Labs Cat# 715-545-150, RRID: AB_2340846
Cy3 polyclonal Goat anti-Rabbit	Jackson Immunoresearch	Jackson ImmunoResearch Labs Cat# 111-165-003, RRID:AB_2338000
Cy5 polyclonal Donkey anti-Chicken	Jackson Immunoresearch	Jackson ImmunoResearch Labs Cat# 703-175-155, RRID:AB_2340365
Dylight 649 monoclonal mouse anti-Rabbit	Jackson immunoresearch	Jackson ImmunoResearch Labs Cat# 211-492-171; RRID:AB_2339164
Chemicals, peptides, and recombinant proteins		
All-trans Retinal	Sigma-Aldrich	Cat# R2500
Schneider's Drosophila medium	Thermo-Fisher	Cat# 21720024
Ethyl butyrate	Sigma-Aldrich	Cat# E15701
Critical commercial assays		
High Pure RNA Tissue Kit	Roche	Cat# 12033674001
Maxima First Strand cDNA Synthesis Kit for RT–quantitative PCR	Thermo Scientific	Cat# K1641
High Pure PCR template preparation kit	Roche	Cat# 11796828001
Experimental models: Cell lines		
D. melanogaster: Cell line S2: S2-DRSC	DGRC	RRID:CVCL_Z992
Experimental models: Organisms/strains		
D. melanogaster :		
w^{1118}	Bloomington Drosophila Stock Center	BDSC:3605

w[1118]; P{y[+t7.7] w[+mC]=GMR35B01-GAL4}attP2	Bloomington Drosophila Stock Center	BDSC: 49898
w[1118]; P{y[+t7.7] w[+mC]=GMR73B01-GAL4}attP2	Bloomington Drosophila Stock Center	BDSC: 39809
w[*]; wg[Sp-1]/CyO; P{w[+mC]=Gr28b.c-GAL4.6.5}3	Bloomington Drosophila Stock Center	BDSC: 57619
w[*]; P{w[+mC]=Gr89a-GAL4.2}11/CyO	Bloomington Drosophila Stock Center	BDSC: 57676
w[1118]; P{y[+t7.7] w[+mC]=GMR22C07-GAL4}attP2	Bloomington Drosophila Stock Center	BDSC: 48975
w[1118]; P{y[+t7.7] w[+mC]=20XUAS-IVS-GCaMP6s}attP40	Bloomington Drosophila Stock Center	BDSC: 42746
w1118; P{20XUAS-IVS-GCaMP6m}attP40	Bloomington Drosophila Stock Center	BDSC: 42748
w[1118]; P{y[+t7.7] w[+mC]=20XUAS-IVS-jGCaMP7s}VK00005	Bloomington Drosophila Stock Center	BDSC: 79032
w[1118]; P{y[+t7.7] w[+mC]=20XUAS-IVS-CsChrimson.mVenus}attP2	Bloomington Drosophila Stock Center	BDSC: 55136
w[1118]; PBac{y[+mDint2] w[+mC]=UAS-CD4-tdGFP}VK00033	Bloomington Drosophila Stock Center	BDSC: 35836
y[1] w[*] Mi{Trojan-GAL4.1}Lgr4[MI06794-TG4.1]	Bloomington Drosophila Stock Center	BDSC: 77775
w TI{TI}Lgr4attP (Lgr4^{ko})*	Bloomington Drosophila Stock Center	BDSC: 84478
w[1118]; PBac{y[+mDint2] w[+mC]=UAS-CD4-tdTom}VK00033	Bloomington Drosophila Stock Center	BDSC: 35837
w[1118]; PBac{y[+mDint2] w[+mC]=UAS-CD4-tdGFP}VK00033	Bloomington Drosophila Stock Center	BDSC: 35836
w[*]; P{w[+mC]=lexAop-nSyb-spGFP1-10}2, P{w[+mC]=UAS-CD4-spGFP11}2; MKRS/TM6B	Bloomington Drosophila Stock Center	BDSC: 64315
w[*]; P{w[+mC]=Gr89a-GAL4.2}11/CyO	Bloomington Drosophila Stock Center	BDSC: 57676
w[1118]; P{y[+t7.7] w[+mC]=GMR22C07-GAL4}attP2	Bloomington Drosophila Stock Center	BDSC: 48975
UAS-spGFP1-10-Syb	M. Gallio, Northwestern University, Evanston, USA	N/A
LexAop-CD4-sp11-CD4-tdTomato	[30]	N/A
A08n-Gal4 (82E12-Gal4AD, 6.14.3-Gal4DBD)	[30]	N/A
Dp7(4-3)-LexA	[30]	N/A

sNPF^{c00448}	30	N/A
sNPF^{MI01807}	30	N/A
Ilp7-LexA	110	N/A
Ilp7^{ko}	111	N/A
w[1118]; LexAop-Kir2.1	30	N/A
w[1118]; LexAop-TnT-HA	112	N/A
Hugin^{VNC} -Gal4	48	N/A
UAS-Kir2.1	113	N/A
Otd-Flp	114	N/A
Dp7(4-3)-Gal4	This paper	N/A
UAS-NPRR^{ilp7}	This paper	N/A
UAS-Ilp7	This paper	N/A
UAS-Lgr4-HA-flag	This paper	N/A
Lk-Gal4	47	N/A
UAS-Cadps-RNAi	Vienna Drosophila Stock Center	VDRC: KK110055
Oligonucleotides		
Primers:		
Table S2	This paper	N/A
Software and algorithms		
Collaborative annotation toolkit for massive amount of image data (CATMAID)	Janelia research campus, USA,[104]	RRID:SCR_006278
Ethovision XT-X2	Noldus Information Technology, Wageningen, Netherlands	RRID:SCR_000441
Pylon Camera Software Suite	Basler, Switzerland	N/A
StreamPix 6	Norpix, Montreal, Quebec, Canada	RRID:SCR_015773
Fiji/Image J	NIH, Bethesda	RRID:SCR_002285
Prism	Graphpad, San Diego, CA, USA	RRID:SCR_00279
StackReg, ImageJ plugin	EPFL, Lausanne, Switzerland [115]	N/A
Time Series analyzer V3, ImageJ plugin	UCLA, California, USA	RRID:SCR_014269
FimTrack	https://www.uni-muenster.de/Informatik.AGRisse/media/fim-media.html, [108]	N/A
Larval distribution analysis scripts	This paper, https://github.com/formozov/larva_tracking_Imambocus_et_al	N/A
Other		
CoolLED pE-4000	CoolLED Ltd., Andover, UK	N/A
RGB-LED plate	Phlox Inc., Provence, France	N/A

Figure 1

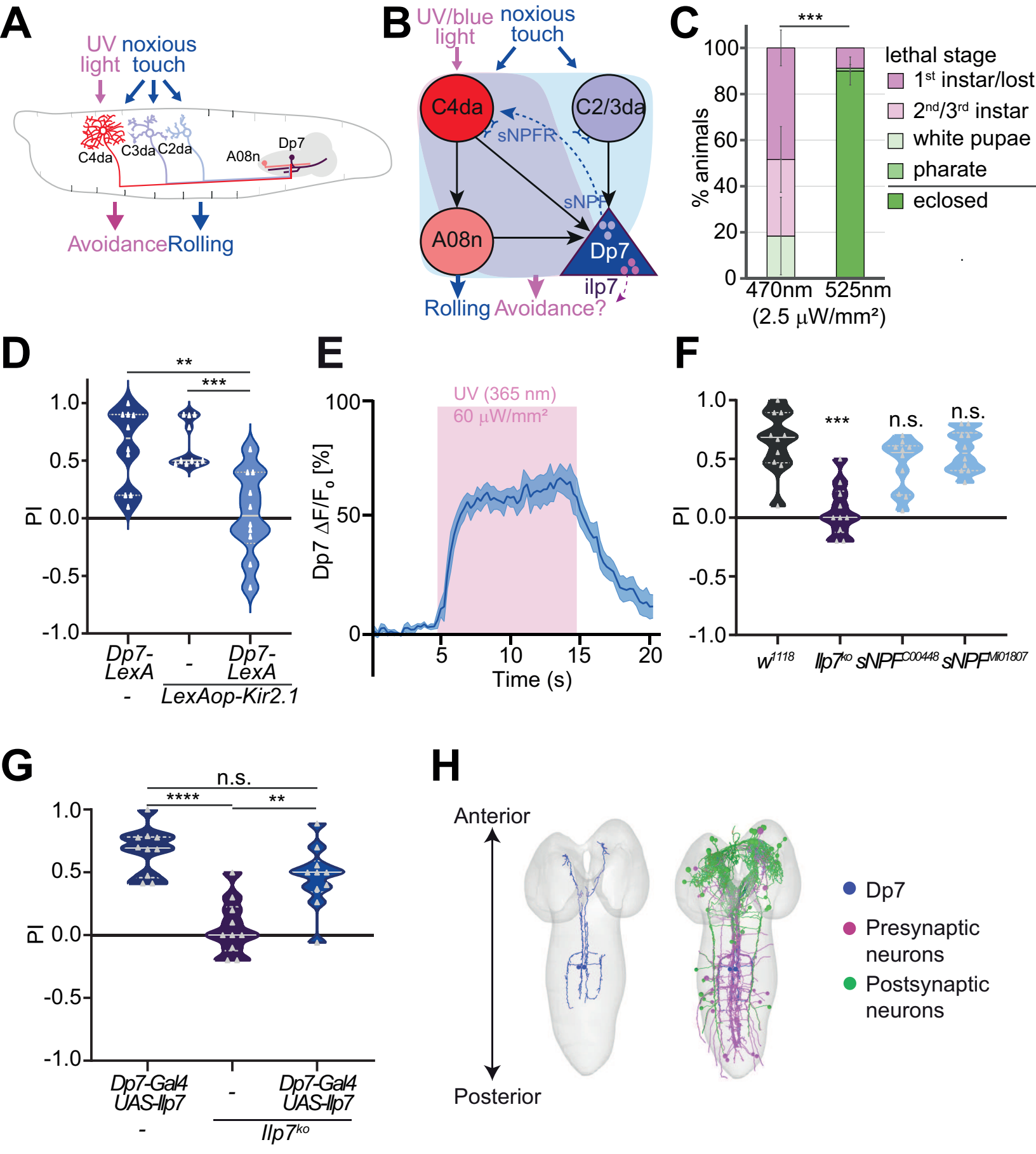
A
UV noxious
light touch
C4da
C3da
C2da
A08n
Dp7
Avoidance
Rolling
B
UV/blue
light
noxious
touch
C4da
C2/3da
sNPFR
sNPF
A08n
Dp7
ilp7
Rolling
Avoidance?
C
***
% animals
100
80
60
40
20
0
lethal stage
1st instar/lost
2nd/3rd instar
white pupae
pharate
eclosed
470nm
525nm
(2.5 µW/mm²)
D
**
***
PI
1.0
0.5
0.0
-0.5
-1.0
Dp7-LexA
-
Dp7-LexA
-
LexAop-Kir2.1
E
UV (365 nm)
60 µW/mm²
Dp7 ΔF/F0 [%]
100
50
0
5
10
15
20
Time (s)
F
PI
1.0
0.5
0.0
-0.5
-1.0
***
n.s.
n.s.
w1118
Ilp7ko
sNPFC00448
sNPFMi01807
G
n.s.
****
**
PI
1.0
0.5
0.0
-0.5
-1.0
Dp7-Gal4
UAS-Ilp7
-
Dp7-Gal4
UAS-Ilp7
-
Ilp7ko
H
Anterior
Posterior
Dp7
Presynaptic neurons
Postsynaptic neurons

Figure 2

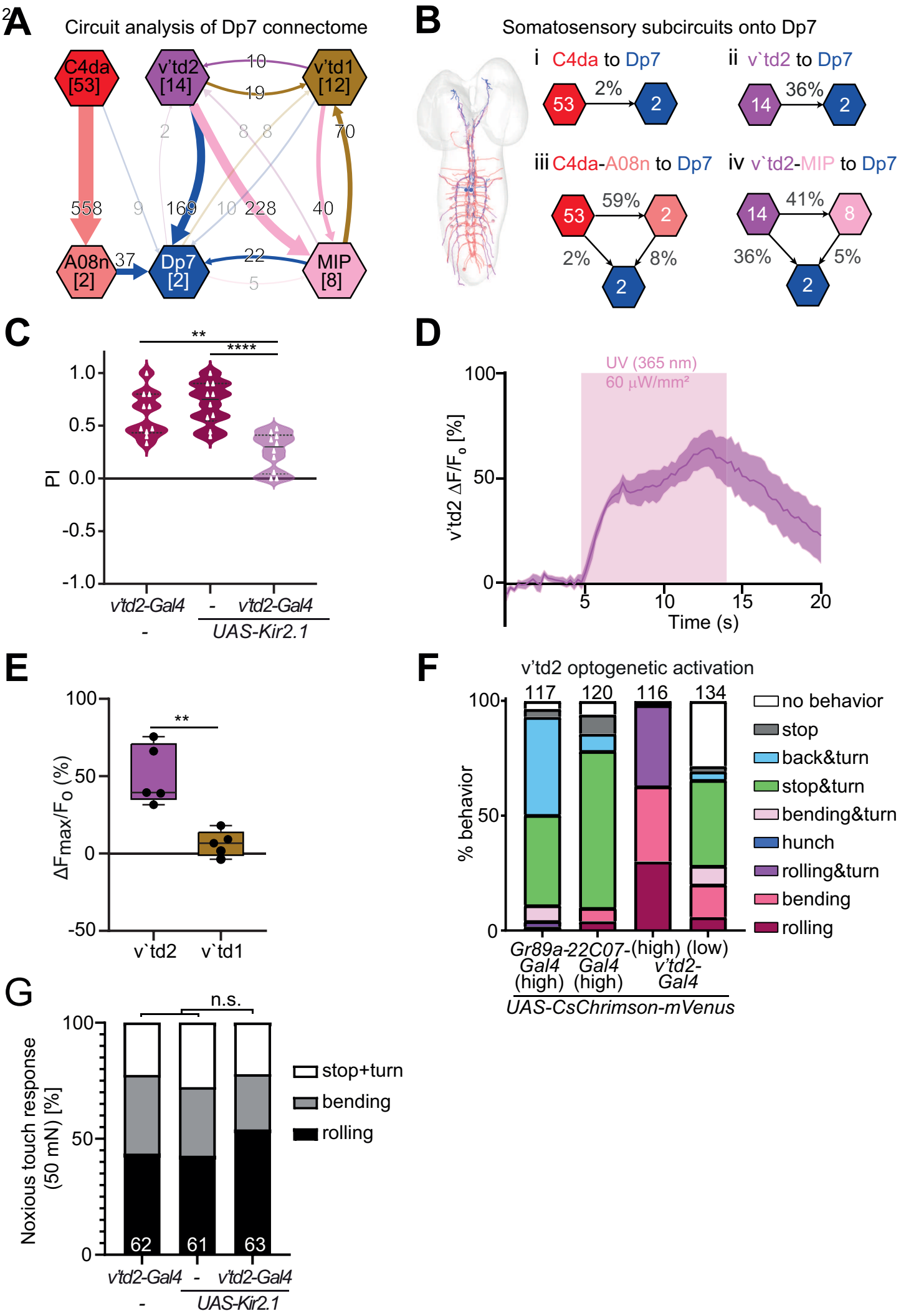
A
Circuit analysis of Dp7 connectome
C4da [53]
v'td2 [14]
v'td1 [12]
A08n [2]
Dp7 [2]
MIP [8]
10
19
2
8
8
70
558
9
169
10
228
40
37
22
5
B
Somatosensory subcircuits onto Dp7
i C4da to Dp7
53
2%
2
ii v`td2 to Dp7
14
36%
2
iii C4da-A08n to Dp7
53
59%
2
2%
8%
2
iv v`td2-MIP to Dp7
14
41%
8
36%
5%
2
C
**
****
1.0
0.5
PI 0.0
-0.5
-1.0
v'td2-Gal4
-
v'td2-Gal4
-
UAS-Kir2.1
D
UV (365 nm)
60 µW/mm²
100
50
0
v'td2 ΔF/F0 [%]
5
10
15
20
Time (s)
E
100
50
0
-50
**
ΔFmax/F0 (%)
v`td2
v`td1
F
v'td2 optogenetic activation
100
50
0
% behavior
117
120
116
134
no behavior
stop
back&turn
stop&turn
bending&turn
hunch
rolling&turn
bending
rolling
Gr89a-Gal4 (high)
22C07-Gal4 (high)
(high) v'td2-Gal4
(low)
UAS-CsChrimson-mVenus
G
n.s.
100
50
0
Noxious touch response (50 mN) [%]
62
61
63
stop+turn
bending
rolling
v'td2-Gal4
-
v'td2-Gal4
-
UAS-Kir2.1

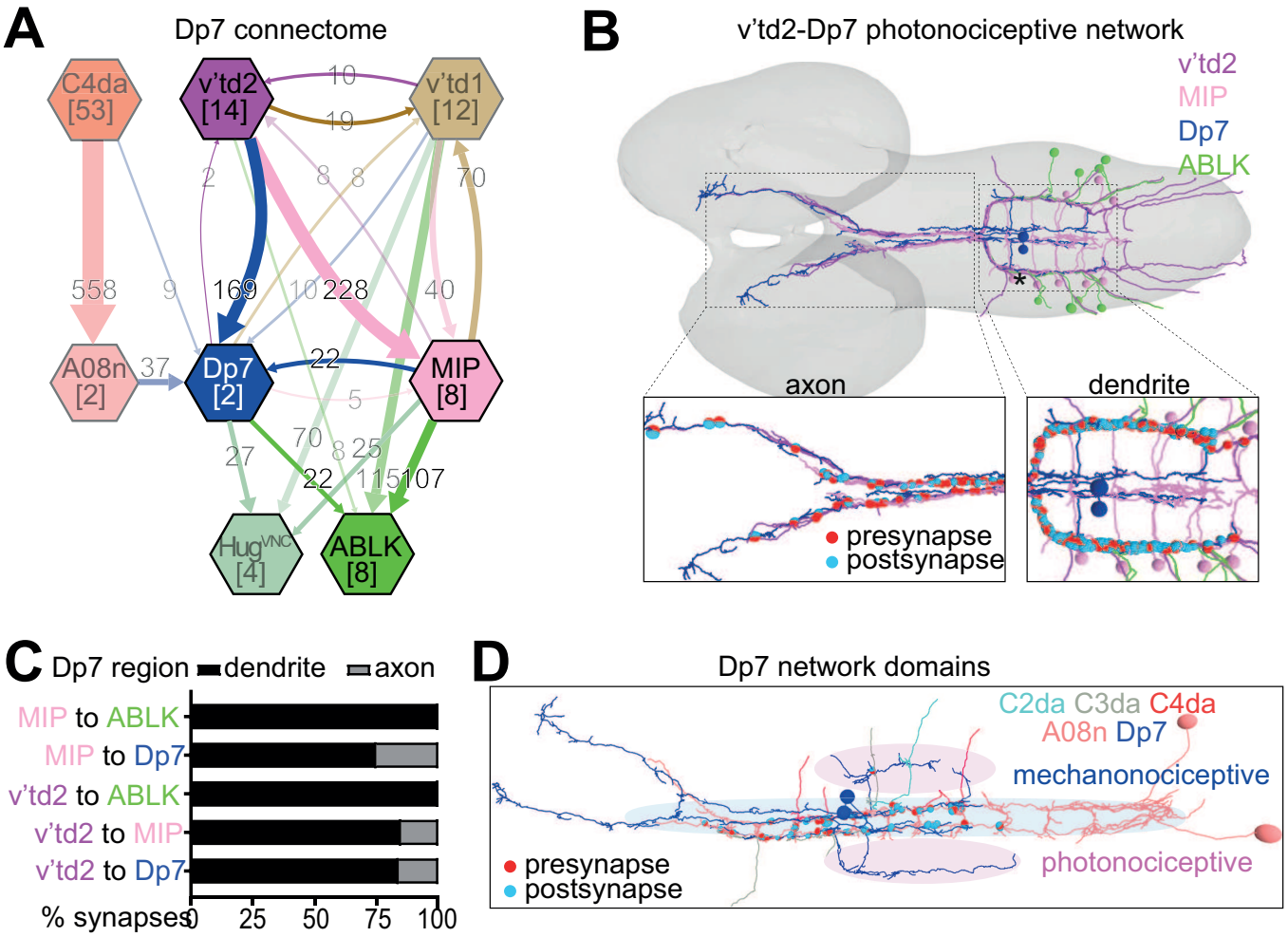
A
Dp7 connectome
C4da [53]
v'td2 [14]
v'td1 [12]
A08n [2]
Dp7 [2]
MIP [8]
Hug^VNC [4]
ABLK [8]
10
19
2
8
8
70
558
9
169
10
228
40
37
22
5
70
8
25
27
22
115
107
B
v'td2-Dp7 photonociceptive network
v'td2
MIP
Dp7
ABLK
*
axon
dendrite
presynapse
postsynapse
C
Dp7 region
dendrite
axon
MIP to ABLK
MIP to Dp7
v'td2 to ABLK
v'td2 to MIP
v'td2 to Dp7
% synapses
0
25
50
75
100
D
Dp7 network domains
C2da C3da C4da
A08n Dp7
mechanonociceptive
photonociceptive
presynapse
postsynapse
E
v'td2 polyads
to MIP and Dp7
F
putative peptide release from Dp7 to ABLK neurons

Figure 4

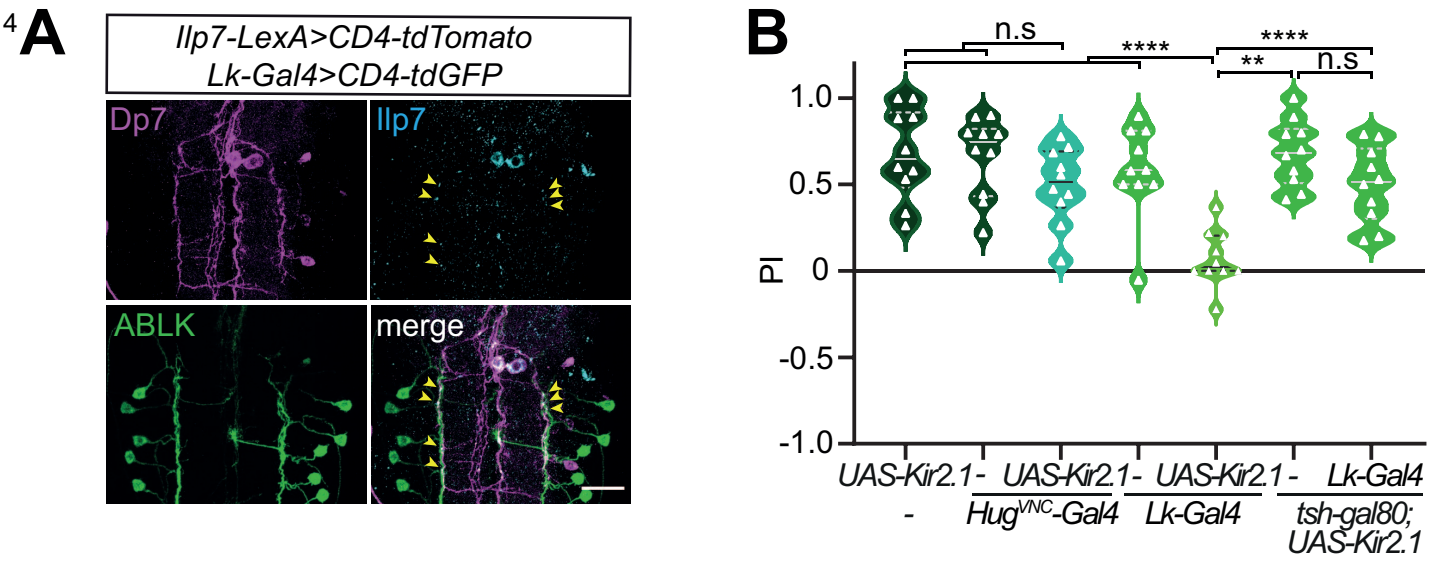

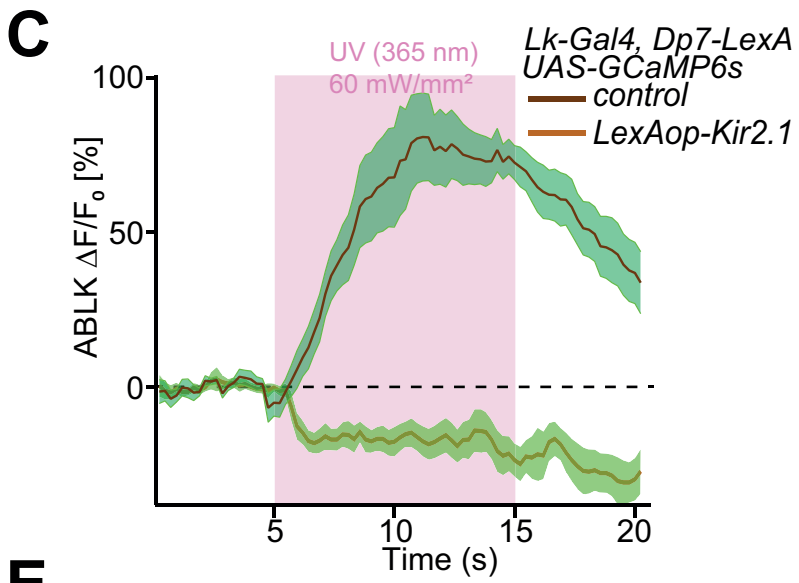

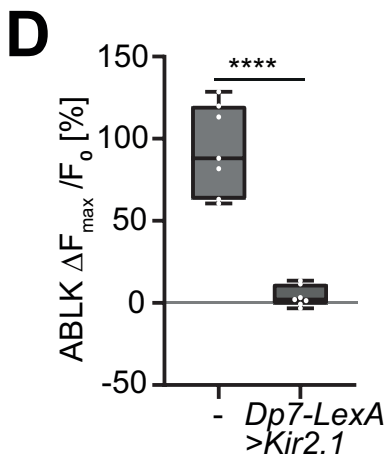

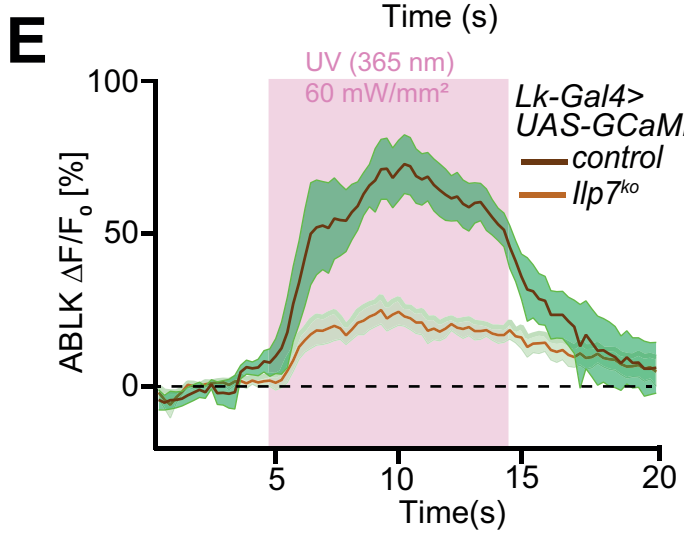

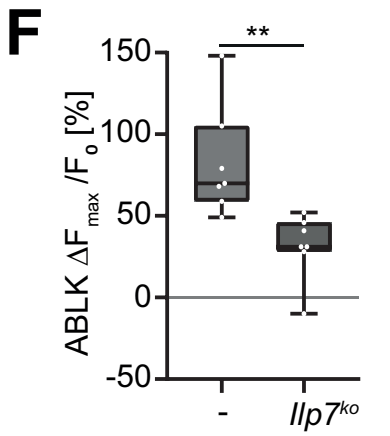

Figure 4, Imambocus et al.

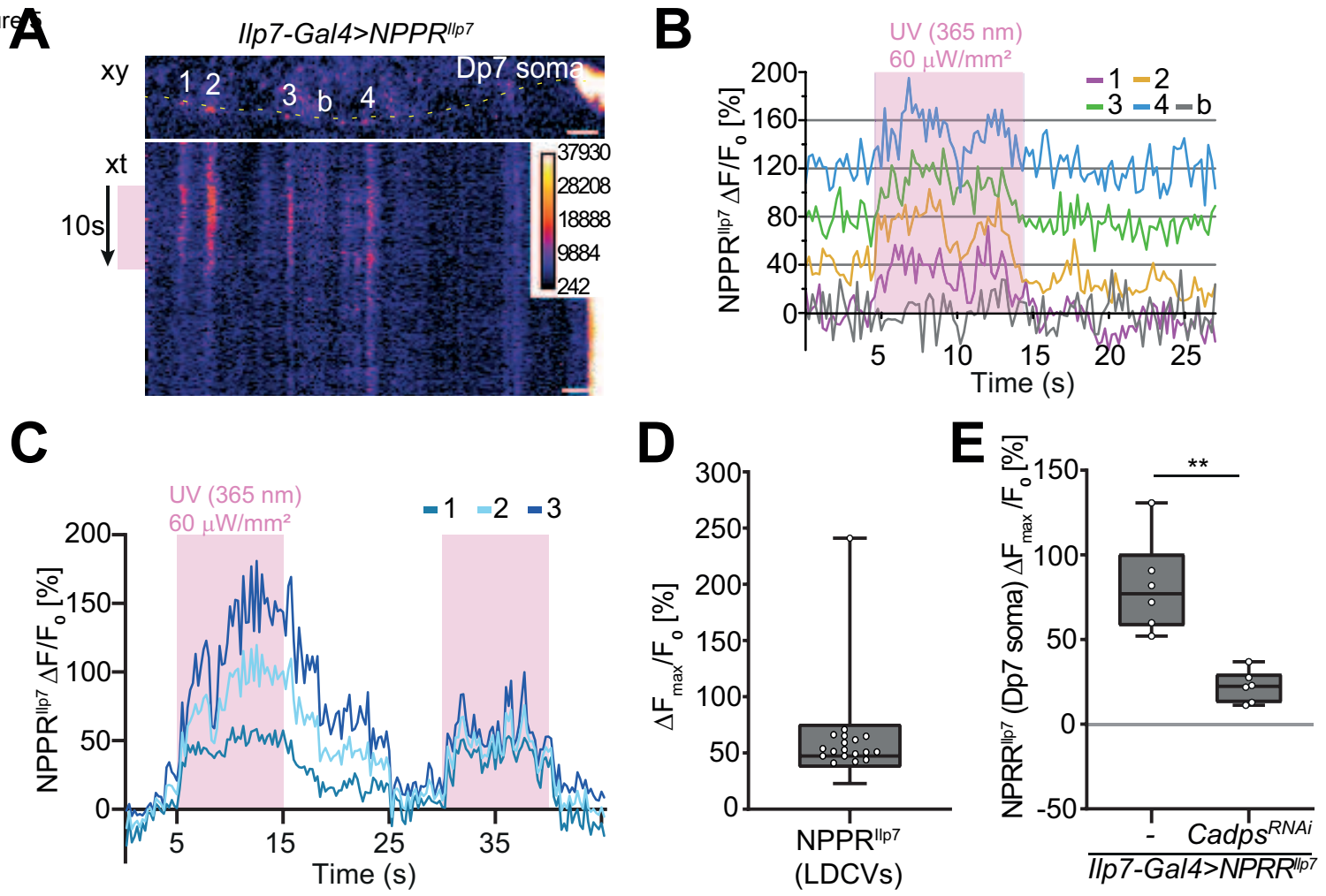

Figure 5, Imambocus et al.

Figure 6

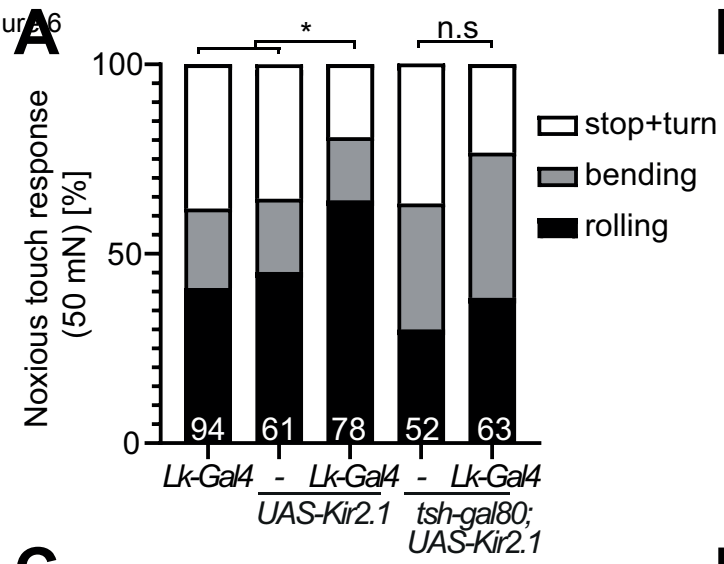
A
*
n.s
100
50
0
Noxious touch response (50 mN) [%]
stop+turn
bending
rolling
94
61
78
52
63
Lk-Gal4
-
Lk-Gal4
UAS-Kir2.1
-
Lk-Gal4
tsh-gal80; UAS-Kir2.1

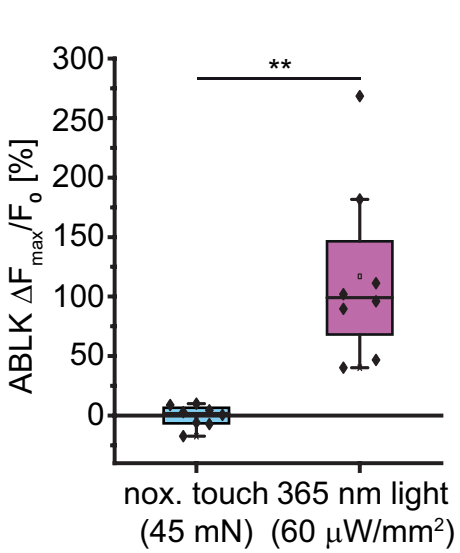
B
**
300
250
200
150
100
50
0
ABLK ΔFmax/Fo [%]
nox. touch 365 nm light
(45 mN) (60 μW/mm²)

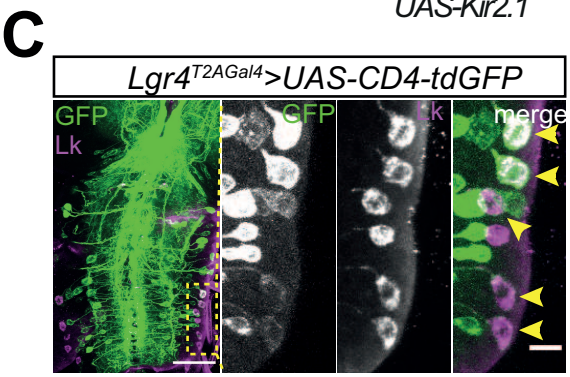
C
Lgr4T2AGal4>UAS-CD4-tdGFP
GFP
Lk
GFP
Lk
merge

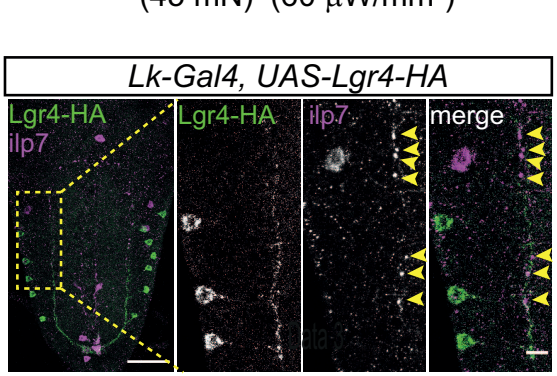
D
Lk-Gal4, UAS-Lgr4-HA
Lgr4-HA
Ilp7
Lgr4-HA
Ilp7
merge

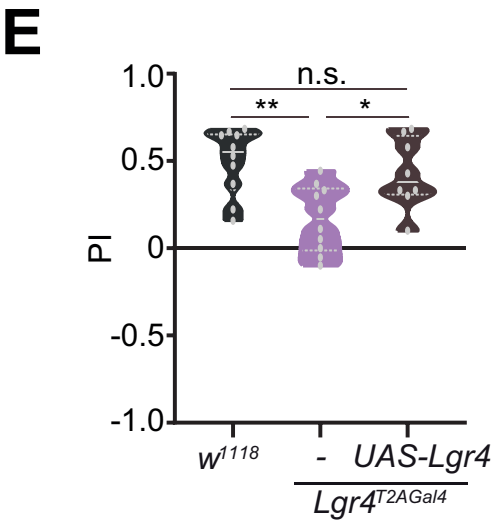
E
n.s.
**
*
1.0
0.5
0
-0.5
-1.0
PI
w1118
-
UAS-Lgr4
Lgr4T2AGal4

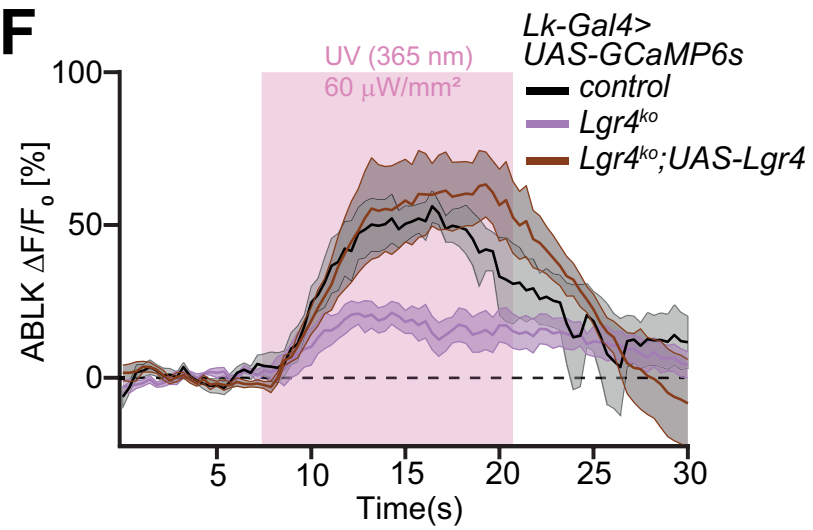
F
Lk-Gal4>
UAS-GCaMP6s
control
Lgr4ko
Lgr4ko;UAS-Lgr4
UV (365 nm)
60 μW/mm²
100
50
0
ABLK ΔF/Fo [%]
5
10
15
20
25
30
Time(s)

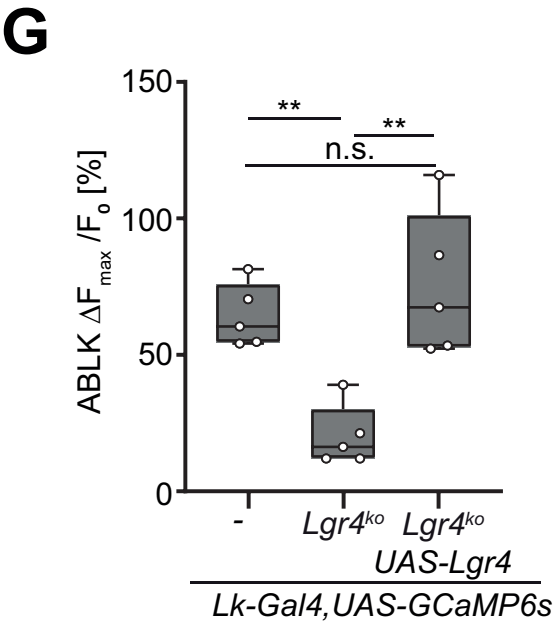
G
**
**
n.s.
150
100
50
0
ABLK ΔFmax/Fo [%]
-
Lgr4ko
Lgr4ko
UAS-Lgr4
Lk-Gal4,UAS-GCaMP6s

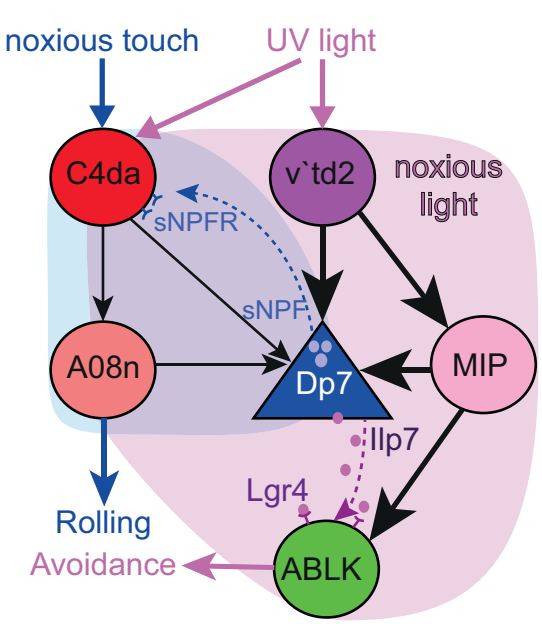
H
noxious touch
UV light
C4da
v`td2
noxious light
sNPFR
sNPF
A08n
Dp7
MIP
Ilp7
Lgr4
Rolling
Avoidance
ABLK

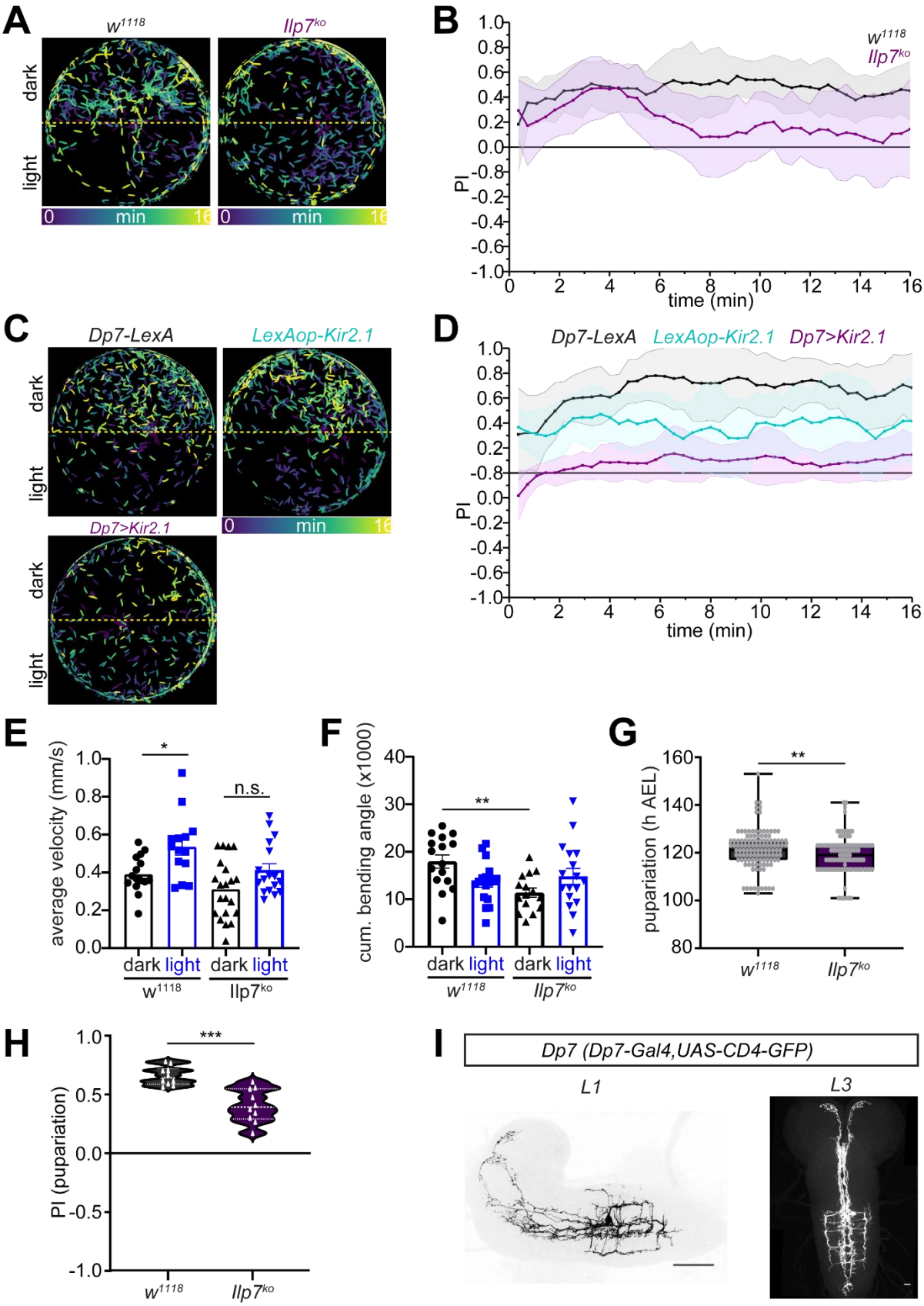
A
w1118
Ilp7ko
dark
light
0 min 16
B
w1118
Ilp7ko
PI
time (min)
C
Dp7-LexA
LexAop-Kir2.1
Dp7>Kir2.1
dark
light
0 min 16
D
Dp7-LexA
LexAop-Kir2.1
Dp7>Kir2.1
PI
time (min)
E
average velocity (mm/s)
*
n.s.
dark light dark light
w1118
Ilp7ko
F
cum. bending angle (x1000)
**
dark light dark light
w1118
Ilp7ko
G
pupariation (h AEL)
**
w1118
Ilp7ko
H
PI (pupariation)
***
w1118
Ilp7ko
I
Dp7 (Dp7-Gal4,UAS-CD4-GFP)
L1
L3

Fig. S1. Dp7 and Ilp7-dependent noxious light avoidance, Related to Figure 1.

A. Time-dependent redistribution of w^{1118} and $Ilp7^{ko}$ larvae in light avoidance assays. Temporal color code indicates larval position at the different time points, dotted line represents light/dark boundary. **B.** Analysis of time-dependent larval distribution of w^{1118} and $Ilp7^{ko}$ larvae during light avoidance assays. Preference index (PI) is based on intensities of larval signals on the dark or light side (see STAR methods). Stable dark preference is reached within the first 5 min for w^{1118}, but not $Ilp7^{ko}$ larvae, which fail to maintain light avoidance. **C.** Time-dependent redistribution of control (*Dp7-LexA* and *LexAop*-Kir2.1) or animals, where Dp7 neurons were silenced (*Dp7-LexA>LexAop-Kir2.1*), in light avoidance assays. Temporal color code indicates larval position at the different time points, dotted line represents light/dark boundary. **D.** Analysis of time-dependent larval distribution in controls and upon Dp7 neuron silencing as indicated. Dp7 neuron function is required for establishing significant light avoidance during the entire assay. **E.** Average velocity and **F.** cumulative bending angle of w^{1118} and $Ilp7^{ko}$ larvae in dark or noxious blue light (4.5 $\mu W/mm^2$) conditions. (n=14-21/genotype, non-significant, *P<0.05, **P<0.01 one-way-ANOVA with Tukey's *post-hoc* test). **G.** Pupariation timing of w^{1118} (median: 121h AEL, n=118) and $Ilp7^{ko}$ larvae (median: 119h AEL, n=103, **P<0.01 Mann-Whitney test). **H.** Dark vs. white light (2.9-4.6 $\mu W/mm^2$) preference index (PI) of pupariation of w^{1118} and $Ilp7^{ko}$ larvae (n=10 trials/genotype, ***P<0.001 two-tailed unpaired *t*-test). Note that control w^{1118} larvae preferentially enter puparium formation in darkness, which is reduced in $Ilp7^{ko}$ animals. **I.** Light microscopic Dp7 neuron morphology at the L1 and L3 stage (*Dp7-Gal4>UAS-CD4-tdGFP*). Dp7 neurons display dendritic arbor extension to the posterior at the L3 stage. In L1, Dp7 neuron dendrites extend to segments A3-A4, while in L3, they extend to the A8 segment. Scale bar=10 μm (L1) and 50 μm (L3).

A

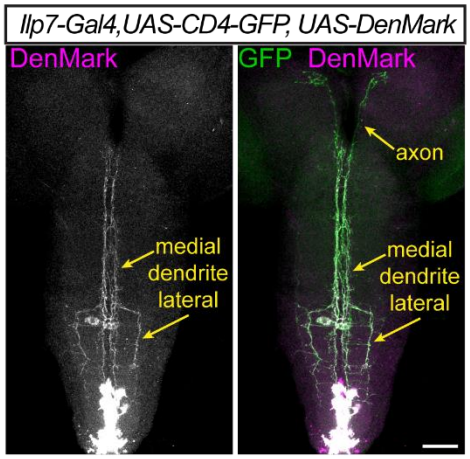

B

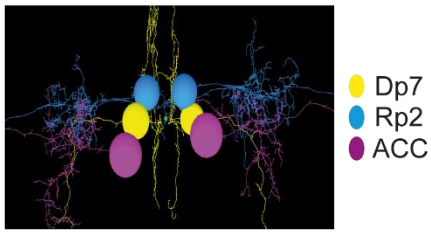

C

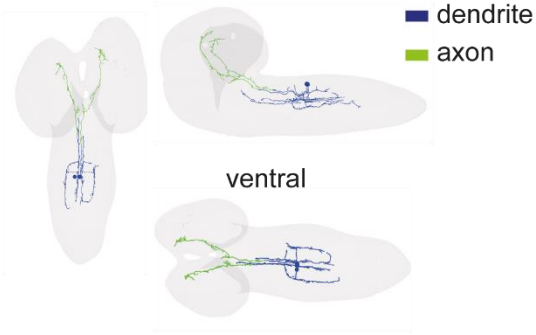

D

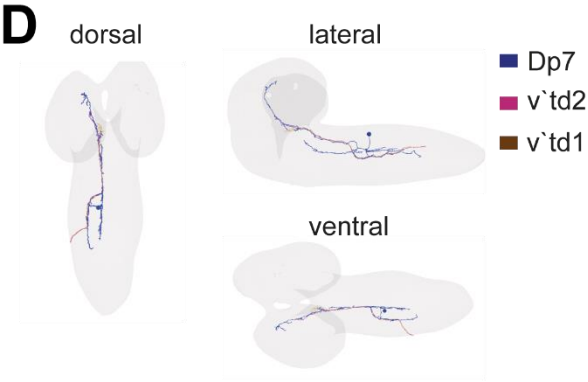

E Dp7 presynaptic connectome

Presynaptic neuron	skeleton ID	synapses Dp7_l	synapses Dp7_r
v`td2	891237		18
v`td2	3915835	21	
v`td2	4061049		14
v`td2	5638694		16
v`td2	7012280	15	
v`td2	12178825		14
v`td2	16303262	4	
v`td2	16911458	15	
v`td2	19017854	17	
v`td2	19037563		14
v`td2	19120772	15	
C2da	3827179		3
C3da	110633	4	
C3da	2777891		4
C3da	7792781	4	
C3da	16307065	4	
C3da	17237088	3	
C4da	18303100	5	1
v`td1	10852875		2
A08n	1927577	1	16
A08n	14899172	19	
MIP	7340664		4
MIP	11291634		3
MIP	11434579		6
MIP	13985838		3
MIP	19040382	3	1
TePn05	2558717		6
TePn05	18981220	18	
	2585319	8	
	2123393	3	
	3629633	3	
	4249897	3	
	6988490	3	
	13674287	3	
	19157404	3	
	2697511		7
	9428865		4
	11512247		4
	4179669		4
	2513992		4
	327601		3
	12617501		2

F Dp7 postsynaptic connectome

Postsynpatic neuron	skeleton ID	synapses Dp7_l	synapses Dp7_r
ABLK	429906	4	
ABLK	3985549	3	
ABLK	10844198	3	
ABLK	19037553		3
ABLK	19166763	5	
Hugin-VNC	6795358	2	5
Hugin-VNC	2613540	4	4
Hugin-VNC	3594705	10	
Hugin-RG	5601924	1	3
Hugin-RG	2138427	7	2
Hugin-RG	5038703	1	2
Hugin-PC	9805520	3	
Bamas	17176866		15
Bamas	17176882	15	
Af6	3946364	3	
BC	3801211		4
DPLm1 contralatera 1 left	6011278		4
DPMm1	3595837		3
DPMpm1	3944626	9	
IPC 6	2357110		3
MIP to the brain	9503414	9	
SN motor neuron	4050398	3	
	5644800	13	5
	8008617	13	5
	3793760	11	
	9524538	10	
	16500055	8	
	6445994	5	
	7345403	5	
	17019327	5	
	18694063	3	5
	16018440	3	1
	3918937	3	
	3945394	3	
	6568902	3	
	14839446	3	
	17415439	3	
	6802553	2	5
	19912140	2	5
	5071140	1	6
	5349961	1	3
	9424902		8
	4411688		6
	11946903		6
	161195633		6
	8546775		5
	15732471		5
	6300434		4
	11278919		4
	3729504		3
	5532548		3
	5613777		3
	6597872		3
	7340664		3
	14162492		3
	15304721		3
	10768709		2
	5378683		2

Fig. S2. Dp7 connectome analysis, Related to Figure 1 and 2.

A. Light microscopic Dp7 neuron morphology and dendritic compartment marked by DenMark at the L3 stage (*Ilp7-Gal4>UAS-CD4-tdGFP, UAS-DenMark*). Dp7 neurons display dendritic arbor extensions within the medial and ventral VNC neuropil. The axon extends anteriorly to the brain lobe region. Scale bar= 50 μm (L3). **B.** Dp7 was identified based on its soma location in abdominal segment A1 on the dorsal side of the VNC in between the two motor neurons Rp2 and ACC and based on the trajectory of its emerging neurites**. C.** Reconstruction of Dp7 neurons illustrated from different angles, Dp7 neuron dendrites shown in blue and axon in green. **D.** V`td1 and v`td2 sensory neurons are anatomically similar and project alongside the lateral and proximal dendritic arbour of Dp7 neurons. **E.** Dp7 presynaptic connectome and **F.** Dp7 postsynaptic connectome from the reconstructed L1 larval EM volume. Numbers indicate synapses with the respective Dp7 neuron (L: left, R: right hemisphere).

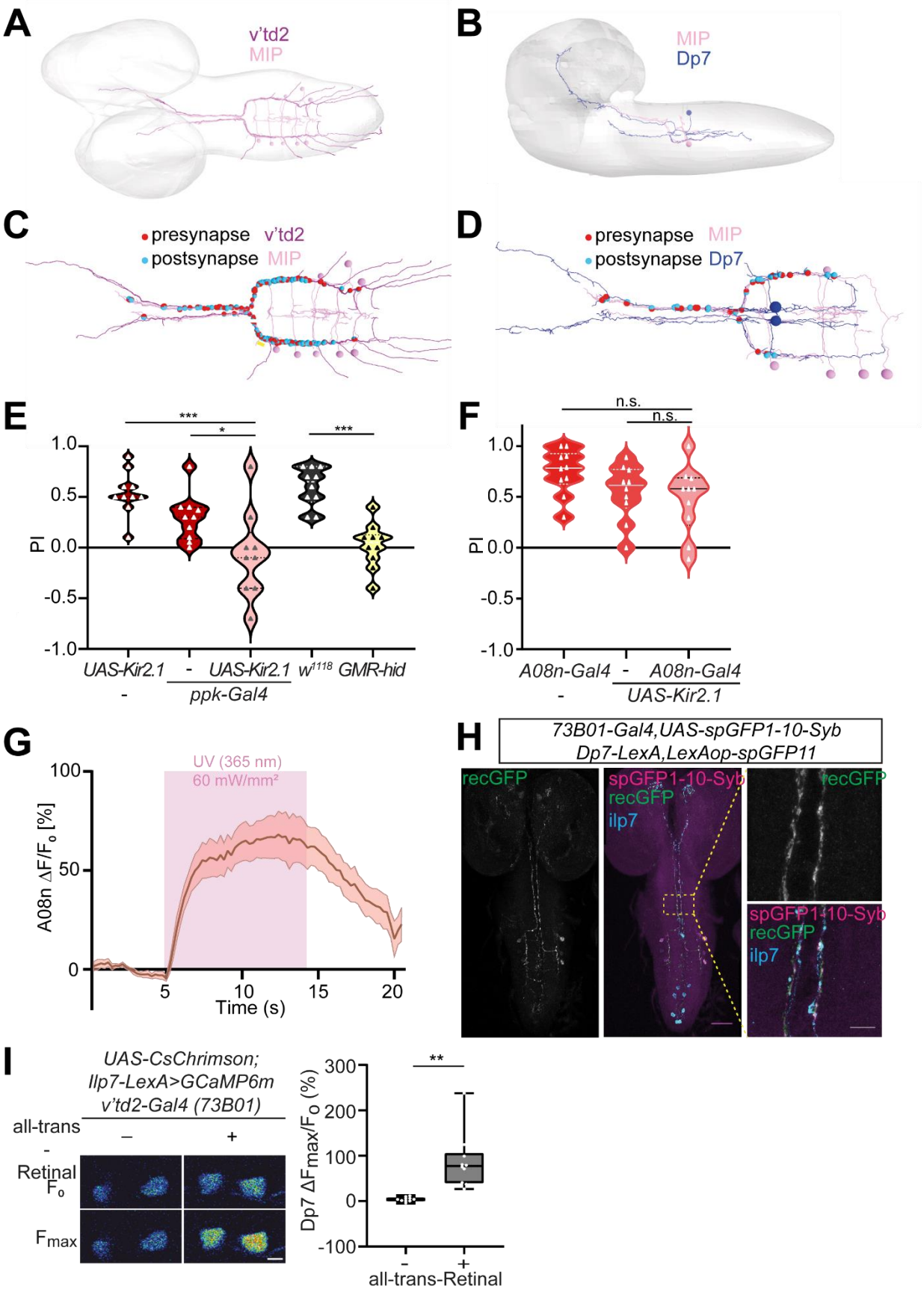
A
v'td2
MIP
B
MIP
Dp7
C
presynapse v'td2
postsynapse MIP
D
presynapse MIP
postsynapse Dp7
E
***
*
***
1.0
0.5
0.0
-0.5
-1.0
PI
UAS-Kir2.1
-
UAS-Kir2.1
w1118
GMR-hid
ppk-Gal4
F
n.s.
n.s.
1.0
0.5
0.0
-0.5
-1.0
PI
A08n-Gal4
-
A08n-Gal4
UAS-Kir2.1
G
UV (365 nm)
60 mW/mm²
100
50
0
A08n ΔF/Fo [%]
5
10
15
20
Time (s)
H
73B01-Gal4,UAS-spGFP1-10-Syb
Dp7-LexA,LexAop-spGFP11
recGFP
spGFP1-10-Syb
recGFP
ilp7
recGFP
spGFP1-10-Syb
recGFP
ilp7
I
UAS-CsChrimson;
Ilp7-LexA>GCaMP6m
v'td2-Gal4 (73B01)
all-trans
-
Retinal
–
+
Fo
Fmax
**
300
200
100
0
-100
Dp7 ΔFmax/Fo (%)
-
+
all-trans-Retinal

Fig. S3. Dp7 neuron upstream network and light sensing circuit, Related to Figure 2.

A. Reconstruction of MIP and v'td2 neurons and **B**. anatomical overlap of MIP (representative member) with Dp7 neurons, lateral view. **C**. Reconstructed synaptic connections between v'td2 and MIP neurons. **D**. Reconstructed synaptic connections between MIP and Dp7 neurons. **E.** Kir2.1 expression in C4da neurons significantly reduces light avoidance responses (*UAS-Kir2.1*, *ppk-Gal4*, *ppk-Gal4>UAS-Kir2.1,* n=10,10,9 trials/genotype, *P<0.05, ***P<0.001, one-way-ANOVA with Tukey's *post-hoc* test). Similarly, genetic ablation of BO by expression of the proapoptotic factor hid strongly impairs light avoidance (*w^{1118} vs. GMR-hid,* n=10 trials/genotype, ***P<0.001, one-way-ANOVA with Tukey's *post-hoc* test). **F.** Kir2.1 expression in A08n neurons does not significantly reduce light avoidance responses (*A08n-Gal4>UAS-Kir2.1,* n=10 trials/genotype, non-significant, one-way-ANOVA with Tukey's *post-hoc* test). **G.** Calcium response to UV light in A08n neuron somata (*82E12-Gal4>UAS-GCaMP6s*, mean ± s.e.m. n=5). **H.** Confocal image showing Syb-GRASP-labelled v`td2 to Dp7 neuron synapses. Presynaptic spGFP1-10-Syb is expressed in v`td2 neurons (*v'td2-Gal4*, magenta), postsynaptic spGFP11-CD4 in Dp7 neurons (*Dp7-LexA*). Reconstituted GFP signal (recGFP, green) labelling v`td2-Dp7 neuron synapses, and Ilp7 neuropeptide immunostaining (cyan). Enlarged boxed area shows proximity of Ilp7 peptide and v'td2-Dp7 neuron synapses along the proximal axon of Dp7 neurons. Scale bars=10 μm. **I.** GCaMP6m signal in Dp7 neurons (using *Ilp7-LexA*) before (F_0) and during (F_{max}) CsChrimson-mediated optogenetic activation of v`td2 neurons (*v'td2-Gal4, UAS-CsChrimson; Ilp7-LexA, LexAop-GCaMP6m*). Maximum responses ($\Delta F_{max}/F_0$) in Dp7 neurons after CsChrimson activation in v`td2 neurons with and without all-trans-retinal (**P<0.01, Mann-Whitney test). Scale bar=10 μm**.**

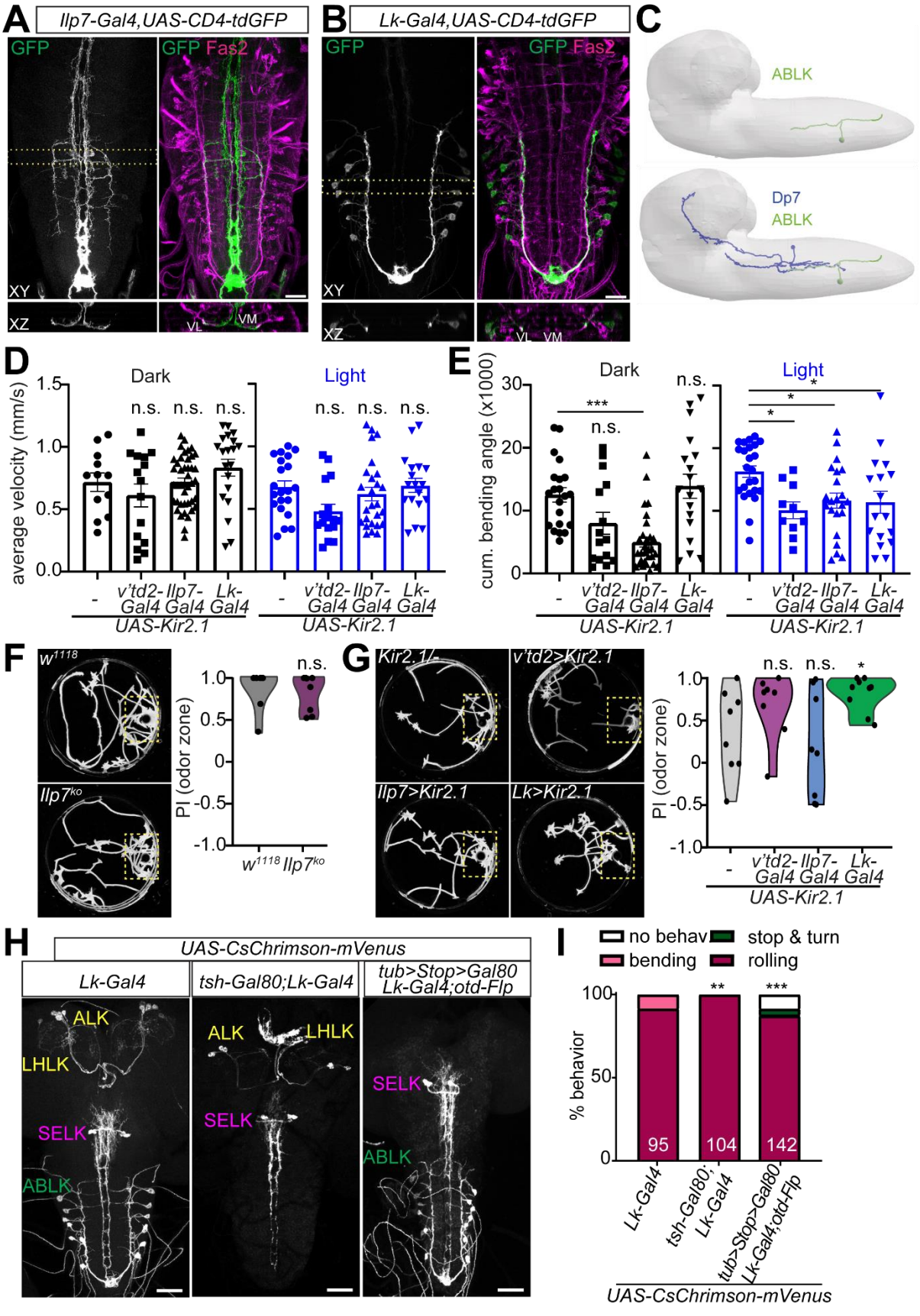
A
Ilp7-Gal4,UAS-CD4-tdGFP
GFP
GFP Fas2
XY
XZ
VL
VM
B
Lk-Gal4,UAS-CD4-tdGFP
GFP
GFP Fas2
XY
XZ
VL
VM
C
ABLK
Dp7
ABLK
D
Dark
Light
average velocity (mm/s)
1.5
1.0
0.5
0.0
n.s.
n.s.
n.s.
n.s.
n.s.
n.s.
-
v'td2-Gal4
Ilp7-Gal4
Lk-Gal4
UAS-Kir2.1
UAS-Kir2.1
E
Dark
Light
cum. bending angle (x1000)
30
20
10
0
***
n.s.
n.s.
*
*
*
-
v'td2-Gal4
Ilp7-Gal4
Lk-Gal4
UAS-Kir2.1
UAS-Kir2.1
F
w1118
Ilp7ko
PI (odor zone)
1.0
0.5
0
-0.5
-1.0
n.s.
w1118
Ilp7ko
G
Kir2.1-
v'td2>Kir2.1
Ilp7>Kir2.1
Lk>Kir2.1
PI (odor zone)
1.0
0.5
0
-0.5
-1.0
n.s.
n.s.
*
-
v'td2-Gal4
Ilp7-Gal4
Lk-Gal4
UAS-Kir2.1
H
UAS-CsChrimson-mVenus
Lk-Gal4
tsh-Gal80;Lk-Gal4
tub>Stop>Gal80 Lk-Gal4;otd-Flp
ALK
LHLK
SELK
ABLK
ALK
LHLK
SELK
SELK
ABLK
I
no behav
stop & turn
bending
rolling
% behavior
100
50
0
**
***
95
104
142
Lk-Gal4
tsh-Gal80;Lk-Gal4
tub>Stop>Gal80 Lk-Gal4;otd-Flp
UAS-CsChrimson-mVenus

Fig. S4. Behavioral functions of noxious light circuit components, Related to Figure 3 and 4.

A. Anatomical localization of Dp7 neuron arbors in relation to Fas2-labelled axon tracts in the larval neuropil. CD4-tdGFP-expression in Dp7 (*Ilp7-Gal4, UAS-CD4tdGFP*) in maximal projection (XY) and a XZ cross-section of the Dp7 soma region (shown region indicated by dotted lines). The primary Dp7 neurite projects from the dorsally located soma (segment A1) to the ventral neuropil forming medial and lateral dendritic branches localizing next to the ventromedial (VM) and ventrolateral (VL) Fas2-positive fascicle, respectively. Scale bar = 50 μm. **B.** Anatomical localization of ABLK neuron arbors in relation to Fas2-labelled axon tracts in the larval neuropil. CD4-tdGFP-expression in ABLK (*Lk-Gal4, UAS-CD4tdGFP*) in maximal projection (XY) and a XZ cross-section of shown region (indicated by dotted lines). ABLK neurons are located in the lateral cortex area (segment A1-A7) and project an axon to body wall muscles, while the resumed dendrites are targeted to the posterior terminal plexus area along the ventromedial (VM) Fas2-positive fascicle. Scale bar = 50 μm. **C.** Reconstruction of ABLK neurons (representative member) and anatomical overlap with Dp7 neurons, lateral view. **D.** Average velocity and **E.** cumulative bending angle of control (*UAS-Kir2.1*) and Kir2.1 expression with different Gal4 lines silencing v'td2 (*v'td2-Gal4*), Dp7 (*Ilp7-Gal4*) or ABLK (*Lk-Gal4*) neurons. Larvae of respective genotypes were tracked in dark or noxious blue light (470 nm, 4.5 $\mu W/mm^2$) conditions. No significant differences were found for average velocity, while cumulative bending angles were significantly reduced under blue light conditions for all groups compared to control (n=15-42, non-significant, *P<0.05, ***P<0.001 one-way-ANOVA with Tukey's *post-hoc* test). **F.** Chemotaxis experiments with a 125mM ethyl butyrate odor source comparing w^{1118} and $Ilp7^{ko}$ larvae. Representative larval tracks are shown, defined odor zone is indicated by dotted yellow box. Both genotypes displayed a high preference index for the odor zone with no significant differences (n=8 trials with 6 larvae each, non-significant, one-way-ANOVA) **G.** Chemotaxis of control (*UAS-Kir2.1*) and Kir2.1 expressing larvae using different Gal4 lines to silence v'td2 (*v'td2-Gal4*), Dp7 (*Ilp7-Gal4*) or ABLK (*Lk-Gal4*) neurons.**.** Representative larval tracks are shown for each genotype, defined odor zone is indicated by dotted yellow box. Preference index for odor zone during the last 2 min of all recorded animals is shown (n=8 trials with 6 larvae each, non-significant, *P<0.05 one-way-ANOVA with Tukey's *post-hoc* test) **H.** CsChrimson-GFP expression with Lk-Gal4 labels ALK and LHLK brain lobe neurons, SELK in the SEZ and ABLK neurons in the VNC. Addition of *tsh-Gal80* (middle panel) selectively eliminates ABLK neuron expression. Otd-Flp-mediated excision of a stop cassette allows brain lobe-specific Gal80 expression (*otd-Flp;tub>Stop>Gal80*), which selectively eliminates ALK an LHLK neuron expression. **I.** Optogenetic activation of CsChrimson in respective genotypes shown in G results in strong rolling responses without significant differences, indicating an involvement of SELK neurons in nociceptive rolling (n= number of animals as indicated in graph, **P<0.01, ***P<0.001, X^2-test).

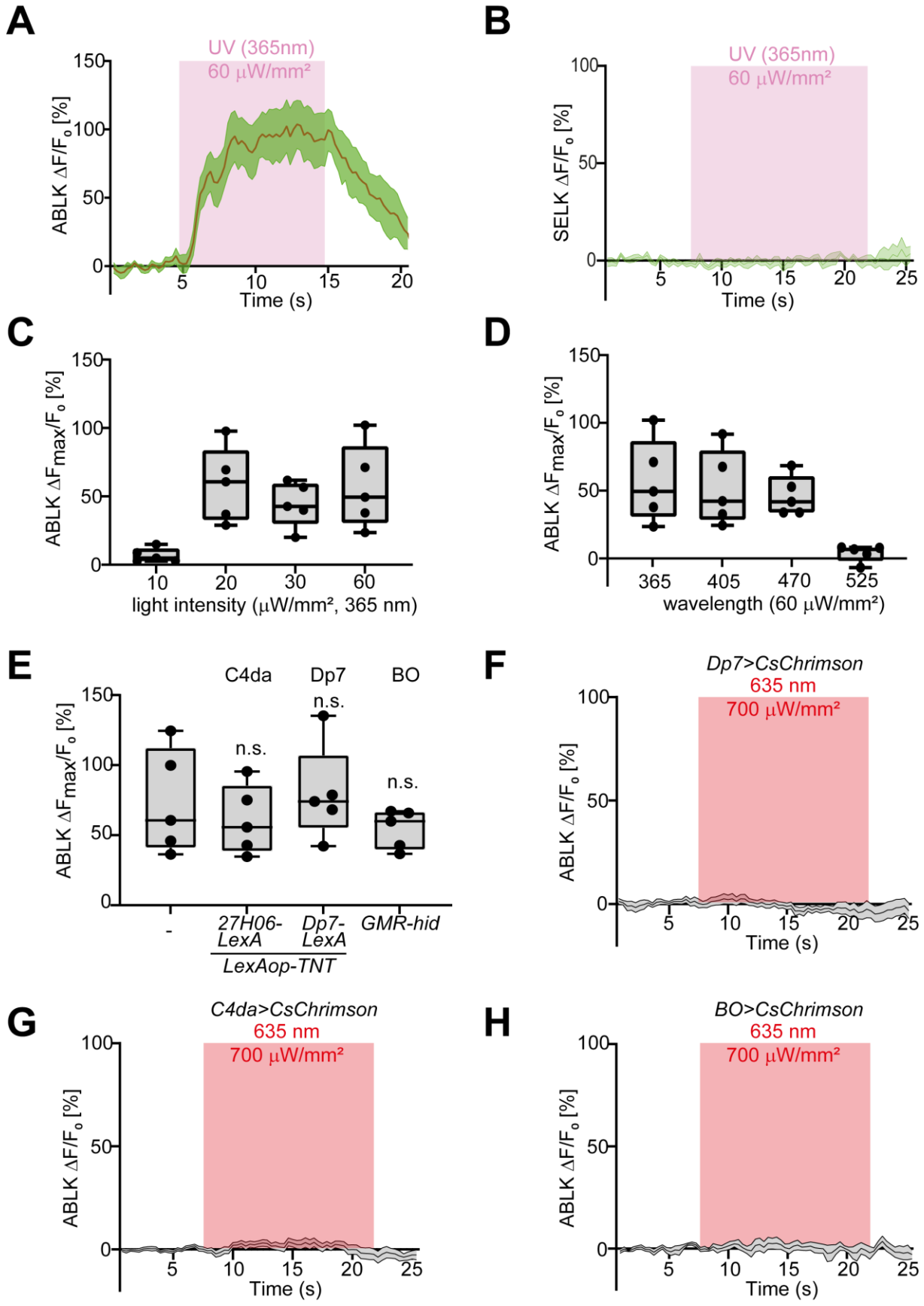
A
UV (365nm)
60 μW/mm²
ABLK ΔF/F₀ [%]
Time (s)
B
UV (365nm)
60 μW/mm²
SELK ΔF/F₀ [%]
Time (s)
C
ABLK ΔFmax/F₀ [%]
light intensity (μW/mm², 365 nm)
D
ABLK ΔFmax/F₀ [%]
wavelength (60 μW/mm²)
E
C4da
Dp7
BO
n.s.
n.s.
n.s.
ABLK ΔFmax/F₀ [%]
-
27H06-LexA
Dp7-LexA
GMR-hid
LexAop-TNT
F
Dp7>CsChrimson
635 nm
700 μW/mm²
ABLK ΔF/F₀ [%]
Time (s)
G
C4da>CsChrimson
635 nm
700 μW/mm²
ABLK ΔF/F₀ [%]
Time (s)
H
BO>CsChrimson
635 nm
700 μW/mm²
ABLK ΔF/F₀ [%]
Time (s)

Fig. S5. Noxious light dependent activation of ABLK neurons, Related to Figure 4.

A. Evoked calcium transients in ABLK neurons by UV-A light (n=5, mean ± s.e.m.). **B**. SELK neurons expressing GCaMP6s do not show UV light-evoked calcium responses light (n=5, mean ± s.e.m.). **C.** Boxplot quantification (% $\Delta F_{max}/F_0$) of ABLK neuron somatic calcium responses (*Lk-Gal4>jRCaMP1b*) in dependence of the UV light intensity (365nm). Strong responses were observed between 20-60 $\mu W/mm^2$ (n=5 larvae/genotype). **D.** ABLK neuron somatic calcium responses (*Lk-Gal4>jRCaMP1b*) to different wavelengths of the same intensity (365nm-525nm, 60 $\mu W/mm^2$). Boxplots of maximum responses (% $\Delta F_{max}/F_0$) show strong activation up to 470nm, but not at 525nm (n=5 larvae/genotype, dataset for 365nm same as in C). **E.** ABLK neuron somatic calcium responses (*Lk-Gal4>GCaMP6s*) to UV light (365nm, 60$\mu W/mm^2$) and synaptic silencing of C4da (*27H06-LexA*) and Dp7 (*Dp7-LexA*) neurons using Tetanus toxin light chain (*LexAop-TNT*) or genetic ablation of BO (*GMR-hid*). Strong ABLK neuron responses without significant differences were observed for all genotypes indicating no major effect of C4da or Dp7 neuron synaptic inactivation or BO ablation (n=5/genotype, non-significant, one-way-ANOVA with Tukey's *post-hoc* test). **F-H**. Expression and activation of CsChrimson (700 $\mu W/mm^2$) for 15s in **F.** C4da (*27H06-LexA*), **G.** Dp7 (*Dp7-LexA*) or **H.** BO (*GMR-LexA*) does not evoke significant somatic ABLK neuron calcium responses (*Lk-Gal4>GCaMP6s,* n=5/genotype).

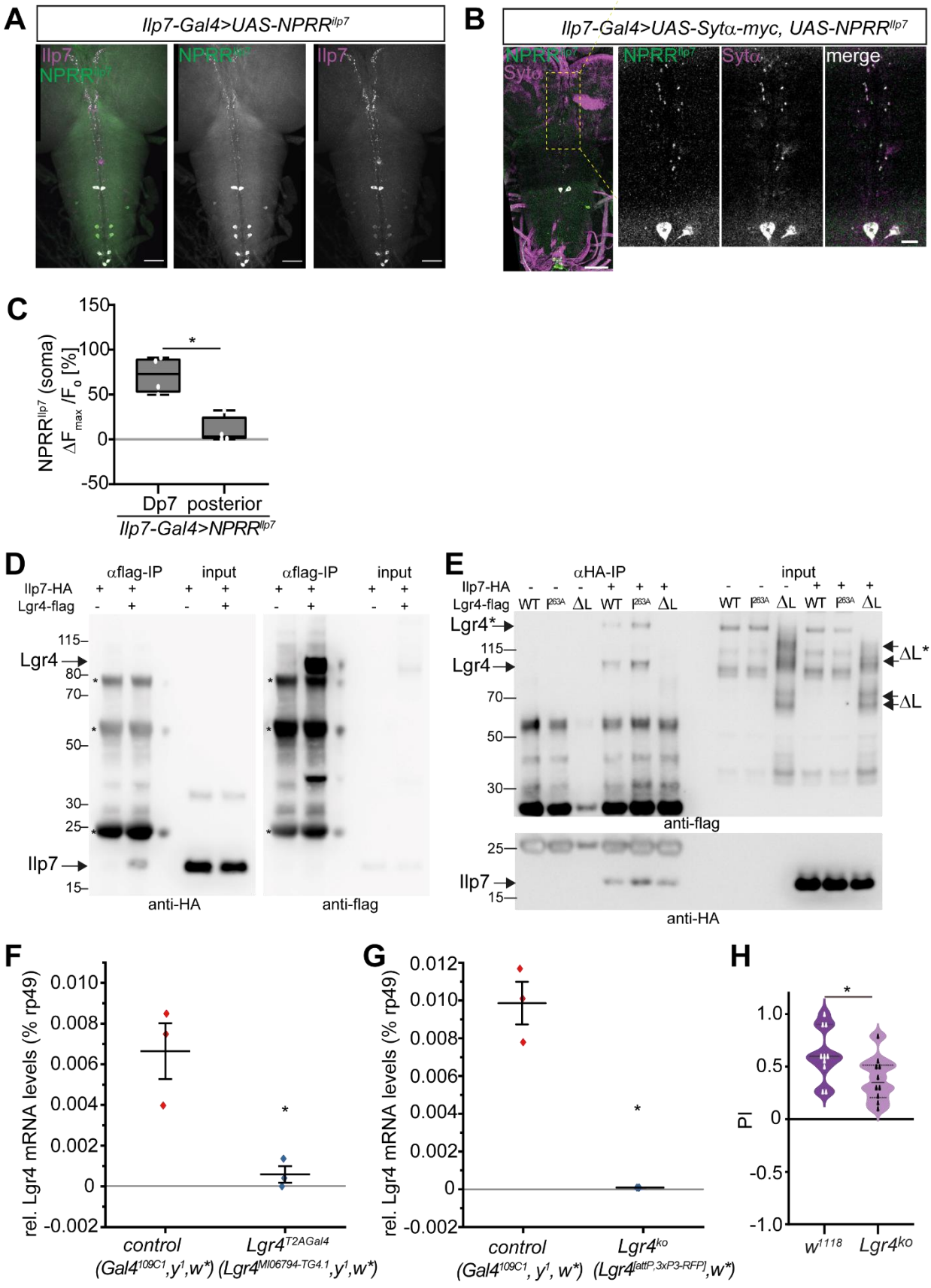
A
Ilp7-Gal4>UAS-NPRR^Ilp7
Ilp7
NPRR^Ilp7
B
Ilp7-Gal4>UAS-Sytα-myc, UAS-NPRR^Ilp7
Sytα
merge
C
NPRR^Ilp7 (soma) ΔF_max /F_0 [%]
Dp7 posterior
Ilp7-Gal4>NPRR^Ilp7
D
αflag-IP
input
Ilp7-HA
Lgr4-flag
Lgr4
Ilp7
anti-HA
anti-flag
E
αHA-IP
input
Lgr4*
ΔL*
ΔL
anti-flag
anti-HA
F
rel. Lgr4 mRNA levels (% rp49)
control
Lgr4^T2AGal4
(Gal4^109C1,y^1,w*) (Lgr4^MI06794-TG4.1,y^1,w*)
G
rel. Lgr4 mRNA levels (% rp49)
control
Lgr4^ko
(Gal4^109C1, y^1, w*) (Lgr4^[attP,3xP3-RFP],w*)
H
PI
w^1118
Lgr4^ko

Fig. S6. *NPRR^{Ilp7}* characterization and biochemical interaction of Lgr4 and Ilp7, Related to Figure 5 and 6.

A. Immunohistochemical analysis of Ilp7 neuropeptide release reporter in Ilp7-expressing neurons (*Ilp7-Gal4>UAS-NPRR^{Ilp7}*, anti-Ilp7 and anti-GFP). Scale bar=50μm. **B**. Immunohistochemical analysis of Ilp7 neuropeptide reporter (NPRR^{Ilp7}, anti-GFP, green) and Sytα-myc (anti-myc, magenta) localization expressed in Ilp7 neurons (*Ilp7-Gal4>UAS-Sytα-myc,UAS-NPRR^{Ilp7}*). Boxed area in overview image is showing enlarged Dp7 neuron proximal dendrite and axon region. Scale bar=50μm, 10μm. **C**. Boxplot quantification (% $\Delta F_{max}/F_0$) of NPRR^{Ilp7} fluorescence changes in Dp7 and posterior Ilp7 neuron somata upon UV light stimulation. Dp7 neurons, but not posterior Ilp7 expressing neurons (A6-A8) show significant responses (n=4 larvae/genotype,*P<0.05, Mann Whitney test). **D-E.** Co-immunoprecipitation of Lgr4 and Ilp7. S2 cells were transfected with flag-tagged Lgr4 and HA-tagged Ilp7, immunoprecipitated with either **D**. anti-flag or **E**. anti-HA antibody beads and detected with antibodies against the coprecipitated Lgr4 or Ilp7, respectively (anti-flag or anti-HA). Specific interaction between Lgr4 and Ilp7 was found under both conditions. In **E**, we also tested interaction with a point mutation (Lgr4-I^{263}A) or deletion (Lgr4$^{\Delta L}$) of the LRR repeats. Lgr4 lacking LRR repeats did not interact with Ilp7 suggesting specific binding of Ilp7 to the Lgr4 extracellular LRR domain. Signals specific for Lgr4 (and ΔL form) and multimeric forms (Lgr4*, ΔL*) are indicated by arrows. Asterisks indicate IP antibody signal. **F**. Quantitative RT-PCR of Lgr4 mRNA comparing *Lgr4^{T2AGal4}* allele to control (n=3, unpaired t-test,**P<0.05*). **G**. Quantitative RT-PCR of Lgr4 mRNA comparing *Lgr4^{ko}* allele to control (n=3, unpaired t-test,**P<0.05*). **H**. *Lgr4^{ko}* animals display reduced light avoidance compared to controls (n=10 trials/genotype, **P<0.05*, unpaired *t*-test).

Table S1.
Exact *P* values and genotypes

Figure	Genotypes compared	Statistical test	Signif-icance	P values	post-hoc test
Fig. 1C	*w*^{1118} blue vs. green light	Chi-Square	***	0.001	
Fig. 1D	*Dp7-LexA/- vs. Dp7-LexA:LexAop-Kir2.1*	One-way Anova	**	0.001	Tukey
	LexAopKir2.1/- vs. Dp7-LexA:LexAopKir2.1	One-way Anova	***	0.0006	Tukey
Fig. 1F	*w*^{1118} vs. *Ilp7*^{ko}	One-way Anova	***	0.001	Tukey
	w ^{1118} vs. *sNPF*^{C00448}	One-way Anova	n.s.	>0.999	Tukey
	w ^{1118} vs. *sNPF* ^{Mi01807}	One-way Anova	n.s.	0.6046	Tukey
Fig. 1G	*Dp7-GAL4*;*UAS-Ilp7* vs. *Ilp7*^{ko}	One-way Anova	****	<0.0001	Tukey
	Dp7-GAL4;*UAS-Ilp7* vs. Ilp7ko;*Dp7Gal4*;*UAS-Ilp7*	One-way Anova	n.s.	0.1083	Tukey
	Ilp7^{ko} vs. Ilp7^{ko};*Dp7-Gal4*;*UAS-Ilp7*	One-way Anova	**	0.0011	Tukey
Fig. 2C	*73B01-GAL4/- vs. 73B01-GAL4;UAS-Kir2.1*	One-way Anova	**	0.0014	Tukey
	UAS-Kir2.1/- vs. *73B01-GAL4;UAS-Kir2.1*	One-way Anova	****	<0.0001	Tukey
Fig. 2E	*35BO1-Gal4, UAS-GCaMP6s*	unpaired t test, two tailed with Welch`s correction	**	0.0044	
Fig. 2G	*73BO1-GAL4*/- vs. *73B01-GAL4; UAS-Kir2.1*	Chi-Square	n.s.	0.5598	
	UAS-Kir2.1/- vs. 73B01-GAL4; UAS-Kir2.1	Chi-Square	n.s.	0.5598	
Fig. 4B	*UAS-Kir2.1*/- vs. *HuginVNC-GAL4; UAS-Kir2.1*	One-way Anova	n.s.	0.5546	Tukey
	HuginVNC-Gal4/- vs. *HuginVNC-GAL4;UAS-Kir2.1*	One-way Anova	n.s.	0.6569	Tukey
	UAS-Kir2.1/- vs. *Lk-Gal4;UAS-Kir2.1*	One-way Anova	****	<0.0001	Tukey
	Lk-Gal4/- vs. *Lk-Gal4;UAS-Kir2.1*	One-way Anova	****	<0.0001	Tukey

	Lk-Gal4;UAS-Kir2.1 vs. -/tsh-gal80; UAS-Kir2.1	One-way Anova	**	0.0013	Tukey
	Lk-Gal4;UAS-Kir2.1 vs. Lk-Gal4; tsh-gal80;UAS-Kir2.1	One-way Anova	****	<0.0001	Tukey
Fig. 4D	*LK-Gal4,UAS-GCamP6s; ilp7-LexA* vs *LK-Gal4,UAS-GCamP6s; Ilp7-LexA, LexAop-Kir2.1*	unpaired t test, two tailed with Welch`s correction	****	<0.0001	
Fig. 4F	*LK-Gal4,UAS-GCaMP6s* vs. *Ilp7^{ko}*; *LK-Gal4,UAS-GCaMP6s*	unpaired t test, two tailed with Welch`s correction	**	0.0064	
Fig. 5E	*ilp7-Gal4,UAS-NPRR^{ilp7}, CapdsRNAi*	unpaired t test, two tailed with Welch`s correction	**	0.0026	
Fig. 6A	*Lk-Gal4/- vs. Lk-Gal4;UAS-Kir2.1*	Chi-Square	*	0.0167	
	UAS-Kir2.1/- vs. Lk-Gal4;UAS-Kir2.1	Chi-Square	*	0.0167	
	Lk-Gal4/- vs. -/tsh-gal80;UAS-Kir2.1	Chi-Square	n.s.	0.1873	
Fig. 6B	*LK-Gal4,UAS-GCaMP6, mechano vs. UV light*	unpaired t test, two tailed with Welch`s correction	**	0.00295	
Fig. 6E	*W^{1118}*vs. *Lgr4$^{T2A-Gal4}$*	One-way Anova	**	0.0023	Tukey
	Lgr4$^{T2A-Gal4}$ vs. *Lgr4$^{T2A-Gal4}$*;UAS-Lgr4	One-way Anova	*	0.0239	Tukey
	W^{1118} vs. *Lgr4$^{T2A-Gal4}$*;UAS-Lgr4	One-way Anova	n.s.	0.7338	Tukey
Fig. 6G	*Lgr4ko; LK-Gal4,UAS-GCaMP6s vs. LK-Gal4,UAS-GCaMP6s*	One-way Anova	**	0.0011	Tukey
	Lgr4ko; LK-Gal4,UAS-GCaMP6s vs. Lgr4ko; LK-Gal4,UAS-GCaMP6s/UASLgr4	One-way Anova	**	0.0058	Tukey
	LK-Gal4,UAS-GCaMP6s vs. Lgr4ko; LK-Gal4,UAS-GCaMP6s/UASLgr4	One-way Anova	n.s.	0.6186	Tukey
Fig. S1E	*w^{1118} dark vs. light*	One-way Anova	*	0.03858	Tukey
	Ilp7^{ko} dark vs. light	One-way Anova	n.s.	0.1457	Tukey
	w^{1118} dark vs. Ilp7^{ko} dark	One-way Anova	n.s.	0. 3687	Tukey

	w^{1118} light vs. Ilp7^{ko} light	One-way Anova	n.s	0.0869	Tukey
Fig. S1F	*w^{1118} dark vs. light*	One-way Anova	n.s.	0.0978	Tukey
	w^{1118} dark vs. Ilp7^{ko} dark	One-way Anova	**	0.0061	Tukey
	w^{1118}light vs. Ilp7^{ko} light	One-way Anova	n.s.	0.8988	Tukey
	Ilp7^{ko} dark vs. light	One-way Anova	n.s.	0.2715	Tukey
Fig. S1G	*w^{1118} vs. Ilp7^{ko}*	Mann-Whitney test, two tailed	**	0.0080	
Fig. S1H	*w^{1118} vs. Ilp7^{ko}*	unpaired t test, two tailed with Welch`s correction	***	0.0002	
Fig. S3E	*ppk-GAL4/-* vs. *ppk-GAL4>UAS-Kir2.1*	One-way Anova	*	0.0439	Tukey
	UAS-Kir2.1/- vs. *ppk-GAL4>UAS-Kir2.1*	One-way Anova	***	0.0001	Tukey
	W^{1118} vs. GMR-hid	One-way Anova	***	0.0002	Tukey
Fig. S3F	*A08n-GAL4/-* vs. *A08n-GAL4;UAS-Kir2.1*	One-way Anova	n.s.	0.0883	Tukey
	UAS-Kir2.1/- vs. *A08n-GAL4;UAS-Kir2.1*	One-way Anova	n.s.	0.8282	Tukey
Fig. S3I	*73B01-Gal4, UAS-Chrimson; Ilp7-LexA,LexAop-GCaMP6m*	Mann-Whitney test, two tailed	**	0.0015	
Fig.S4D	*UAS-Kir2.1/- vs. 73B01-Gal4>UAS-Kir2.1 (dark)*	One-way Anova	n.s.	0.7290	Tukey
	UAS-Kir2.1/- vs. Ilp7-Gal4>UAS-Kir2.1 (dark)	One-way Anova	n.s.	>0.9999	Tukey
	UAS-Kir2.1/- vs. Lk-Gal4>UAS-Kir2.1(dark)	One-way Anova	n.s.	0.6197	Tukey
	UAS-Kir2.1/- vs. 73B01-Gal4>UAS-Kir2.1 (light)	One-way Anova	n.s.	0.0862	Tukey
	UAS-Kir2.1/- vs. Ilp7-Gal4>UAS-Kir2.1 (light)	One-way Anova	n.s.	0.863	Tukey
	UAS-Kir2.1/- vs. Lk-Gal4>UAS-Kir2.1(light)	One-way Anova	n.s.	0.9985	Tukey
Fig.S4E	*UAS-Kir2.1/- vs.*	One-way	n.s.	0.1264	

	v'td2-Gal4>UAS-Kir2.1 (dark)	Anova			
	UAS-Kir2.1/- vs. Ilp7-Gal4>UAS-Kir2.1 (dark)	One-way Anova	***	0.0002	
	UAS-Kir2.1/- vs. Lk-Gal4>UAS-Kir2.1(dark)	One-way Anova	n.s.	0.8929	
	UAS-Kir2.1/- vs. 73B01-Gal4>UAS-Kir2.1 (light)	One-way Anova	*	0.022	
	UAS-Kir2.1/- vs. Ilp7-Gal4> UAS-Kir2.1 (light)	One-way Anova	*	0.0308	
	UAS-Kir2.1/- vs. Lk-Gal4> UAS-Kir2.1(light)	One-way Anova	*	0.0354	
Fig. S4F	*W1118 vs Ilp7ko*	One-way Anova	n.s.	0.6167	
Fig. S4G	*UAS-Kir2.1/- vs. 73B01-GAL4;UAS-Kir2.1*	One-way Anova	n.s.	0.1857	
	UAS-Kir2.1/- vs. ilp7-Gal4;UAS-Kir2.1	One-way Anova	n.s.	0.5927	
	UAS-Kir2.1/- vs. Lk-Gal4;UAS-Kir2.1	One-way Anova	*	0.0247	
Fig. S4I	*Lk-Gal4 ; UAS-ChrimsonGFP vs. Lk-Gal4;tub>STOP>Gal80xotdFlp;UAS-ChrimsonGFP*	Chi-Square	***	0.0001	
	Lk.Gal4 ; UAS-ChrimsonGFP vs. LkGAl4+ tshGal80; UAS-ChrimsonGFP	Chi-Square	**	0.0025	
Fig. S5E	*ctrl vs. Lk-Gal4>UAS-GCaMP6s ; 27H06-LexA >LexAop-TNT*	One-way Anova	n.s.	0.899	Tukey
	ctrl vs. Lk-Gal4>UAS-GCaMP6s; Ilp7-LexA >LexAop-TNT	One-way Anova	n.s.	0.9859	Tukey
	ctrl vs. Lk-Gal4>UAS-GCaMP6s; GMR-hid	One-way Anova	n.s.	0.7331	Tukey
Fig. S6C	*Ilp7-Gal4>UAS-NPRRilp7*	Mann-Whitney test, two tailed	*	0.0286	
Fig. S6F	*ctl vs. Lgr4-T2A-Gal4*	unpaired t test, two tailed with Welch`s correction	*	0.03858	
Fig. S6G	*ctl vs. Lgr4ko*	unpaired t test, two tailed with Welch`s correction	*	0.01311	

Fig. S6H	*Lgr4ko vs. W1118*	unpaired t test, two tailed with Welch`s correction	*	0.0361	

Table S2.

Primer sequences

Primers:	
Ilp7-NotI-c (Ilp7-HA)	aaGCGGCCGCATGACCAGAATGATAATAC
Ilp7-HA-nc (Ilp7-HA)	This paper
ILP7-Nde_nc (Ilp7-GCaMP6s) agaCATATGGTAGTGATTGCGTCGCTTG	AGCATCTCGAGACCCTCCTCGGTGTGCTGCAGcagagatgcgtagtctggcacgtcgtatgggtagctCTGCAGTGCCTC
GCaMP6s-Nde-c (Ilp7-GCaMP6s)	tggCATATGggttctcatcatcatcatc
GCaMP6s-Xba-nc (Ilp7-GCaMP6s)	atctagattacttcgctgtcatcatttgtac
Lgr4-Not-c	acGCGGCCGCATGTGTATAGCTCACCTGC
Lgr4-Xho-nc (Lgr4-flag)	TTGCCTCGAGCAGATAGCTCATCTGCCGGTg
Lgr4-over-c (Lgr4-I263A)	ATTGAGTATTCTCgccTTGGCACGCAACCACCTGCACC
Lgr4-over-nc (Lgr4-I263A)	TGGTTGCGTGCCAAggcGAGAATACTCAATTGATTGC
Lgr4^{T2AGal4} forward	TCACCTCGACAGGGACAGGAA
Lgr4^{T2AGal4} reverse	ACTGCGTGAACGAGGTGGAC
Lgr4^{ko} forward	TGCAGCGATAAGCAGACACCAT
Lgr4^{ko} reverse	GTCCTACGCCTTCTGCTGTTGT
rp49 forward	TTGAGAACGCAGGCGACCGT
rp49 reverse	CGTCTCCTCCAAGAAGCGCAAG

Video S1

Click here to access/download

Supplemental Videos and Spreadsheets

video S1_w11118_light avoidance masked.avi

Video S2

Video S3

Click here to access/download

Supplemental Videos and Spreadsheets

video S3 Combined Stacks S3 S4v2.avi

Video S4

Click here to access/download

Supplemental Videos and Spreadsheets

video S4 Combined Stacks S5-8v4.avi

Video S5

Click here to access/download

Supplemental Videos and Spreadsheets

video S5 LK opto.avi

Video S6